Subducted fragments of the Liguro-Piemont ocean, Western Alps: Spatial correlations and offscraping mechanisms during subduction

Clément Herviou, Philippe Agard, Alexis Plunder, Kevin Mendes, Anne Verlaguet, Damien Deldicque, Nadaya Cubas

Subducted fragments of the Liguro-Piemont ocean, Western Alps: spatial correlations and offscraping mechanisms during subduction

Clément Herviou[a*], Philippe Agard[a], Alexis Plunder[b], Kevin Mendes[a], Anne Verlaguet[a], Damien Deldicque[c], Nadaya Cubas[a]

[a] Sorbonne Université, CNRS-INSU, Institut des Sciences de la Terre de Paris, ISTeP UMR 7193, F-75005 Paris, France

[b] BRGM, F-45060, Orléans, France

[c] Laboratoire de Géologie, Ecole Normale Supérieure PSL, F-75005 Paris, France

□ Corresponding author: clement.herviou@sorbonne-universite.fr (C. Herviou)

Keywords:

Oceanic subduction, Liguro-Piemont, Schistes Lustrés, Western Alps, Tectonic slicing, HP-LT metamorphism

Abstract

Fragments of subducted slow-spreading oceanic lithosphere are exposed continuously in the Liguro-Piemont domain of the Western Alps. By combining new and literature petrological data, interpolated maps of maximum temperatures, maximum Si contents of phengite as a proxy for peak pressure and thermodynamic modelling, we provide a detailed framework of the peak metamorphic conditions experienced by the distinct subduction slices. High-resolution mapping confirms the marked eastward increase in metamorphic grade throughout the domain, as well as within some slices. The compilation of lithostratigraphic, structural and radiochronological data and the estimation of sediment/mafic-ultramafic ratio for each slice allow refining the origin of these tectonometamorphic units within the former oceanic domain. The refined structural sketchmap allows to restore the geometries of the Alpine subduction at peak burial conditions. Results point to a trimodal distribution of the units with an increase in metamorphic conditions from the Upper (LPU; 320-400°C- 1.2-1.9 GPa) to the Middle (LPM; 415-475°C- 1.7-2.2 GPa) and to the Lower units (LPL; 500-580°C- 2.2-2.8 GPa). The blueschist-facies LPU and LPM units are dominated by sediments (>90%), whereas the eclogitic LPL units are far richer in mafic-ultramafic rocks (>40%). These characteristics, along with lithostratigraphic differences, reflect major differences in their initial paleogeography and/or in the mechanisms responsible for material offscraping from the downgoing slab. The peak burial depths of the LPU, LPM and LPL units are similar to those inferred for slicing and underplating in both modern and fossil subduction zones. Petrological and lithostratigraphic data suggest that the offscraping of the LPU and LPM units was mostly

controlled by lithological contrasts, within pelagic shales or along contacts within the uppermost serpentinized mantle. In contrast, major dehydration reactions (such as lawsonite breakdown in sediments) likely controlled the offscraping of the LPL units at eclogite-facies conditions, possibly through high fluid pressure conditions and rocks embrittlement.

1. Introduction

Subduction zones trigger devastating earthquakes and volcanic eruptions (e.g. Ruff and Kanamori, 1980; Tatsumi, 1986; Stern, 2002). Understanding mechanical coupling and mass transfer occurring at the subduction plate boundary, and the complex interplay of short and long-term processes, is therefore critical to decipher subduction dynamics and risk assessment (Rüpke et al., 2004; Agard et al., 2018; Behr and Bürgmann, 2021). During convergence, some material is removed from the downgoing plate (the 'slab') sporadically and accreted, or 'underplated', to the upper one (Karig and Sharmann, 1975; Scholl et al., 1980; Platt, 1986). At shallow depth, offscraping at the roof of the oceanic crust results in the formation of accretionary wedges dominated by sediments (Platt, 1988). Deeper accretion also takes place along the subduction plate interface (Willner, 2005; Agard et al., 2009) and leads to the juxtaposition, and later exhumation, of deeply subducted slices with distinctive subduction histories (Plunder et al., 2012, 2015; Angiboust et al., 2013, 2014, 2016, 2018; Tewksbury-Christle et al., 2021). The removal of oceanic material from the slab, and potential accretion to the upper plate, require the down-stepping of the plate interface décollement into the slab (Kimura and Ludden, 1996; Kimura et al., 2007), hence an increase in mechanical coupling (Agard et al., 2016, 2020) and strain localization into weakness zones (Kimura and Ludden, 1996; Kimura et al., 2007; Angiboust et al., 2012c; Ruh et al., 2015). The worldwide record of blueschist- and eclogite-facies subducted oceanic fragments shows that this happens transiently (Agard et al., 2009; Monié and Agard, 2009; Bonnet et al., 2018) and at non-random depths (Plunder et al., 2015; Agard et al., 2018).

The processes leading to coupling and slicing in the slab are still debated, despite suggestions that large sediment inputs (Behr and Becker, 2018) and serpentinization of the slab (Ruh et al., 2015) or of the mantle wedge (Agard et al., 2009, 2016; Guillot et al., 2009, 2015), or fluid-mediated deformation mechanisms (Agard et al., 2020), may enhance the lubrication of the plate interface, and thereby promote decoupling (Agard et al., 2018; Garber et al., 2020b). More specifically, what are the mechanical processes driving deep slicing of the downgoing plate and the recovery of slivers at the surface? Do rock recovery clusters correspond to downdip changes of the mechanical behavior along the plate interface or to

lithological heterogeneities? How do dehydration reactions impact slab fragments, from the base of the seismogenic zone down to sub-arc depths?

Since direct access through deep drilling is limited to the few first kilometers (e.g. Tobin et al., 2019), the investigation of fossil subduction fragments with a diagnostic high pressure low temperature (HP-LT) imprint is paramount. In the Western Alps, remnants of subducted slow-spreading oceanic lithosphere (Lagabrielle and Cannat, 1990) are exposed along the 200 km-long and up to 50 km-wide Liguro-Piemont domain (L-P; or Piemonte-Liguria domain; Deville et al., 1992; Agard, 2021; Agard and Handy, 2021). This nappe-stack is one of the largest, better-preserved and most studied examples of fossil subduction complexes, spanning a range from ~30 to 80 km depth (Berger and Bousquet, 2008; Agard et al., 2002, 2018; Agard, 2021), and providing an access to subduction processes along those depths (Bebout et al., 2013; Herviou et al., 2021).

In the L-P domain, a major distinction can be made between the metamafic-ultramafic dominated (MUM units of Agard, 2021) eclogite-facies units and the metasedimentary dominated (S units of Agard, 2021) blueschist (BS)-facies units (Dal Piaz, 1974b; Caby et al., 1978; Droop et al., 1990; Pognante, 1991; Agard et al., 2001a). Within these distinct zones, several slices, generally three to four in total, were identified along different transects of the L-P domain (Fudral, 1996; Agard et al., 2001a; Tricart and Schwartz, 2006; Lagabrielle et al., 2015). However, tectonic contacts preserving the pristine, initial juxtaposition of the units sliced during subduction are often obscured by later deformation and almost impossible to follow over great distances. Consequently, very few studies (e.g. Deville et al., 1992) have attempted to correlate these tectonic slices across the entire domain, and their extension and distribution across the L-P domain remain poorly known. A detailed knowledge of this tectonometamorphic set-up is nevertheless critical to reconstruct the 2D and 3D geometries and to understand subduction-related processes along the L-P domain.

In the Liguro-Piemont domain, metamafic and ultramafic bodies are generally embedded in volumetrically dominant sediments. These sediments, more sensitive to P-T changes (Goffé and Chopin, 1986; Bousquet et al., 2008) are also cropping out continuously along the complex and across the different slices. They provide the opportunity to follow in detail the evolution of (i) the index mineralogy (Goffé et al., 2004; Bousquet et al., 2008), (ii) the variation of their stratigraphic succession (Deville et al., 1992; Lemoine, 2003), (iii) the maximum temperature experienced by these rocks during peak burial (Beyssac et al., 2002), and (iv) the peak pressure, through adequate indicators (Agard et al., 2001a, 2001b).

This study tightly and systematically combines lithostratigraphic, structural and petrologic data, both new and from the literature, across the entire L-P domain of the Western Alps, in

order to precise its tectonometamorphic set-up. A refined model of the distribution of equivalent tectonic slices along the L-P complex is proposed. We then discuss the mechanisms driving the recovery of the distinct rock types (MUM versus S units) from selective depths and the insights gained on Alpine subduction dynamics, as well as on the processes driving slab slicing and nappe stacking at depth.

2. Geological setting

2.1 Fragments of subducted oceanic lithosphere in the Western Alps

The Western Alps formed as a result of an east- to south-east-dipping and slow (~1 cm/yr) subduction of the 100 to 1000 km wide Valais and Liguro-Piemont oceans below Adria/Apulia (Le Pichon et al., 1988; Schmid et al., 1996, 2017; Lapen et al., 2003; Handy et al., 2010; Agard and Handy, 2021). Subduction of these slow-spreading oceanic domains (Lagabrielle and Cannat, 1990) started in the Late Cretaceous and was over by ~35 Ma (Stampfli et al., 1998; Schmid et al., 2017). Subduction of oceanic material was followed by a phase of continental subduction (Chopin, 1984; Rubatto and Hermann 2001; Bonnet et al., submitted) before Eurasia-Adria/Apulia collision started (Simon-Labric et al., 2009; Bellahsen et al., 2014).

Remnants of subducted Liguro-Piemont oceanic lithosphere are now exposed in the internal domain of the Western Alps and form a nappe-stack known as the Liguro-Piemont (L-P) domain (Agard, 2021; Agard and Handy, 2021; Fig. 1a) or Schistes Lustrés complex (Caron, 1977; Agard et al., 2001a, 2009), owing to their characteristic sedimentary features. Metasediments (Schistes Lustrés s.s.) are volumetrically dominant in this complex and range from the Late Jurassic (De Wever and Caby, 1981; Lagabrielle, 1987) to the Late Cretaceous (Lemoine et al., 1984; Lagabrielle, 1987). They correspond to an initial ~200-400 m thick sequence of pelagic and hemipelagic seafloor deposits (marls, shales and limestones metamorphosed as calcschists, metapelites and marbles; Lemoine et al., 1984; Lemoine and Tricart, 1986; Lemoine, 2003; Deville et al., 1992; Michard et al., 1996) embedding variable amounts of mafic and ultramafic rocks (Fig. 1a). The serpentinized mantle generally contains sparse pockets of Jurassic mafic material (e.g. Decrausaz et al., 2021) highlighting the discontinuous character of the oceanic crust (Lagabrielle, 1987; see Agard, 2021 and references therein). Exposed fragments of L-P lithosphere often preserve pre-alpine oceanic structures (Lagabrielle et al., 2015, Balestro et al., 2018, 2019; Decrausaz et al., 2021).

During subduction, these rocks were buried between ~30 and 80 km depth (Agard et al., 2002, 2009) and were intensely folded, leading to significant thickening of the initial sedimentary pile (Agard et al., 2002; Tricart and Schwartz, 2006). Agard et al. (2009) roughly

estimated that approximatively 30% to 50% of the sedimentary deposits were scraped off from the downgoing plate and exhumed, whereas only ~5% of the oceanic crust and serpentinized mantle were.

After a peak burial between 60 and ~40 Ma (e.g. Agard et al., 2002; Rubatto and Hermann, 2003), these rocks were detached as slices from the subducting plate and were exhumed from the Late Eocene to the Miocene (Agard et al., 2002, 2009; Schwartz et al., 2007, 2020; Malusà et al., 2005; Angiboust and Glodny, 2020). This complex stack of slices formed a deep accretionary complex, probably built by progressive underplating (Platt, 1986; Marthaler and Stampfli, 1989; Agard et al., 2009, 2018; Agard, 2021), where structurally upper slices may have been underplated earlier (Kimura et al., 2007; Dumitru et al., 2010; Plunder et al., 2012; Agard and Vitale-Brovarone, 2013; Angiboust et al., 2016).

Rocks from the Western Alps L-P domain, metamorphosed under BS- to eclogite-facies conditions, exhibit an almost continuous increase of metamorphic grade from west (~1.2 GPa-330°C) to east (~2.5 GPa-550°C), along a ~8°C metamorphic gradient characteristic of subduction zones (Agard et al., 2001a; Gabalda, 2009; Plunder et al., 2012; Schwartz et al., 2013; Agard, 2021). This gradient is recognizable by the evolution of metamorphic mineral assemblages and notably by the subtle evolution of index minerals in metasediments (Goffé and Chopin, 1986; Agard et al., 2001a; Goffé et al., 2004; Bousquet et al., 2008; Fig. 1b). For example, in the western part of the Schistes Lustrés complex, and especially south of Ambin massif, Fe-Mg carpholite is frequently present in pelitic layers (Fig. 1b; Goffé et Chopin, 1986; Agard et al., 2001a). Further east, Fe-Mg capholite gradually disappears at the expense of chloritoid (Fig. 1b; Goffé et Chopin, 1986; Agard et al., 2001a). In both areas lawsonite can be observed in the metasedimentary matrix as well as in metamorphic veins (Caron, 1974; Bocquet, 1974; Saliot et al., 1978; Lefeuvre et al., 2020; Herviou et al., 2021). Finally, the easternmost part of the L-P domain is characterized by the occurrence of garnet, generally coexisting with chloritoid (Agard et al., 2001a; Plunder et al., 2012; Ghignone et al., 2021a). In these metasediments, Fe-Mg carpholite is characteristic of low-temperature BS-facies while chloritoid generally appears in high-temperature BS-facies (Goffé et Chopin, 1986; Goffé et al., 2004). Lawsonite is present over a wide range of P-T conditions in these BS-facies rocks (Herviou et al., 2021), whereas the presence of garnet is indicative of eclogite-facies metamorphism (Agard et al., 2001a; Plunder et al., 2012; Vitale-Brovarone et al., 2014) except for rare spessartine and grossular-rich garnet in marbles (Ballèvre and Lagabrielle, 1994; Manzotti et al., 2021).

Besides this metamorphic gradient, several units/slices were identified in the L-P domain of the Western Alps based on lithostratigraphic and tectonometamorphic contrasts (Lagabrielle,

1987; Fudral, 1996; Agard, 2021). In particular, the metamafic-ultramafic dominated eclogite-facies units crop out eastward of and tectonically below the BS-facies metasedimentary-dominated units (Fig. 2c; Dal Piaz, 1974b; Caby et al., 1978; Droop et al., 1990; Pognante, 1991; respectively MUM and S units of Agard, 2021 and Agard and Handy, 2021). These zones are separated by a major extensional tectonic contact (Philippot, 1990; Ballèvre et al., 1990; Ballèvre and Merle, 1993). Inside these different zones, distinct slices, generally 3 to 4 were described in different transects of the L-P domain (Lagabrielle, 1987; Fudral, 1996; Agard, 2021) and are described in the next section.

3. Subduction slices across the Western Alps Liguro-Piemont domain

3.1 Valais-Aosta transect

In this northern zone, the identification of a major sharp divide was first made in the Zermatt-Saas area by Bearth (1959, 1962, 1967). Kienast (1973), Dal Piaz (1974a, 1974b) and Caby et al. (1976, 1978) later described a similar divide in the Aosta Valley. These authors identified a zone of "Lower Schistes Lustrés" rich in mafic and ultramafic rocks metamorphosed in eclogite-facies that they distinguish from a zone of "Upper Schistes Lustrés" only metamorphosed in blueschist- and greenschist-facies and almost devoid of ophiolites. The eclogite-facies slices or Zermatt-Saas zone are cropping out eastward of the Dent Blanche klippe and are tectonically overlain by the blueschist slices named Combin zone (or Tsaté Nappe). These zones are separated by a Late Cretaceous-Early Tertiary extensional fault, the Combin fault (Ballèvre et Merle, 1993, Fig. 1a-c).

Different tectonic slices were identified in the Zermatt-Saas zone: the Zermatt-Saas and Avic slices found on both sides of the Aosta fault (ZS and AV in Fig. 1c; Dal Piaz et al., 2010; Polino et al., 2015). Thermodynamic modelling, multi-equilibrium thermobarometry and Raman Spectroscopy on Carbonaceous Material (RSCM) allowed to estimate peak P-T conditions around 550 ± 50°C and 2.5 ± 0.5 GPa for the Zermatt-Saas unit (Bucher et al., 2005; Bucher and Grapes, 2009; Angiboust et al., 2009; Angiboust and Agard 2010; Negro et al., 2013; Zanoni et al., 2016) and around 550 ± 50°C and 2.1-2.3 GPa for the Avic unit (Martin et al., 2008; Angiboust et al., 2009; Angiboust and Agard 2010; Dragovic et al., 2020). While the homogeneity of the P-T conditions recorded in these two units may hint to largely coherent slices (Angiboust et al., 2009), these two units show at smaller scale a series of tectonic slices separated by serpentinite layers (Angiboust and Agard, 2010). Near Lago di Cignana, a small 2 km^2 ZS slice contains diamond- and coesite-bearing metasediments indicative of ultra-high pressure (UHP) conditions of 2.8-3.2 GPa and 600°C (Reinecke, 1991, 1998; Compagnoni and Rolfo, 2003; Groppo et al., 2009; Frezzotti et al.,

2011). Finally, south of the Avic unit, an eclogite-facies slice is cropping out around the Gran Paradiso massif, the Grivola-Urtier unit (GU in Fig. 1c; Bocchio et al., 2000; Dal Piaz et al., 2010; Polino et al., 2015). P-T conditions of 550°C, 2.3-2.5 GPa are estimated for this slice mostly made of calcschists enveloping mafic blocks (Bousquet, 2008; see also Reynard and Ballèvre, 1988).

Based on multiple methods, most peak burial ages range between 40 and 50 Ma for the Zermatt-Saas unit (Bowtell et al., 1994; De Meyer et al., 2014; Skora et al., 2015; Weber et al., 2015; Rebay et al., 2018), between 42-46 Ma for the Avic unit (Dal Piaz et al., 2001; Dragovic et al., 2020) and between 40 and 49 Ma for the Lago di Cignana slice (Rubatto et al., 1998; Amato et al., 1999; Lapen et al., 2003; Gouzu et al., 2006, 2016; Skora et al., 2015). For the Grivola-Urtier unit, peak burial ages were constrained between 42 and 48 Ma by Rb-Sr and Ar-Ar on white mica in both metasediments and metamafics (Dal Piaz et al., 2001; Villa et al., 2014) and between 55 and 60 Ma by Lu-Hf on bulk garnet-omphacite or garnet-glaucophane assemblages (Villa et al., 2014). D1 syn-peak deformation stage is dated at 48 Ma while D2 syn-BS facies exhumation is dated at 40 Ma (Villa et al., 2014). K-Ar data on white-micas from two localities of the Grivola-Urtier unit gave 54-39 Ma ages (Delaloye and Desmons, 1976).

In the BS-facies Combin zone, below the Dent Blanche klippe, the presence of a synformal stack of slices was inferred from the distribution of RSCM temperatures (Negro et al., 2013; Angiboust et al., 2014; Manzotti et al., 2021), possibly two or three slices (Angiboust et al., 2014). Recently, Manzotti et al. (2021), based on petrological data and field observations, suggested the presence of two slices, the Cornet unit separated from the underlying By unit by a major tectonic discontinuity (respectively CO and BY in Fig. 1c). Based on this distinction, peak temperatures range between 364 and 422°C in the Cornet unit and between 421 and 530°C in the By unit (Negro et al., 2013; Angiboust et al., 2014; Decrausaz et al., 2021; Manzotti et al., 2021). The large By unit may comprise several slices (Broilliot and Aouilletta slices; Ellero and Loprieno, 2018; Polino et al., 2015), but their extension is unknown. Peak pressures are estimated at 1.6-1.7 GPa for the By unit and 0.8-0.9 GPa for the Cornet unit (Manzotti et al., 2021). The D2 to D3 exhumation-related episodes of these units were dated between 41 and 37 Ma (Reddy et al., 2003; Angiboust et al., 2014). Potentially independent tectonic slices, rooted in the Briançonnais area and belonging to the complex Valsavarenche mega-fold (Bucher et al., 2003), crop out around the Valgrisenche, Val de Rhêmes and Valsavarenche valleys. These slices, grouped in the Avise-Tsaboc-Feluma unit (ATF in Fig. 1c), seem to have recorded BS-facies conditions (Debelmas et al., 1991; Caby, 1996; Polino et al., 2015). In the Avise area, D1 deformation was dated a 45.4 Ma and followed by a 39.5 Ma D2 deformation. Finally, a slice may be present in the eastern

side of Grand Paradiso between the Grivola-Urtier slice and the Sesia complex, featured as a thin tongue of BS-facies L-P rocks in literature maps and cross-sections (Ballèvre et al., 1986; Dal Piaz et al., 2001; West-Sesia, i.e. W-SS in Fig. 1c).

3.2 Savoy-Susa transect

A similar contrast between the BS-facies “Upper Schistes Lustrés” and eclogite-facies “Lower Schistes Lustrés” was observed in the Savoy area by Bocquet (1974), Caby et al. (1976), Chopin (1979) and Robert (1979), and in the Susa Valley by Pognante (1980, 1984). Chopin (1979) first distinguished two sets of slices within the BS-facies zone, with the “Upper Unit” characterized by low-grade BS-facies metamorphism atop the “Intermediate Unit” composed by a thick series of calcschist metamorphosed in BS-facies. Based on lithostratigraphic and structural arguments, Deville (1987), Fudral et al., (1987) and Fudral (1996) refined Chopin's (1979) distinction by also suggesting the presence of three units in the Savoy region and by mapping their distribution. These units are the eclogite-facies “Lower Oceanic Unit”, the BS-facies “Middle Oceanic Unit” and the “Upper Oceanic Unit” also metamorphosed in BS-facies.

The “Upper Oceanic Unit” (Savoy Upper Unit) crops out as rare klippen scattered across the region (Lamet, Jovet, Sana, Grand Vallon; respectively LA, JO, SN-U and GV in Fig. 1c, see also 2a). Their limited extent across the area precludes assessing whether they are independent slices or instead correspond to a single one. Nevertheless, the Grand Vallon klippe (Fig. 1c) contains a stratigraphic succession distinct from the other “Upper Oceanic Unit” klippen (Deville, 1986, 1987; Fudral, 1996). Its detrital-rich sediments were dated as Late Maastrichtian by the presence of foraminifera, as for the unmetamorphosed Helminthoid Flysch (Deville, 1986). Such deposits are rarely encountered in the Schistes Lustrés, suggesting that this klippe constitutes an independent slice (Deville, 1986; Deville et al., 1992; Fudral, 1996). The “Upper Oceanic Unit” is characterized by a low-grade BS-facies, marked by the presence of Fe-Mg carpholite or lawsonite and absence of chloritoid (Fig. 1b). Peak burial temperatures range between 376 and 404°C in the Savoy region (Gabalda et al., 2009; Plunder et al., 2012). No pressure or age constraints are available for these tectonic slices.

The “Middle Oceanic Unit” (Savoy Middle Unit, i.e. SMU in Fig. 1c) predominates in this region and seems to be made of several slices with uncertain boundaries (Fudral, 1996). These slices mostly crop out across the Haute-Maurienne valley and have also been identified in the Grande Sassière and Chardonney klippen and at the base of the Sana klippe (Deville, 1987, Fudral, 1996; respectively GS, CH and SN-L in Fig. 1c). Near Susa, a distinct Venaus slice was recognized (Polino et al., 2002; Cadoppi et al., 2002; VN in Fig. 1c) within

the previously defined Savoy slices (Fudral, 1996). The “Middle Oceanic Unit” is mostly made of massive calcschist slices and characterized by the presence of chloritoid, lawsonite and relics of Fe-Mg carpholite (Fig. 1b). Peak P-T are 384-503°C and 1.6-1.9 GPa (Rolland et al., 2000; Gabalda et al., 2009; Plunder et al., 2012). Recent in situ Ar-Ar white-mica dating of the “Middle Oceanic Unit” around Susa gave ages for an early foliation S1 between 49 and 40 Ma, while retrograde fabrics (S2 and mylonitic foliation) range between 40 and 37 Ma (Ghignone et al., 2021b). Previous Ar-Ar dating on white mica for this unit gave 42-37 Ma ages (Chopin and Maluski, 1980).

The eclogite-facies “Lower Oceanic Unit” (Savoy Lower Unit, i.e. SLU in Fig. 1c) crops out in the eastern part of the Haute-Maurienne area, immediately above the Gran Paradiso massif (Fig. 2a; Chopin, 1979) and in the Susa, Viu and Ala Valleys (Fig. 1c). At least two slices named Ciamarella-Gran Uia and Averole where recognized in this unit (Fudral, 1996), but their exact distribution remains uncertain. A large slice of eclogitized mantle is also present in the eastern part of this transect, the Lanzo massif (Lagabrielle et al., 1990; Debret et al., 2013; Fig. 1a, b, c). Its ultramafic lithology contrasts with those of the “Lower Oceanic Unit”, and whether it represents oceanic or sub-continental mantle is disputed (Bodinier et al., 1991; Müntener et al., 2005; Pelletier and Müntener, 2006; Piccardo et al., 2007). The “Lower Oceanic Unit” is characterized by the appearance of garnet coexisting with chloritoid, suggesting the existence of a pressure gap with the “Middle Oceanic Unit” (Plunder et al., 2012; Vitale-Brovarone et al., 2014). Estimated peak P-T are 460-570°C and 2.2-2.9 GPa (Rolland et al., 2000; Gabalda et al., 2009; Plunder et al., 2012; Ghignone et al., 2021a). Recent in-situ Ar-Ar dating on an early S1 foliation gave 47-42 Ma ages, while retrograde fabrics (S2 and mylonitic foliation) range between 40 and 36 Ma (Ghignone et al., 2021b). Previous Ar-Ar on white micas data for the HP stages of this unit yielded a wide range between 68 and 39 Ma (Chopin and Maluski, 1980).

3.3 Cottian Alps transect

In this transect, the different L-P units are particularly well-exposed across a long ridge between Susa and the Chisone valley, which constitutes a reference cross-section (Caron, 1977; Agard et al., 2001a, 2001b, 2009; Agard, 2021; Fig. 2b). A strong eastward metamorphic gradient was identified by the progressive increase of the tschermak substitution in white-mica (which serves as proxy for pressure; Velde, 1967; Massonne and Schreyer, 1987) and by the evolution of index minerals in sediments (Agard et al., 2001a, 2001b; Fig. 1b). These trends are also reflected in the eastward increase of RSCM temperatures (Beyssac et al., 2002). In this region, as well, a zone of BS-facies metasedimentary-dominant slices stands out from an eclogite-facies zone containing more

metamafics and ultramafic rocks (Agard, 1999; Agard et al., 2001a; Fig.1a, c). These zones are separated by a major tectonic contact, well exposed at the Finestre Pass (Fig. 2b; Ballèvre et al., 1990; Agard et al., 2001a).

Several tectonic slices were described in the BS-facies zone. Structurally on top, the Lago Nero unit (Polino et al., 2002; Barféty et al., 2006; LN in Fig. 1c, see also 2b) shows Fe-Mg carpholite-bearing metasediments and the appearance of chloritoid in the eastern outcrops (Agard et al., 2001a, 2001b). These rocks also contain massive amounts of lawsonite (Lefeuvre et al., 2020). Peak P-T range from 300-350°C- 1.2-1.3 GPa at west to ~380°C- 1.8 GPa at east (Agard, 1999; Agard et al., 2001a, 2001b; Beyssac et al., 2002; Gabalda et al., 2009). The Lago Nero unit was considered as analogous to the “Oceanic Upper Unit” of the Savoy transect (Plunder et al., 2012; Agard, 2021). Below this slice, five BS-facies tectonic slices were identified: (i) the Cerogne-Ciantiplagna unit (Polino et al., 2002; Cadoppi et al., 2002; CC in Fig. 1c, see also 2b); (ii) the Albergian unit, separated from the Cerogne-Ciantiplagna unit by a major tectonic contact nicely exposed in the Chisone valley (Polino et al., 2002; ALB in Fig. 1c); (iii) the Puys unit, considered as an equivalent of the Venaus slice from the Savoy-Susa transect (Polino et al., 2002; Barféty et al., 2006; PY in Fig. 1c); (iv) the Aigle unit (Polino et al., 2002; Barféty et al., 2006; AG in Fig. 1c) and (v) the small Vin Vert unit (Polino et al., 2002; Barféty et al., 2006; VV in Fig. 1c) immediately above the Ambin massif. The Cerogne-Ciantiplagna and Albergian units are characterized by the presence of chloritoid (Fig. 1b) and peak P-T conditions of 423-463°C- ~1.9 GPa (Agard et al., 2001a, 2001b, Beyssac et al., 2002). These slices were inferred to be equivalent to the “Middle Oceanic Unit” of the Savoy-Susa transect (Plunder et al., 2012; Agard, 2021). The Puys, Aigle and Vin Vert slices are essentially lacking P-T constraints, although a RSCM temperature of 386°C was estimated in the Aigle unit (Gabalda et al., 2009). In metasediments from the Lago Nero and Albergian units, several deformation stages were identified and dated (Agard et al., 2001a, 2002; see also Ghignone et al., 2021a). D1 deformation relates to the development of early fabrics, km-scale folds and crystallization of peak metamorphic assemblages at 61-55 Ma for the Lago Nero unit and 64-49 Ma for the Albergian unit. A second phase (D2), dated at 51-43 Ma for the Lago Nero, corresponds to the ductile east-vergent deformation accompanying early exhumation under BS-facies conditions. The third fabric (D3), between ~38 and 36 Ma for the Lago Nero unit, is marked by top-to-the-west ductile to brittle deformation associated with greenschist-facies exhumation. Two K-Ar ages on white mica from the Lago Nero unit gave 67-62 Ma ages (Delaloye and Desmons, 1976).

In the eclogite-facies zone, the presence of different slices is unclear. In the Orsiera-Rocciavrè unit (OR in Fig. 1c, Cadoppi et al., 2002), the Rocciavrè massif is a large eclogitic

gabbroic and ultramafic body containing negligible amounts of metasediments (Pognante, 1985). In contrast, to the west, from Monte Orsiera to Finestre pass, mafic and ultramafic rocks are embedded in metasediments that seem to be volumetrically equivalent to the ophiolitic bodies (Fig. 1c). The existence of a tectonic contact between these two parts of the unit was suggested by Cadoppi et al. (2002). Metasediments contain garnet and chloritoid (Fig. 1b) and their estimated P-T conditions are 500-542°C and ~2-2.1 GPa (Agard, 1999; Agard et al., 2001a, 2001b, Beyssac et al., 2002; Gabalda et al., 2009). No recent P-T estimates are available for the mafic rocks. The Orsiera-Rocciavrè unit is interpreted as the southern extension of the "Lower Oceanic Unit" of the Savoy-Susa transect (Plunder et al., 2012). In metasediments from the Orsiera-Rocciavrè unit, the same D1 to D3 events of BS-facies slices were described (Agard et al., 2001b). An early-HP stage, close to D1 deformation is dated at 61-53 Ma by in situ Ar-Ar in white mica, whereas D2 is dated at 46-42 Ma and D3 at 42-38 Ma (Agard et al., 2002). In Rocciavrè metagabbros, Rb-Sr on phengite with high Si content gave a 46 Ma age (Angiboust and Glodny, 2020).

3.4 Queyras-Monviso and Ubaye transects

Along these southernmost transects, the BS-facies slices are separated from eclogite-facies units by a major extensional contact (Philippot, 1990; Ballèvre et al., 1990; Fig. 2c).

Three BS-facies slices were identified in the Queyras region around the Guil valley, from west to east (Lagabrielle, 1987; Lagabrielle et Polino, 1988; Lagabrielle et al., 2015): (i) the Calcschist unit (CS in Fig. 1c, see also 2c), almost devoid of ophiolitic material, is characterized by Fe-Mg carpholite and lawsonite occurrences (Herviou et al., 2021; Fig. 1b, c); (ii) the Pelvas-Taillante unit (PT in Fig. 1c, see also 2c) also contains Fe-Mg carpholite and lawsonite occurrences, and chloritoid appears in the eastern part (Fig. 1b); (iii) the Mirabouc-Bouchet unit (MB in Fig. 1c, see also 2c), which is characterized by the presence of lawsonite and chloritoid (Fig. 1b). Estimated P-T conditions are 320-340°C- ~1 GPa for the Calcschist unit, 338-373°C- ~1.2 GPa for the Pelvas-Taillante Unit and 383-469°C- ~1.3 GPa for the Mirabouc-Bouchet unit (Schwartz, 2000; Tricart and Schwartz, 2006; Schwartz et al., 2013).

The eclogite-facies zone of this transect corresponds to the Monviso massif, a large mafic-ultramafic body (Lombardo et al., 1978) comprising at least two tectonic slices (Schwartz et al., 2000a; Angiboust et al., 2012b; Locatelli et al., 2018, 2019a). The Monviso Unit (MV in Fig.1c, see also 2c), to the west, recorded 476-498°C- ~2.2 GPa P-T conditions (Angiboust et al., 2012b; Schwartz et al., 2013) and the Lago Superiore unit to the east (LS in Fig. 1c, see also 2c) recorded 514-580°C- 2.5-2.8 GPa (Groppo and Castelli, 2010; Angiboust et al.,

2012b, Schwartz et al., 2013; Locatelli et al., 2018). Metasediments from these two slices are characterized by garnet-chloritoid-bearing assemblages (Fig. 1b).

The Lago Superiore unit peak-burial conditions were dated between 50 and 45 Ma by multiple methods (Duchène et al., 1997; Rubatto and Hermann, 2003; Rubatto and Angiboust, 2015; Garber et al. 2020a). The D2 and D3 exhumation-related deformation episodes were dated at 38-37 Ma and 35 Ma in the Lago Superiore and Monviso slices (Angiboust and Glodny, 2020; Rb-Sr on phengite). For the BS-facies slices, a 42-40 Ma Ar-Ar age on white mica, supposedly close to peak P-T conditions, was obtained for the Calcschist unit (Lanari, 2012). In the Pelvas-Taillante unit, two ages between 43 and 41 Ma were obtained by bulk K-Ar on white mica (Delaloye and Desmons, 1976). Finally, Ar-Ar dating on white mica on a sample from the Mirabouc-Bouchet unit gave 68-58 Ma for an early S1 fabric (prograde to peak?), 45 Ma for a second fabric (S2) and a <30 Ma age for a S3 foliation (Lanari, 2012). D3 deformation in the same slice was dated at ~35 Ma by Rb-Sr on phengite (Angiboust and Glodny, 2020). All these BS- and eclogite-facies units were stacked and exhumed from late Eocene to Miocene times (Angiboust and Glodny, 2020; Schwartz et al., 2007, 2020). Along the Ubaye transect, an eastward metamorphic increase was identified from the Briançonnais units to the Liguro-Piemont domain (Michard et al., 2004), with no distinction of L-P slices. We will consider that the Queyras-Monviso slices extend across this valley (Fig. 1c).

4. Compilation of lithostratigraphic data and size of the recovered slices

4.1 Stratigraphic columns of the different slices

In order to identify similarities between the tectonic slices of the different transects and gain information on the paleogeography of the L-P slices (Fig. 3a), we compiled lithostratigraphic columns across the Western Alps L-P domain (Fig. 3b).

In the Western Alps, the Chabrière series (stratigraphic column 1, Fig. 1a, 3b; Lemoine et al., 1970; Tricart, 1974) is considered as the characteristic and idealized sequence of L-P deposits. This stratigraphic column allowed to differentiate the L-P series deposited on an oceanic basement from the Gondran-type series (Lemoine, 1959, 1971), which are made of sediments deposited on the Piemont/Pre-Piemont continental margins (Fig. 1a-c; Lemoine, 1971; Elter, 1971; Bourbon et al., 1979; Lemoine et al., 1986). The Chabrière-type series starts with radiolarian cherts or shales deposited on an oceanic basement. This formation, dated between the Oxfordian and the Kimmeridgian (De wever and Caby, 1981; De Wever et al., 1987a, 1987b; Lagabrielle, 1987) corresponds to the first argillite-dominated episode of

the series (A2; Fig. 3b; Lemoine, 2003), characterizing sediments deposited below the CCD. These A2 deposits are often composed by manganese-rich quartzite layers instead of cherts (Chopin, 1978, 1979). Overlying the cherts, there is a level of whitish to bluish marbles attributed to the Late Jurassic (Tithonian and up to Berriasian?) by analogy with the "Calpionelles Limestones" of the Ligurian Appenines (Decandia and Elter, 1969, 1972; Lagabrielle, 1987). This formation corresponds to the first calcareous-dominated episode of the series (C3; Fig. 3b; Lemoine, 2003), with deposition above the CCD. The above, younger formation, made of shales with intercalations of calcareous beds with a characteristic reddish patina, is named "Replatte formation" (Lemoine et al., 1970). This formation is attributed to the Lower Cretaceous by analogy with the "Palombini shales" of the Ligurian Appenines (Lemoine et al., 1970, Lemoine and Tricart, 1986; Lagabrielle, 1987). Just above, there is a characteristic formation of black shales, often called the "Roche Noire formation" (Fig. 3b; Tricart, 1974), assigned to the Mid-Cretaceous (Aptian-Albian?) given their similarity with the "Val Lavagna Schists" of Ligurian Appenines (Decandia and Elter, 1972; Tricart, 1974; Lagabrielle, 1987). These two Lower Cretaceous formations correspond to the second argillite-dominated episode of the series (A3; Fig. 3b; Lemoine, 2003). For the sake of clarity, we herein use A3a for the "Replatte formation" and A3b for the "Roche Noire formation" (Fig. 3b). Finally, these series end by a thick and fairly homogeneous formation of massive calcschists dated as Late Cretaceous (Cenomanian-Turonian) by the presence of planktonic foraminifera in various localities (Marthaler, 1984; Lemoine et al., 1984; Lagabrielle, 1987; Deville, 1987). In scarce places the L-P series ends with a formation of Maastrichtian calcareous flyschs considered as lateral equivalents of the unsubducted Helminthoid Flysch (Deville, 1986; Deville et al., 1992). These Late Cretaceous formations correspond to the last calcareous-dominated deposit of the series (C4; Fig. 3b; Lemoine, 2003; C4a is used below for the Cenomanian-Turonian calcschists and C4b for the Maastrichtian flyschs). Some of these C4 flyschs may correspond to trench-filling deposits (Marthaler, 1984). The different formations of the Chabrière-type series generally contain detritic and breccia horizons made of continental and/or oceanic material (e.g., Deville et al., 1992) not considered here.

The Chabrière series therefore consists of pelagic/hemipelagic and rarer clastic deposits overlying mafic and ultramafic rocks. Changes of the stratigraphic record and/or tectonic repetition of this succession may help reveal the distinct paleogeography and/or preferential zones of detachment inside the sequences (Kimura et al., 1996).

In the Western Alps L-P domain, stratigraphic columns equivalent to the Chabrière series were described in several of the blueschist-facies slices.

In the Queyras-Ubaye region, the complete Chabrière series was observed in the Pelvas-Taillante slice (Fig. 1a, 3b, stratigraphic columns 1,2; Lemoine et al., 1970; Tricart, 1974; Lemoine and Tricart, 1986; Lagabrielle, 1987). In the Calcschist unit, the deposits are mainly made of a thick C4a calcschist formation overlying a thin A3b formation (Fig. 3b, stratigraphic column 3; Lagabrielle, 1987; Deville et al., 1992). The lack of Jurassic deposits and ophiolites led the authors to suggest that the Calcschist unit sediments may have been deposited on continental margin rather than oceanic basement (Lagabrielle, 1987; Deville et al., 1992). The lithostratigraphic column of the Mirabouc-Bouchet (Fig. 1a, 3b, stratigraphic column 4; Lagabrielle, 1987) is close to the complete Chabrière series but differs by the absence of A2 cherts and the presence of a thick C4a calcschist formation.

In the Cottian Alps region, a series close to the Chabrière one was described in the Lac des Cordes (Fig. 1a, 3b, stratigraphic column 5; Dumont et al., 1984; Lemoine and Tricart, 1986). This series is nevertheless lacking the Middle Jurassic cherts and contains a A3a calcschist formation instead of the Replatte formation. In general, Chabrière-type series were identified in the Lago Nero (Fig. 1a, 3b, stratigraphic columns 6 and 7; Caron, 1977; Polino and Lemoine, 1984; Lemoine and Tricart, 1986) and Aigle slices (Fig. 1a, 3b, stratigraphic column 9; Barféty et al., 2006). C4a is characterized by a calcareous flysch rather than calcschists in the Lago Nero locality (Fig. 3b, stratigraphic column 6; Polino and Lemoine, 1984). Deposits in the Puys slice consist of undifferentiated Cretaceous calcschists probably corresponding to C4a (Fig. 1a, 3b; stratigraphic column 8; Barféty et al., 2006), whereas the Vin Vert slice contains massive C4a calcschists and C3 marbles (Fig. 1a, 3b; stratigraphic column 10; Barféty et al., 2006). Very few sedimentary descriptions are available for the Cerogne-Ciantiplagna and Albergian slices. The Cerogne-Ciantiplagna sediments nevertheless mostly comprise massive calcschists with very few pelitic alternations (Fig. 2b), as for C4a calcschists. For the Albergian slice, where ophiolites are present in greater amounts (Fig. 1a), the sedimentary sequence rather corresponds to a Chabrière-like series analogous to that of the Mirabouc-Bouchet unit (Caron, 1977; Fig. 1a, 3b, stratigraphic column 4).

Around the Savoy region, different series where identified in the Savoy Upper Unit klippen. In most of them, such as for the Lamet klippe (Fig. 1a, 3b, stratigraphic column 11; Fudral, 1996), the metasediments correspond to C4a calcschists whereas the Grand Vallon klippe is composed by the Maastrichtian C4b flysch (Fig. 1a, 3b, stratigraphic column 13; Deville, 1986, 1987; Deville et al., 1992). However, the Savoy Middle Unit stratigraphic column seems to correspond to an incomplete Chabrière-type series (Fig. 1a, 3b, stratigraphic column 12; Fudral, 1996; Deville et al., 1992): these C4 calcschists overly deposits markedly from the A3 sediments, and this series may therefore lack Lower Cretaceous sediments.

Finally, around the Valais region, the Combin sediments resemble a Chabrière-like series with C4 composed by a calcareous flysch (Fig. 1a, 3b, stratigraphic column 14; Marthaler, 1984; Sartori, 1987; Kunz, 1988; Marthaler and Stampfli, 1989; Stampfli and Marthaler, 1990; Deville et al., 1992).

In the eclogite-facies slices, stratigraphic columns are always lacking Upper Cretaceous formations (Fig. 1a, 3b, stratigraphic columns 15-18; Lagabrielle, 1987; Sartori, 1987; Stampfli and Marthaler, 1990; Deville et al., 1992; Balestro et al., 2019; Tartarotti et al., 2021). These sedimentary series are generally exposing A2 cherts and C3 marbles, overlain by Lower Cretaceous A3a Replatte-like deposits or calcschists. In these slices, the thickness variation of the sedimentary-series is interpreted as reflecting deposition on a rugged seafloor (De Togni et al., 2021).

4.2 Sediment/ophiolitic ratios and surface extension of the slices

The ratio of sedimentary versus ophiolitic material (mafic and ultramafic rocks) cropping out in each L-P slice was calculated using imagej©. This software was also used to compute the approximate aerial exposure of each L-P slice using the geological outlines of the 1:250000 BRGM maps (Gap; Annecy and Thonons-les-Bains). For the different contours we used 1:50000 ISPRA maps (Aosta; Bardonecchia; Chatillon, Monte Cervino and Susa), 1:50000 BRGM maps (Lanslebourg-Mont d'Ambin; Névache-Bardonecchia-Modane; Tignes) and some articles/PhD. theses (Lagabrielle, 1987; Fudral, 1996; Lagabrielle et al., 2015; Manzotti et al., 2021). The Chenaillet and Lanzo massifs (Fig. 1a-c) were not considered in the calculations.

The results highlight the predominance of sediments in the Western Alps L-P domain (71%; Table 1). Almost all BS-facies slices surfaces have more than 90% (Table 1) of sediments except for the Combin domain (By + Cornet slices) where numerous volcano-sedimentary horizons (prasinites) are mapped, but where sediments still prevail (76%; Table 1). The whole BS-facies zone surface only contains 9% of mafic and ultramafic rocks (Table 1). The eclogite-facies slices surfaces drastically differ from the BS-facies slices (Table 1). Indeed, four out of the six studied areas contain less than 40% of sediments, whereas the two remaining areas contain around 60% of sediments (Table 1). The whole eclogite-facies zone displays 62% of mafic and ultramafic rocks at the surface. Finally, in the two slices for which few metamorphic informations are available (Avise-Tsaboc-Feluma and West-Sesia; Fig. 1c) sediments predominate (more than 90%; Table 1).

The outcropping surface of the L-P slices ranges from a few km^2 in the Savoy Upper Unit klippen (less than 1 km^2 for the Lamet klippe; Table 1) to several hundred of km^2 (Table 1). In the blueschist-facies zone, most of the slices (14 over 19) represent less than 100 km^2,

whereas the Lago Nero and Calcschist units are respectively around 130 and 160 km^2 (Table 1). The three remaining zones correspond to greater surfaces but the poor knowledge of the boundaries between the slices imposed some grouping (By+Cornet, Savoy Middle Unit, Albergian+Mirabouc Bouchet; Table 1). In the eclogite-facies zone, most of the slices are larger than 100 km^2 (5 over 6; Table 1), which may suggest the presence of several slices in these areas.

5. Evolution of temperature and pressure in the Western Alps Liguro-Piemont slices

5.1 Raman Spectroscopy of Carbonaceous Material temperatures

Methodology

The abundance of carbonaceous material in the almost continuously exposed L-P metasediments allows quantifying the maximum temperature (T_{max}) experienced by these metasediments during peak burial, using the Raman Spectra of Carbonaceous Material technique (RSCM; Beyssac et al., 2002, 2003). Despite previous studies across the L-P domain of the Western Alps, large gaps remain across the studied transects (Beyssac et al., 2002; Gabalda et al., 2009; Angiboust et al., 2009, 2012b, 2014; Angiboust and Agard, 2010; Plunder et al., 2012; Negro et al., 2013; Decrausaz et al., 2021; Manzotti et al., 2021; see Fig. 4a). Complementary sampling (108 new samples added to the existing 289 ones) was therefore conducted to constrain the maximum temperature of the entire domain (as for the Central Alps; Wiederkehr et al., 2011), as well as to characterize the thermal imprint of individual tectonic slices (Fig. 4a). Note that two samples, one from this study and another form Schwartz et al. (2013), belong to the west-Chenaillet Gondran sediments, which may rather correspond to Piemont margin deposits (Fig. 4a; Lemoine, 1971).

Raman spectra of carbonaceous material, were obtained using a Renishaw inVia Spectrometer at ENS Paris. The excitation light was provided by a laser (Cobolt Fandango) at 514.5 nm and at a power of 50 mW, focused on the sample using a x100 objective (Leica). Thirteen to seventeen spectra per sample were acquired in the 1000-2000 cm^{-1} range; acquisition time was 30-90 seconds with 10% of laser power following the spectral acquisition parameters of Beyssac et al. (2002). Peak position, baseline correction and band width were determined using Peakfit© software and Matlab© codes. Temperatures were determined using Beyssac et al. (2002) method for most of the samples (105 samples) and using Lahfid et al. (2010) method for the very rare low-temperature samples (<330°C; 3 samples). The RSCM data from the literature and this study were then interpolated using the

inverse distance weighted interpolation method of QGis© software (Fig. 4b, c). Temperature estimates, mineralogy and GPS coordinates of the samples can be found in Sup. mat. 1.

Results

RSCM temperatures and their interpolation illustrate the eastward increase of metamorphic grade across the Western Alps L-P domain (Fig. 4a-c). This is particularly conspicuous south of the Gran Paradiso massif, where western samples recorded 300-350°C peak temperatures while eastward samples are generally greater than 500°C (Fig. 4a-c). The distribution of the L-P tectonic contacts allows studying the specific maximum temperature of each slice (Fig. 4c). It reveals the presence of both intra-slice metamorphic gradients, where temperature overlaps rather smoothly across the slices, and temperature gaps matching tectonic contacts (Fig. 4c). For example, some BS-facies slices (Fig. 1c; §3) are dominantly in bluish-color in the interpolation maps, exposing temperatures below 400°C, while others have greenish to yellowish colors outlining a temperatures range between 400°C and 500°C (Fig. 4b-c). The eclogite-facies slices exhibit almost only orange to red colors suggesting temperatures above 500°C (Fig. 4b-c). More irregular patterns in the temperature interpolation, especially south of Gran Paradiso massif, result from the lack of data in these areas (Fig. 4b).

The temperature distribution for each slice (mean, median, standard deviation, number of samples and temperature range) is compiled in Table 2. While many slices show a wide range of temperatures, reflecting their internal metamorphic gradient (Table 2; Fig. 4a-c), the mean-median temperatures of slices appear clustered around three temperature ranges in each of the four studied transect (Valais-Aosta, Savoy-Susa, Cottian Alps and Queyras-Monviso; Table 2). These clusters are around 350-390°C (Cornet, Savoy Upper Unit, Lago Nero, Puys, Aigle, Calcschist Unit and Pelvas-Taillante), 415-475°C (By, West-Sesia, Savoy Middle Unit, Venaus, Vin Vert, Cerogne-Ciantiplagna, Albergian, Mirabouc-Bouchet) and 490-540°C (Zermatt-Saas, Avic, Grivola-Urtier, Avise-Tsaboc-Feluma, Savoy Lower Unit, Orsiera-Rocciavrè, Monviso and Lago Superiore). Temperatures indeed follow a trimodal distribution with Gaussian-like curves centered around 370-380°C, 460-470°C and 530-550°C (Fig. 5a). Cumulative histograms of the RSCM temperatures for each transect, where individual slices were grouped into the three distinct temperature clusters (Fig. 5b-e), show that these groups have specific temperature distributions and only overlap around the minimum and/or maximum values (Fig. 5b-e).

5.2 Si^{max} values of phengite

Methodology

Tschermak substitution (Al^{IV} + Al^{VI} = Si^{IV} + Fe^{VI}, Mg^{VI}) in phengite is known to be highly sensitive to pressure variations in K-feldspar- or talc-bearing assemblages (Velde, 1967; Massonne and Schreyer, 1987,1989; Massone, 1995) and in HP-LT metapelites (Saliot and Velde, 1982; Massonne, 1992; Jolivet et al.,1996, 1998; Goffé and Bousquet, 1997; Bousquet et al., 1998, 2002; Agard et al., 2001a, 2001b). The maximum Si values ($Si^{max}Ph$) of highly substituted early phengite therefore provide an estimate of the peak pressure experienced by the rocks during burial (Si values also depend on rock composition, see §6 below). This is a minimum value since phengite may have reequilibrated during the retrograde path. In the Western Alps L-P domain, the map of $Si^{max}Ph$ isopleths revealed an eastward increase in peak-pressure along the Cottian Alps transect (Agard, 1999; Agard et al., 2001a). In the Savoy-Susa transect, the differences between the Savoy Lower Unit and the Savoy Middle Unit are further supported by their contrasting $Si^{max}Ph$ values (Plunder et al., 2012).

In order to map out the peak pressure distribution across the Western Alps L-P domain, emphasis was placed on the southern half of the domain (Cottian Alps to Ubaye valley), where a strong eastward metamorphic gradient was detected along several transects (Agard et al., 2001a; Gabalda et al., 2009; Schwartz et al., 2013). This is also where numerous slices were identified and very few P-T constraints are available for most of them (see § 3.3; 3.4). Thirty-two samples were selected (see Sup. mat. 1 for location and mineralogy). In each sample, the different generations of white mica were carefully studied in order to locate early, highly substituted phengite. In optimal samples, where up to three successive schistosities (S1, S2 and S3) could be recognized, similar to those of Agard et al. (2001a; Fig. 6a-b), phengite from the S1 generation was selected.

Electron Probe Microanalyis (EPMA) was performed at Camparis (Sorbonne Université, Paris) using both Cameca SX-5 and SX-100 instruments. Point measurements were made in classical analytical conditions (15 kV acceleration voltage, 10 nA beam current allowing ~2 µm beam size in wavelength-dispersive spectroscopy mode) using diopside (Ca, Mg, Si), $MnTiO_3$ (Mn, Ti), orthoclase (K, Al), Fe_2O_3 (Fe), albite (Na) and Cr_2O_3 (Cr) as standards for calibration of elements in parentheses. Representative electron microprobe compositions of phengite are presented in Sup. mat. 2.

Phengite structural formulae were calculated on an 11 oxygen basis and the $Si^{max}Ph$ value of each sample is considered as a proxy for the minimum peak-pressure recorded by the rocks. In order to complete this dataset $Si^{max}Ph$ value from the same region were compiled from literature (Bocquet, 1974; Liewig, 1981 and Agard et al., 2001a; Bonnet et al., submitted). Selected $Si^{max}Ph$ values from this work and from the literature are given in Sup. mat. 3.

627 **Results**

628 Phengite microprobe data are shown in the muscovite-celadonite-pyrophyllite ternary
629 diagram (Fig. 7a). Most analyses plot close to the muscovite-celadonite axis, i.e. along the
630 tschermak substitution trend (Fig. 7a), and generally contain less than 20% of pyrophyllite.
631 We discard phengite containing more than 20% of pyrophyllite to avoid considering Si values
632 related to the pyrophyllitic substitution rather than to peak pressure (see Agard et al., 2001b).

633 $Si^{max}Ph$ values range between 3.25 and 3.67 atoms per formula units (a.p.f.u.) highlighting a
634 large range of tschermark substitution. Selected $Si^{max}Ph$ values from our data and the
635 literature were plotted against their corresponding RSCM temperatures (Fig. 7b). Most of the
636 points expose a relatively clear trend of $Si^{max}Ph$ increase with temperature, evidencing a
637 subduction-related HP-LT gradient in these rocks (Fig. 7b). Some points, especially for high
638 temperature (> to 440°C), are plotting away from the trend. These points may represent
639 samples where the most substituted phengite formed at peak burial was not preserved.

640 The selected $Si^{max}Ph$ are superimposed on the simplified structural sketch map of the
641 Cottian Alps-Queyras region in order to discern the evolution of peak-pressure across the L-
642 P domain (Fig. 8). Except for samples that may not have preserved peak Si values (Fig. 7b),
643 these data reveal an increase of $Si^{max}Ph$ values from west (generally lower than 3.35 a.p.f.u.)
644 to east (generally greater than 3.55 a.p.f.u.), consistent with previous findings on specific
645 sections (Agard et al., 2001a, 2001b) and with the strong eastward increase in metamorphic
646 grade. Our dense sample distribution allows to draw approximate $Si^{max}Ph$ isopleths for 0.10
647 a.p.f.u. steps and to map out the distribution of estimated peak pressure across the L-P
648 domain (Fig. 8). A finer resolution would nevertheless be necessary to scrutinize the
649 pressure evolution across individual tectonic contacts between the L-P slices (Fig. 1c),
650 except maybe for the contact between the BS and eclogite-facies slices, which appears close
651 to the Si 3.55 a.p.f.u. isopleth.

652

653 ## 6. Themodynamic modelling for an average composition, peak pressure and
654 ## dehydration in the tectonic slices

655 **Methodology**

656 In order to compare the peak pressure of the different slices, a reference P-T pseudosection
657 was calculated with the Perple_X software (version 6.9.1; Connolly, 1990, 2005, 2009; Fig.
658 9a). The updated thermodynamic database is that of Holland and Powell (1998), with the
659 corresponding solution models (for chloritoid, Fe-Mg carpholite, garnet, phengite) except for

chlorite (after Holland et al., 1998). For this pseudosection, we used the bulk composition CBas912m of Henry et al. (1996; Fig. 9a) since that is considered as a representative L-P calcschist (and was already used for the Schistes Lustrés by Bebout et al., 2013). The used Na_2O-CaO-K_2O-FeO-MgO-Al_2O_3-SiO_2-H_2O (NaCaKFMASH) chemical system is assumed to describe realistically most of the L-P metasediments. Manganese is largely restricted to garnet cores and was thus neglected in the calculations. TiO_2 and BO_3 are only present in accessory phases (rutile, titanite, tourmaline). Cr_2O_3 is minor and dominantly stored in phengite (and/or lawsonite) and was therefore neglected. The pseudosection was calculated with H_2O in excess in the P-T range of 0.9-2.5 GPa and 300-600°C encompassing most of the peak P-T conditions in the Western Alps L-P domain. The Si-in-phengite isopleths (a.p.f.u.), shown on the P-T grid (Fig. 9a), are relatively flat-lying, outlining the good sensitivity of the phengitic tschermak substitution to pressure variations. The relative peak pressure conditions were determined from the intersection of $Si^{max}Ph$ values (along Si-in-phengite isopleths) of this study and literature samples with their respective RSCM temperatures. The estimated P-T ranges for the studied slices are given in Table 3 (see Sup. mat. 3 for all P-T estimations). These pressure estimates must be considered with caution since the Si content in phengite depends, to a minor extent, on each bulk rock composition. Varying randomly the weight percent of each system component by a few percents results in pressure variations of ± 0.1-0.15 GPa.

In order to track the evolution of metamorphic assemblages during burial, mineral proportions were calculated along the 8°C/km gradient inferred for the Western Alps (Fig. 9b; Agard et al., 2001a; Agard, 2021). We computed the evolution of water content bound in minerals along the same gradient (Fig. 9c) to identify the major dehydration steps and assess their potential impact on slicing mechanisms.

Results

The pseudosection reproduces mineral assemblages observed in L-P sediments (Fig. 1a, 9a, b). Quartz and phengite are the dominant phases and are present in all fields (Fig. 9a, b). Fe-Mg carpholite is present in low-grade sediments and progressively disappears at the expense of chloritoid (Fig. 9a, b). Across a 8°C/km gradient, garnet appears around ~525°C and ~2.2 GPa. This is in good agreement with the almost systematic lack of garnet in BS-facies slices (Fig. 1a; §2.2, 3). Along the same gradient lawsonite is stable up to ~575°C and ~2.4 GPa, fitting with the presence of lawsonite in the ~470°C peak P-T assemblages of the L-P domain (Herviou et al., 2021). The major mismatch is the presence of Na-bearing silicates (glaucophane, jadeite) and kyanite in minor proportions above 2 GPa (glaucophane <6 vol%; jadeite ~1 vol%; kyanite 6-7 vol%), as already noticed by Bebout et al. (2013). The

amount of mineral-bound water first decreases significantly when crossing the chloritoid-in reaction (Fig. 9b-c), and then progressively as Fe-Mg carpholite (~12% H_2O) is gradually replaced by chloritoid (~7.5% H_2O; Fig. 9b). At higher grade two major steps of dehydration are observed along this gradient (Fig. 9b, c): (i) the first one corresponds to chlorite breakdown at ~500°C and 2 GPa (~3.5 to ~2.8 wt% H_2O in the system), followed by final disappearance of carpholite (ii) the second one to lawsonite and chloritoid breakdown reactions, at ~575°and 2.4 GPa (~2.5 to ~1.2 wt% H_2O in the system).

Peak pressures estimated using the $Si^{max}Ph$ and RSCM temperatures intersection range between ~1.3 and 2.5 GPa (Table 3; Sup. mat. 3). Above 500°C, however, pressure determination is limited by the steepening of the Si-in-phengite isopleths (Fig. 9a). The obtained pressures are in good agreement with data available from literature, at least for Cottian Alps (Agard et al., 2001a, 2001b). Indeed, for Lago Nero slice, the pressures obtained range between ~1.3 GPa at west to ~1.9 GPa at east (Table 1) versus 1.2-1.3 and 1.8 GPa for Agard et al. (2001a) in the same samples. In Albergian slice, peak pressure ranges between 1.8 and 2.3 GPa (Table 3) with most samples clustering around 2 GPa (Sup. mat. 3) while Agard et al. (2001a) obtained ~1.9-2 GPa in the same slice. These pressures are a bit higher than those of Agard et al. (2001a) but fit the 2-2.3 GPa peak pressure recently estimated by Corno et al. (2021) for extensional allochtons embedded within the Albergian slice (Corno et al., 2019; Fig. 1a-c). For the Orsiera-Rocciavrè sediments, we obtained slightly higher pressure (~2.2 to ~2.5 GPa; Table 3) than Agard et al. (2001a; 2-2.1 GPa). These values nevertheless fit better with the eclogitic sediments of the other L-P slices (Bousquet, 2008; Angiboust et al., 2012b; Plunder et al., 2012), as well as the 8°C/km gradient of the Western Alps. In the Puys, Vin Vert and Cerogne-Ciantiplagna units, where no pressure estimates exist, the obtained ranges are repectively 1.7-1.8 GPa, 2.1 GPa and 1.7- ~2.2 GPa.

For the Queyras-Monviso BS-facies slices, the estimated pressures are higher than the scarce literature values. Pressure is in the range 1.4-2 GPa for the Calcschist unit, 1.4-1.7 GPa for the Pelvas-Taillante unit and 1.9- ~2.4 GPa for the Mirabouc-Bouchet unit (with most data around 1.9-2 GPa in the latter unit; Table 3; Sup. mat. 3). These pressure values significantly contrast with those previously estimated for metamafic rocks of the same slices (Schwartz, 2000; Tricart and Schwartz, 2006), i.e. respectively ~1 GPa (for ~300°C), ~1.2 GPa and ~1.3 GPa (for ~450°C). These older P-T estimates align along a ~16-17 °C/km gradient, which seems inconsistent with the HP-LT gradient usually considered for Western Alps (Agard, 2021), suggesting that peak pressure was strongly underestimated in these previous works. Finally, the estimated peak pressure for the Lago-Superiore slice is >2.4

GPa (Table 3), in good agreement with literature data (see §3.4; Angiboust et al. 2012b; Locatelli et al., 2018).

Individual slices were then plotted in a P-T space considering their mean RSCM temperature and their approximate mean peak pressure (Fig. 10a). For the slices where no pressure was determined by our study, the compiled P-T estimates from the literature of §3 were used. No pressure data is available, however, for the Avise-Tsaboc-Feluma, West-Sesia, Savoy Upper Unit, Venaus and Aigle slices, which are not shown in figure 10a. The slices were color-coded on the basis of the trimodal temperature distribution (Fig. 5b-e; §5.1). The different slices are also shown considering their peak pressure and age (see references in §3) in figure 10b.

Figure 10a strengthens the existence of a trimodal distribution of tectonic slices with respect to peak burial conditions. The first cluster is characterized by mean peak conditions of 350-400°C and ~1.5-1.7 GPa. These slices (Calcschist unit, Lago Nero, Pelvas-Taillante and Puys) mosty consist of sediments (>90%; Table 1; Fig. 1a, 10a, b). Cornet unit has the same range of mean temperature (390°C; Table 2) but lower pressure (0.8-0.9 GPa; Manzotti et al., 2021). Some pressure estimates for the lower grade rocks of Lago Nero and Calcschist units (Agard et al., 2001a, 2001b; Tricart and Schwartz, 2006) are relatively close to those of Cornet unit, then considered to belongs to the same cluster. The second cluster shows mean peak conditions of 415-475°C and ~1.7-2.1 GPa. These units (Albergian, By, Cerogne-Ciantiplagna, Mirabouc-Bouchet, Savoy Middle Unit and Vin Vert) are also dominantly composed by sediments (Table 1, Fig. 1a, 10a). The third cluster is characterized by mean RSCM temperature of ~490-540°C and mean peak pressures of 2.2- ~2.6 GPa. These slices (Avic, Lago Superiore, Monviso, Savoy Lower Unit, Zermatt-Saas) are mostly composed by mafic and ultramafic rocks (~60%; Table 1; Fig. 1a, 10a) except for the Grivola-Urtier and Orsiera-Rocciavrè, which nevertheless show a higher ophiolitic content than all BS-facies slices.

7. Discussion

7.1 Correlations between tectonic slices, distribution, and revised structural sketchmap

Using the peak P-T conditions, lithostratigraphy, zoneography of index minerals and structural constraints, three groups of tectonic slices can be recognized in the L-P domain (Figs. 11,12a-d):

— the Liguro-Piemont Upper units (LPU):

These units, which make up ~18% of the Western Alps L-P surface (~440 km^2; Table 1), crop out in the west of the L-P domain (Figs. 11, 12a-d) and are dominated by metasediments (>90%, Table 1; Fig. 1a). They are largely exposed in the southern L-P domain (Queyras-Monviso and Cottian Alps, Fig. 11) while gradually disappearing from the Savoy-Susa to the Valais-Aosta region, where they are relatively rare (except for the Cornet slice; Fig. 11). From north to south, the LPU include the Cornet slice (Valais-Aosta), the Savoy Upper Unit with the Jovet, Grand Vallon, Upper Sana and Lamet klippen (Savoy-Susa region), the Lago Nero, Aigle and Puys slices (Cottian Alps) and the Calcschist and Pelvas-Taillante slices (Queyras-Monviso). Some of these slices exhibit an almost complete Chabrière-type stratigraphic succession (Lago Nero, Pelvas-Taillante, Cornet; Fig. 3b), whereas some only contain C4a-b calcschists-flyschs (Calcschist unit, Puys, Savoy Upper Unit; Fig. 3b). The lack of Lower-Cretaceous and Jurassic deposits in the latter units may indicates a more proximal origin (Fig. 3a) or reflects differences in décollement depth (see §7.4). These LPU units are characterized by low- to medium-temperature BS-facies peak metamorphism highlighted, in metasediments, by the presence of Fe-Mg carpholite and lawsonite (Fig. 1b). Chloritoid only appears in their higher-grade metasediments, in the eastern part of these units (Fig. 1b). Peak P-T conditions range mostly between 320-400°C and 1.2 to 1.9 GPa (Fig.4a-c, 5b-e, 10a; Table 2, 3, see §3). Mean and median RSCM temperatures for these units are ~373°C (86 samples; Fig. 13a), while mean/median values of $Si^{max}Ph$ are 3.40/3.42 a.p.f.u. (30 samples; Fig. 13b).

Some uncertainties remain on the exact distribution of the LPU slices. In Savoy-Aosta, the extent of the Cornet slice and the precise location of its contact with the underlying By slice (Manzotti et al., 2021) still need to be investigated to the east of the Dent Blanche Nappe (Fig. 11). In the Queyras-Monviso region, we have considered that Acceglio's half-window separates the Pelvas-Taillante (LPU) to the west from the Mirabouc-Bouchet to the east of Acceglio, the two samples closest to the contact nevertheless show temperatures <400°C, which is significantly lower than most temperatures obtained for the Mirabouc-Bouchet slice (Fig. 4a-c) and may indicate that the Pelvas-Taillante slice is cropping out over a short distance to the east of Acceglio. Finally, only few temperature constraints are available for the Savoy Upper Unit (4 samples), Puys (1 sample) and Aigle (3 samples) slices, and almost no pressure constraints (only 1 sample for Puys). While their estimated RSCM temperatures are similar to LPU units (Table 2, Fig. 5b-e, 10a), more P-T estimates are needed to confirm this interpretation.

— the Liguro-Piemont Middle units (LPM):

These units make up ~42% of the L-P aeral exposure (~1050 km^2; Fig. 11, Table 1) and are also dominated by metasediments (generally >90%, Table 1; Fig. 1a). They crop out eastward of the LPU units (Fig. 11, 12a-d), except in Savoy-Susa where the LPU is found as klippen and in Valais-Aosta where the Cornet slice (LPU) forms a synformal stack atop the By slice (LPM; Fig. 12a). The Liguro-Piemont Middle units comprise the By slice (Valais-Aosta), the Savoy Middle Units (including Grande Sassière, Lower Sana and Chardonnet klippen) and the Venaus slice (Savoy-Susa), the Albergian, Cerogne-Ciantiplagna and Vin Vert slices (Cottian Alps) and the Mirabouc Bouchet slice (Queyras-Viso), and possibly the West-Sesia and Avise-Tsaboc-Feluma slices (see below). These slices generally exhibit a stratigraphic succession corresponding to an incomplete Chabrière-like series, commonly with a thick sequence of – and in places restricted to – Upper-Cretaceous C4a deposits (Fig. 3b). The LPM are characterized by a high-temperature blueschist-facies and up to transitional BS-eclogite-facies metamorphism highlighted in metasediments by the appearance of chloritoid in peak assemblages, the disappearance of Fe-Mg carpholite, the presence of lawsonite and the absence of garnet (Fig. 1b). Most P-T conditions range between 415-475°C and 1.7-2.2 GPa (Fig.4a-c, 5b-e, 10a; Table 2, 3, see §3). Mean/median RSCM temperatures for these units are 459°C/463°C (191 samples; Fig. 13a), while mean/median values of $Si^{max}Ph$ are 3.52/3.51 a.p.f.u. (23 samples; Fig. 13b).

Uncertainties on the spatial extent of the LPM concern slices with limited lithostratigraphic and P-T data. While the Venaus slice was already considered as an equivalent of the Savoy Middle Unit (Fudral, 1996) and shows a RSCM temperature of 485°C consistent with LPM, the attribution is less clear for the West-Sesia and Avise-Tsaboc-Feluma slices. The RSCM temperature for the West-Sesia slice (433°C; Fig. 4a-c; Table 2) fits LPM temperatures (no such low value was found in the eclogite-facies units; Table 2, Fig. 5b-e, 10a). It is furthermore largely dominated by metasediments (~93%; Table 1), in contrast with the LPL lithology (Table 1, Fig. 1a), and would be the only BS-facies slice eastward of eclogite-facies LPL (Fig. 11). We therefore suggest that this slice may be analogous to the other LPM units and reflect the doming of Savoy Middle Unit-like slices above the Gran Paradiso massif (Fig. 11). For the Avise-Tsaboc-Feluma slice(s), while the RSCM temperature of 522°C fits in the LPL temperature range (Table 2; Fig. 5b-e, 10a), its estimated sediment/mafic-ultramafic ratio does not fit with the LPL units (~99% of sediments; Table 1), notwithstanding the fact that a few temperatures are close to 500°C in the LPM Savoy Middle Unit, and even higher in the LPM By and Mirabouc-Bouchet slices. Further P-T constraints are needed to confirm these attributions.

— the Liguro-Piemont Lower units (LPL)

These units occupy ~40% of the L-P surface (~990 km^2) and contain much more mafic and ultramafic material than the LPU and LPM units (Table 1; Fig. 1a). Most LPL slices contain >60% of ophiolitic material (Avic, Zermatt-Saas, Savoy Lower Unit, Monviso, Lago Superiore; Table 1) and correspond to the MUM units of Agard (2021), while a few have ~40% of ophiolites (Grivola-Urtier, Orsiera-Rocciavrè; Table 1). The Liguro-Piemont Lower units comprise the Avic, Grivola-Urtier and Zermatt-Saas slices (Valais-Aosta), the Savoy Lower Unit (Savoy-Susa), the Orsiera-Rocciavrè slice (Cottian Alps) and the Monviso and Lago Superiore slices (Queyras-Monviso). The LPL units are characterized by a specific, incomplete Chabrière-type series, devoid of Upper Cretaceous deposits (Fig. 3b), which may reflect a distinct paleogeography and/or high topography on the seafloor or a tectonic removal of its sedimentary cover during the subduction/exhumation processes. These LPL slices were metamorphosed from BS-eclogite-facies to eclogite-facies as outlined by the presence of chloritoid-garnet assemblages in metasediments (Fig. 1b). Most P-T conditions range between 500 and 580°C and 2.2 to 2.8 GPa (Fig.4a-c, 5a-e, 10a; Table 2, 3, see §3). Mean/median RSCM temperatures for these units are 529°C/534°C (118 samples; Fig. 13a), while mean/median values of $Si^{max}Ph$ are 3.55/3.54 a.p.f.u. (4 samples; Fig. 13b). Note that some Alpine units fit the LPL in term of peak P-T conditions but appear slightly different in terms of lithology, containing either almost only ophiolitic material for the Lanzo massif (>90% of mafic and ultramafic rocks; Lagabrielle et al., 1990) or almost only metasediments for the small Lago di Cignana UHP slice (e.g., Compagnoni and Rolfo, 2003).

The LPL units are exposed on the eastern side of the domain and appear separated from the BS-facies LPM by a major extensional contact (Philippot, 1990; Ballèvre et al., 1990; Ballèvre and Merle, 1993; Fig. 2a-c, 11, 12a-d). One might further sub-divide the LPL between mafic-ultramafic-dominated (~60% mafic-ultramafic; Table 1) and sediment-dominated slices (~60% sediments; Table 1), with the latter potentially representing the former cover of the MUM units (Agard, 2021). Indeed, some of the described slices (Savoy Middle Unit, Orsiera-Rocciavrè; §3) contain large amount of sediments embedding mafic-ultramafic rocks in their western side and are almost devoid of sediments in their eastern side (Fig. 1a). This distribution may either be explained by the west-dipping foliation of the slices (i.e., with the oceanic basement at the base) or by the presence of tectonic contacts juxtaposing sedimentary dominated eclogite-facies slices on top of mafic-ultramafic dominant slices. The different peak burial age inferred for the Orsiera massif metasediments (61-53 Ma, Agard et al., 2001a; Fig. 10b; §3, 7.3) and the Rocciavrè metagabbros (46 Ma, Angiboust and Glodny, 2020; Fig. 10b; §3, 6.3) rather supports this distinction. The Grivola-Urtier slice, which is richer in metasediments than most LPL units, would be an analogous of these sediments-dominated eclogite-facies slices.

7.2 Diachronous burial and stacking, and possible paleogeographic origin

The similar peak P-T conditions, structural position and lithological content among slices in each of the three L-P groups (§7.1) suggest that they may have recorded similar subduction histories and processes. The plot of RSCM temperatures versus longitude for each transect highlights the similarity of slice-stacking of LPU, LPM and LPL units across the L-P domain (Fig. 14a-e). The eastward-trend of temperature increase exposes the HP-LT subduction gradient, less conspicuous for the Valais-Aosta transect where a stronger collisional imprint on the nappe-stack (synformal-stack implying upper plate fragments) slightly erased this trend (Fig. 14e). Subtle differences in lithostratigraphy nevertheless point out to differences in their paleogeographic origin (Fig. 15a-c; see §7.3, 7.4), and all slices with similar P-T were probably not buried, sliced and juxtaposed at the same time. While the formation of deeply underplated nappe stacks suggests that the structurally lower units may have been buried, detached and underplated later (Kimura et al., 2007; Bachmann et al., 2009; Dumitru et al., 2010; Plunder et al., 2012), available metamorphic ages are here discussed to precise the slicing and underplating sequence of the LPU, LPM and LPL units (Fig. 10b, 14a, 15b).

Very few robust ages are available for the BS-facies LPU and LPM units (Fig. 10b; §3). The Lago Nero slice (LPU) was dated by in-situ Ar-Ar on phengite and gave 61-55 Ma, 51-43 Ma and 38-36 Ma ages for D1 (peak P-T), D2 and D3 fabrics respectively (Agard et al., 2002). Moreover, bulk Ar-Ar on separated generations of phengite from the Calcschist unit (LPU) gave a 42-40 Ma age for a peak P-T foliation (Lanari, 2012; Fig. 10b). These ages suggest a diachronous slicing of the LPU characterized by Chabrière-type series, which were buried and underplated earlier than the LPU units lacking deposits older than the Upper Cretaceous (Fig. 3b, 10b, 14a, 15a, b). The latter ones may have been originally located close to Piemont margin and been underplated on top of the L-P stack at the very end of oceanic subduction (Fig. 15b, 14a; see also Herviou et al., 2021, their Fig. 13 and §7.2.1).

In LPM (Albergian slice, Fig. 11), in situ Ar-Ar dating on phengite gave 64-49 Ma and ~50 Ma ages for D1 (peak P-T) and D2 fabrics (Agard et al., 2002; Fig. 10b). This method also gave 47-42 Ma and 40-36 Ma for S1(peak) and S2 (potentially equivalent to D3 of Agard et al., 2002; Fig. 10b) foliation in the Savoy Middle Unit (Ghignone et al., 2021b; Fig. 10b). Bulk Ar-Ar on isolated generation of phengite from the Mirabouc-Bouchet slices (LPM) gave 68-58 Ma for an early foliation (prograde to peak?), 45 Ma for a S2 (peak or early retrograde?) and an age younger than 30 Ma for a late S3 foliation (Lanari, 2012; Fig. 10b) while Rb-Sr on D3 phengite from the same slice gave ~35 Ma (Angiboust and Glodny, 2020; Fig. 10b). In the Valais-Aosta region, D2 to D3 exhumation-related episodes of By (LPM) and Cornet (LPU)

slices were dated between 41 and 37 Ma (Reddy et al., 2003; Angiboust et al., 2014; Fig. 10b). These peak burial ages of the LPM units, either undistinguishable from or younger than those for the Lago Nero unit, are broadly consistent with a slicing and underplating somewhat later than the LPU Chabrière-serie slices (Fig. 10b, 14a, 15a, b) and with their present structural position (Fig. 12a-d).

Finally, for LPL mafic-ultramafic-dominated units, most of the peak burial ages (from various methods; see §3) range between 50 and 40 Ma (§3; Fig. 10b) and may represent the sampling of a mafic-rich zone close to the Piemont margin units (Fig. 14a, 15a), as pointed out by Agard (2021). Sediment-dominated units have older ages: 61-53 Ma, 46-42 Ma, 42-38 Ma in D1 (peak P-T), D2 and D3 fabrics of Orsiera massif sediments (in situ Ar-Ar in phengite; Agard et al., 2002; Fig. 10b) and 60-48 Ma for Grivola-Urtier slice (bulk Lu-Hf and Ar-Ar on phengite, Villa et al., 2014; Fig. 10b) suggesting that the few sediment-dominated eclogite-facies units may have been stripped from and underplated before the ophiolitic-dominated MUM LPL units (Fig. 14a, 15a). For each transect, the corresponding slices successively detached from the Alpine slab during a short-lived period prior to continental burial and were stacked together during exhumation around 40-35 Ma at ~20 km depth (Fig. 10b, 14a, 15a).

7.3 Trimodal distribution of units: insights into subduction processes

The three groups of L-P slices show peak P-T conditions comparable to those of subducted oceanic fragments recovered worldwide, for which two major recovery depths were recognized at 30-40 km and 80 ± 10 km, with a potential third cluster at 55-60 km (Fig. 16a-c; Agard et al., 2018; see also Plunder et al., 2015). The same distinct recovery depths were detected in continental-subduction slivers (Agard and Vitale-Brovarone, 2013; Soret et al., 2021). These rock clusters are thought to reflect major changes in mechanical coupling along the plate interface (Agard et al., 2018), which occur transiently (Monié and Agard, 2009) and in places coevally across-dip (Bonnet et al., 2018). While offscraping from the downgoing slab requires an increase in mechanical coupling (Agard et al., 2016, 2020), the stepping down of the plate interface décollement into the slab and strain localization into zones of weakness (Kimura and Ludden, 1996; Kimura et al., 2007; Angiboust et al., 2012c; Ruh et al., 2015), mechanical processes controlling slicing are unknown. Similar depth clusters (35 ± 10 km and 60 ± 5 km) for the locus of interplate deformation bounding earthquakes were also recently identified by a mechanical analysis of the topography along the Chilean margin (Cubas et al., submitted; Fig. 16a). These depths are interpreted as zones of distributed deformation ultimately leading to slicing of the slab, underplating and topographic build-up

(Menant et al., 2019, 2020), which are responsible for stress build-up eventually leading to the nucleation of earthquakes propagating across the domains B and C as defined by Lay et al. (2012; Cubas et al., submitted; see Fig. 16c). The LPU, LPM and LPL units, with their slicing depths of ~35-45 km, ~55-65 km and ~70-80 km, respectively, may therefore provide insights into the mechanisms that control strain localization and slicing along the plate interface (Fig. 16b).

— *Offscraping mechanisms in the LPU units*

The LPU ~35-45 km depth coincides with the downdip end of the seismogenic zone, where the transition from upper plate continental crust to mantle wedge likely induces a strong change in interplate coupling (Agard et al., 2018), and where ductile shear and dissolution-precipitation creep (DPC) may be the dominant deformation mechanisms (Wassmann and Stöckhert, 2013; Platt et al., 2018; Agard et al, 2018). Both geophysical and petrological data suggest the presence of fluids and high pore fluid pressure (Audet et al., 2009; Saffer and Tobin, 2011; Behr and Bürgmann, 2021), which reduces shear strength and enhances strain localization in weak zones (Kimura and Ludden, 1995; Kimura et al., 2007; Saffer and Tobin, 2011; Kameda et al., 2017).

In the LPU units, the presence of fluids at peak burial conditions is attested by the large amount of hydrated phases in sediments and metamorphic veins (Goffé and Chopin, 1986; Lefeuvre et al., 2020; Herviou et al., 2021). The formation of lawsonite-bearing extensional cracks in these rocks reflects near-lithostatic fluid-pressure (Lefeuvre et al., 2020; Herviou et al., 2021). At these depths and for such a cold subduction gradient, however, no major dehydration reaction is predicted (Peacock, 1993; Van Keken et al., 2011). Only the eastern samples contain chloritoid (Fig. 1b), showing that the progressive carpholite-out reaction is only crossed by the highest grade samples of LPU units, as predicted by our thermodynamic modelling (Fig. 9a-c; see also Agard et al., 2001a; Bebout et al., 2013; Herviou et al., 2021). Veins therefore likely formed by the local redistribution of material in the fluid through DPC-controlled deformation (Herviou et al., 2021). Slicing of the LPU units may then be related to inherited heterogeneities in the lithological succession and/or high fluid pressure rather than to embrittlement by major fluid release (e.g., Hacker et al., 2003).

In the LPU slices limited to Upper Cretaceous deposits (Fig. 3b, §4.1, 7.1, 7.2), strain may have localized between the Lower Cretaceous pelagic A3 and the more clastic Upper Cretaceous C4 calcschists-flyschs (Fig. 15c; see also Fig. 3b; §4.1), as observed between pelagic sediments and trench-filling turbidites in accretionary prisms (Karig and Sharman, 1975; Moore, 1975; Kimura et al., 2007). The Middle Cretaceous A3b shales would have served as a zone of rheological weakness (weaker than more siliceous hemipelagic

sediments; Ikari et al., 2018) leading to deformation localization and slicing as in silty clays at slow aseismic creep conditions (Vannucchi et al., 2017).

In the LPU Chabrière-series slices (3b, 14; §4.1, 7.1, 7.2), which contain a dismembered ophiolitic basement (Table 1; Fig; 3b), slicing occurred deeper in the oceanic lithosphere (Fig. 15a, c), possibly along the numerous pre-Alpine structures identified in the L-P domain (e.g., oceanic-detachments; Manatschal et al., 2011; Lagabrielle et al., 2015; Balestro et al., 2018; Decrausaz et al., 2021; Agard, 2021). Fluid infiltration along theses structures, as notably attested by the strong hydrothermal alteration of the L-P oceanic fragments (Selvertsone and Sharp, 2013; Busigny et al., 2011, 2018; see also Herviou et al., 2021), promoted strain localization (Fig. 15c). Strain localization in serpentinized horizons, in particular, is commonly considered for slicing in the slab (Angiboust et al., 2011; Agard et al., 2018; Tewksbury-Christle et al., 2021) and supported by modeling (e.g., Ruh et al., 2015).

— *Offscraping mechanisms in the LPM units*

At ~55-65 km, the slab is juxtaposed against the partly serpentinized and decoupled mantle wedge, explaining the lesser recovery of rocks for this range of subduction depths (Guillot et al., 2015; Agard et al., 2018; Fig. 16c). In the LPM units, fresh lawsonite is found in both metasediment matrix and veins (Fig. 1a; Herviou et al., 2021) and therefore considered to have remained stable during burial, as predicted by our pseudosection (Fig. 9a-c; 10a). In these slices, Fe-Mg carpholite is only found as micrometric needles in quartz crystals preserved from recrystallization (Agard et al., 2000; 2001a), whereas chloritoid is widespread in pelitic layers (Fig. 1a). The Fe-Mg carpholite (~12 wt% H_2O) to chloritoid (~7-8 wt% H_2O) reaction is therefore well under way. The carpholite-out reaction along a 8°C/km gradient is predicted at ~500°C-2 GPa (Fig. 9b, c, 10a), which fits the highest P-T conditions recorded by the LPM units (Fig. 5b-e; table 2, 3). However, no other major dehydration reaction releasing a large amount of water during a short P-T window is predicted for the LPM metasediments (Fig. 9b-c) or mafic-ultramafic rocks (Angiboust and Agard, 2010). The slicing of the LPM units may therefore be related to a combination of inherited lithological heterogeneities and fluid release (Fig. 15c, 16b). We therefore consider that strain localized in the Middle Cretaceous A3b shales for the Upper Cretaceous LPM slices (as for the LPU units; Fig. 3b, 15c) and around oceanic detachment faults for the Chabrière-like LPM (Fig. 3b, 16c).

— *Offscraping mechanisms in the LPL units*

The third cluster at ~70-80 km coincides with the depth beyond which rocks are generally not recovered, due to density and slab pull changes as well as to viscous recoupling (Wada and Wang, 2009; Syracuse et al., 2010, see also Kerswell et al., 2021; Fig. 16c) dragging down

irreversibly the slab into the mantle once serpentinite is fully dehydrated (Agard et al., 2009; 2018; Duesterhoeft et al., 2014). A change in deformation mechanisms from fluid-assisted DPC to dislocation creep may drive this viscous coupling (Agard et al., 2020).

The transition from BS- to eclogite-facies is considered as a major dehydration-step for the downgoing plate (Peacock, 1993; Angiboust and Agard, 2010; Van Keken et al., 2011; Paulatto et al., 2017). The boundary between these two facies coincides with the location of intermediate-depth earthquakes, suggesting that rocks undergo weakening and embrittlement during dehydration at eclogite-facies conditions (Hacker et al., 2003; Kita et al., 2006; Abers et al., 2006, 2013), especially for the coldest slabs (Abers et al., 2013). Dehydration reactions such as the lawsonite-out (~12 wt% H_2O) were suggested because crustal intermediate-depth seismicity coincide with the thermal stability of lawsonite (Abers et al., 2006), and because lawsonite dehydration may trigger brittle failure as unstable fault slip (Okazaki and Hirth, 2016; Incel et al., 2017). Brittle-deformation was furthermore evidenced in exhumed eclogites and may reflect an increase in fluid pressure induced by dehydration reactions (Angiboust et al., 2017; Hertgen et al., 2017; Behr et al., 2018).

In LPL units, eclogitic breccias and veins reveal rupture events along rheological contrasts and during fluid ingression at ~80 km (Angiboust et al., 2011, 2012a; Locatelli et al., 2018, 2019a, b; Broadwell et al., 2019). Furthermore, pseudotachylites formed in the same depth range were reported in Lanzo massif, adjacent to the LPL units (Scambelluri et al., 2017; Pennacchioni et al., 2020). At peak P-T conditions, in LPL units mafic crust, lawsonite is supposedly still stable (Angiboust and Agard, 2010; Angiboust et al., 2011, 2012b; Locatelli et al., 2018) whereas chlorite (~12 wt% H_2O) is predicted to breakdown at the BS- to eclogite-facies transition (Angiboust and Agard, 2010). In the LPL ultramafic rocks, antigorite (~12 wt% H_2O) is still stable at peak P-T conditions (Angiboust et Agard, 2010; Schwartz et al., 2013). In the LPL mafics and ultramafics, the only reaction that may contribute to high fluid pressure and affect rheology is therefore chlorite breakdown. Dehydration reactions occurring deeper, such as antigorite breakdown, may also affect rocks at LPL units peak-burial depths (Angiboust et al., 2012a).

The P-T estimates for the LPL units lie close to predicted major dehydration reactions for metasediments (Fig. 9a-c; 10a), supporting the potential role of fluids in LPL slicing. While the chlorite and Fe-Mg carpholite breakdown in sediments is predicted at ~500°C-2 GPa (with a decrease in water content from ~3.5 wt% to ~2.8 wt% H_2O; Fig. 9b-c, 10a), another major step of dehydration (leading to a decrease from ~2.5 wt% to ~1.2 wt% H_2O) is predicted at ~575°C-2.4 GPa for chloritoid (~7-8 wt% H_2O) and lawsonite breakdown (Fig. 9b-c, 10a). We note that this second step coincides with most of the maximum P-T

conditions recorded in LPL units (Fig. 9c, 10a, see §3, 7.1), where lawsonite is no longer stable, and that large amounts of lawsonite, up to ~40 vol% of the host rocks, were present in metasediments (Lefeuvre et al., 2020). We therefore propose that the destabilization of these large amounts of lawsonite, accompanied by chloritoid-out reaction and/or chlorite breakdown (in mafic rocks), may have induced high fluid pressure and embrittlement able to slice LPL units from the downgoing slab (Fig. 15c, 16b; as supported by experiments; Okazaki and Hirth, 2016). These reactions would have helped localize strain deeper in the downgoing slab than for the LPU and LPM units, explaining the larger volume of mafic and ultramafic rocks in the present-day stack of LPL units (Fig. 1a, 10a, 15a, c; see §4, 7.1, 7.2). As for the LPU and LPM units, inherited detachment faults may have served as rheological weaknesses to localize the strain (Fig. 15a, 16c).

Conclusions

Through the compilation of petrological data (peak P-T estimations, zoneography of index minerals) and report of new RSCM temperatures, RSCM interpolation, maximum Si values of phengite (as a proxy for peak pressure) and thermodynamic modelling, this study provides a detailed framework of the peak P-T conditions recorded by the various Liguro-Piemont slices. A strong eastward increase in metamorphic grade through the Liguro-Piemont domain, as well as inside some slices, is notably highlighted by the distribution of RSCM temperatures and maximum Si values of phengite. In addition, the compilation of lithostratigraphic, structural and radiochronological data, together with the estimation of the sediment versus mafic-ultramafic content from aerial exposures, for each slice, allow refining the origin and evolution of these tectonometamorphic units/slices across the Liguro-Piemont domain. The revised structural organization of the various Liguro-Piemont units allows restoring the geometries of the Alpine subduction at peak burial conditions. Results point to a trimodal distribution of units with an almost continuous increase in metamorphic conditions from the Liguro-Piemont Upper units (LPU; 320-400°C- 1.2-1.9 GPa) to the Liguro-Piemont Middle units (LPM; 415-475°C- 1.7-2.2 GPa) and to the Liguro-Piemont Lower units (LPL; 500-580°C- 2.2-2.8 GPa). The LPU and LPM units, metamorphosed under blueschist-facies conditions at peak P-T conditions, are dominated by sediments (>90%) whereas the LPL units, metamorphosed at eclogite-facies conditions at peak burial, are much richer in mafic-ultramafic rocks (>40%). These two types exhibit major differences in terms of initial paleogeography and/or mechanisms responsible for material-offscraping from the downgoing slab. Peak burial depths of the LPU, LPM and LPL units are similar to those deduced for the slicing and underplating of rocks in modern and fossil subduction zones, pointing to specific

mechanisms controlling transient changes in interplate coupling at these depths. Combined petrological and lithostratigraphic data suggest that strain localization leading to the offscraping of the LPU and LPM units was mostly controlled by lithological contrasts across sedimentary packages, within the shales or along the contacts within the uppermost serpentinized mantle (some of which may have been inherited from former oceanic detachment faults), which acted as rheological weaknesses, possibly under high fluid pressure conditions. In contrast, major dehydration reactions (such as lawsonite breakdown in sediments and chlorite breakdown in mafics) likely controlled the offscraping of the LPL units at eclogite facies conditions, possibly through high fluid pressure conditions and rock embrittlement. In these units too, strain localization may have been guided by preexisting heterogeneities such as inherited oceanic detachment faults.

Acknowledgments

This study was funded by the BRGM in the frame of the RGF Alpes project. The authors thank S. Angiboust, O. Beyssac and T. Decrausaz for their help in locating samples of their articles. N. Rividi and M. Fialin are thanked for analytical support and E. Delairis for sample preparation. M. Ballèvre and an anonymous reviewer are thanked for their remarks and suggestions which have greatly helped to improve this work as Z.-X. Li for his editorial handling. We also thank G. Bonnet, B. Lefeuvre, S. Schwartz, L. Jolivet, H. Raimbourg, C. Chopin, B. Dubacq, T. Gyomlai and A. Lahfid for discussions.

References

Abers, G.A., van Keken, P.E., Kneller, E.A., Ferris, A., Stachnik, J.C., 2006. The thermal structure of subduction zones constrained by seismic imaging: Implications for slab dehydration and wedge flow. Earth and Planetary Science Letters 241, 387–397. https://doi.org/10.1016/j.epsl.2005.11.055

Abers, G.A., Nakajima, J., van Keken, P.E., Kita, S., Hacker, B.R., 2013. Thermal–petrological controls on the location of earthquakes within subducting plates. Earth and Planetary Science Letters 369–370, 178–187. https://doi.org/10.1016/j.epsl.2013.03.022

Agard, P, 1999. Evolution métamorphique et structurale des métapélites océaniques dans l'orogène Alpin : l'exemple des Schistes Lustrés des Alpes occidentales (Alpes Cottiennes). PhD thesis Université de Paris 6.

Agard, P., 2021. Subduction of oceanic lithosphere in the Alps: Selective and archetypal from (slow-spreading) oceans. Earth-Science Reviews 214, 103517. https://doi.org/10.1016/j.earscirev.2021.103517

Agard, P., Vitale-Brovarone, A., 2013. Thermal regime of continental subduction: The record from exhumed HP–LT terranes (New Caledonia, Oman, Corsica). Tectonophysics 601, 206–215. https://doi.org/10.1016/j.tecto.2013.05.011

Agard, P., Handy, M.R., 2021. Ocean Subduction Dynamics in the Alps. Elements 17, 9–16. https://doi.org/10.2138/gselements.17.1.9

Agard, P., Goffé, B., Touret, J.L.R., Vidal, O., 2000. Retrograde mineral and fluid evolution in high-pressure metapelites (Schistes lustrés unit, Western Alps). Contributions to Mineralogy and Petrology 140, 296–315. https://doi.org/10.1007/s004100000190

Agard, Philippe, Jolivet, L., Goffe, B., 2001a. Tectonometamorphic evolution of the Schistes Lustres Complex; implications for the exhumation of HP and UHP rocks in the Western Alps. Bulletin de la Société Géologique de France 172, 617–636. https://doi.org/10.2113/172.5.617

Agard, P., Vidal, O., Goffé, B., 2001b. Interlayer and Si content of phengite in HP-LT carpholite-bearing metapelites. Journal of Metamorphic Geology 19, 479–495. https://doi.org/10.1046/j.0263-4929.2001.00322.x

Agard, P., Monie, P., Jolivet, L., Goffe, B., 2002. Exhumation of the Schistes Lustres complex: in situ laser probe 40Ar/39Ar constraints and implications for the Western Alps. J Metamorph Geol 20, 599–618. https://doi.org/10.1046/j.1525-1314.2002.00391.x

Agard, P., Yamato, P., Jolivet, L., Burov, E., 2009. Exhumation of oceanic blueschists and eclogites in subduction zones: Timing and mechanisms. Earth-Science Reviews 92, 53–79. https://doi.org/10.1016/j.earscirev.2008.11.002

Agard, P., Yamato, P., Soret, M., Prigent, C., Guillot, S., Plunder, A., Dubacq, B., Chauvet, A., Monié, P., 2016. Plate interface rheological switches during subduction infancy: Control on slab penetration and metamorphic sole formation. Earth and Planetary Science Letters 451, 208–220. https://doi.org/10.1016/j.epsl.2016.06.054

Agard, P., Plunder, A., Angiboust, S., Bonnet, G., Ruh, J., 2018. The subduction plate interface: rock record and mechanical coupling (from long to short timescales). Lithos 320–321, 537–566. https://doi.org/10.1016/j.lithos.2018.09.029

Agard, P., Prigent, C., Soret, M., Dubacq, B., Guillot, S., Deldicque, D., 2020. Slabitization: Mechanisms controlling subduction development and viscous coupling. Earth-Science Reviews 208, 103259. https://doi.org/10.1016/j.earscirev.2020.103259

Amato, J.M., Johnson, C.M., Baumgartner, L.P., Beard, B.L., 1999. Rapid exhumation of the Zermatt-Saas ophiolite deduced from high-precision SmNd and RbSr geochronology. Earth and Planetary Science Letters 171, 425–438. https://doi.org/10.1016/S0012-821X(99)00161-2

Angiboust, S., Agard, P, 2010. Initial water budget: The key to detaching large volumes of eclogitized oceanic crust along the subduction channel? 22.

Angiboust, S., Agard, P., Jolivet, L., Beyssac, O., 2009. The Zermatt-Saas ophiolite: the largest (60-km wide) and deepest (c. 70-80 km) continuous slice of oceanic lithosphere detached from a subduction zone? Terra Nova 21, 171–180. https://doi.org/10.1111/j.1365-3121.2009.00870.x

Angiboust, S., Agard, P., Raimbourg, H., Yamato, P., Huet, B., 2011. Subduction interface processes recorded by eclogite-facies shear zones (Monviso, W. Alps). Lithos 127, 222–238. https://doi.org/10.1016/j.lithos.2011.09.004

Angiboust, S., Agard, P., Yamato, P., Raimbourg, H., 2012a. Eclogite breccias in a subducted ophiolite: A record of intermediate-depth earthquakes? Geology 40, 707–710. https://doi.org/10.1130/G32925.1

Angiboust, S., Langdon, R., Agard, P., Waters, D., Chopin, C., 2012b. Eclogitization of the Monviso ophiolite (W. Alps) and implications on subduction dynamics. Journal of Metamorphic Geology 30, 37–61. https://doi.org/10.1111/j.1525-1314.2011.00951.x

Angiboust, S., Wolf, S., Burov, E., Agard, P., Yamato, P., 2012c. Effect of fluid circulation on subduction interface tectonic processes: Insights from thermo-mechanical numerical modelling. Earth and Planetary Science Letters 357–358, 238–248. https://doi.org/10.1016/j.epsl.2012.09.012

Angiboust, S., Agard, P., De Hoog, J.C.M., Omrani, J., Plunder, A., 2013. Insights on deep, accretionary subduction processes from the Sistan ophiolitic “mélange” (Eastern Iran). Lithos 156–159, 139–158. https://doi.org/10.1016/j.lithos.2012.11.007

Angiboust, S., Glodny, J., Oncken, O., Chopin, C., 2014. In search of transient subduction interfaces in the Dent Blanche–Sesia Tectonic System (W. Alps). Lithos 205, 298–321. https://doi.org/10.1016/j.lithos.2014.07.001

Angiboust, S., Kirsch, J., Oncken, O., Glodny, J., Monié, P., Rybacki, E., 2015. Probing the transition between seismically coupled and decoupled segments along an ancient subduction interface: CATACLASIS ON THE SUBDUCTION INTERFACE. Geochem. Geophys. Geosyst. 16, 1905–1922. https://doi.org/10.1002/2015GC005776

Angiboust, S., Agard, P., Glodny, J., Omrani, J., Oncken, O., 2016. Zagros blueschists: Episodic underplating and long-lived cooling of a subduction zone. Earth and Planetary Science Letters 443, 48–58. https://doi.org/10.1016/j.epsl.2016.03.017

Angiboust, S., Yamato, P., Hertgen, S., Hyppolito, T., Bebout, G.E., Morales, L., 2017. Fluid pathways and high- P metasomatism in a subducted continental slice (Mt. Emilius klippe, W. Alps). J. Metamorph. Geol. 35, 471–492. https://doi.org/10.1111/jmg.12241

Angiboust, S., Cambeses, A., Hyppolito, T., Glodny, J., Monié, P., Calderón, M., Juliani, C., 2018. A 100-m.y.-long window onto mass-flow processes in the Patagonian Mesozoic subduction zone (Diego de Almagro Island, Chile). GSA Bulletin 130, 1439–1456. https://doi.org/10.1130/B31891.1

Angiboust, S., Glodny, J., 2020. Exhumation of eclogitic ophiolitic nappes in the W. Alps: New age data and implications for crustal wedge dynamics. Lithos 356–357, 105374. https://doi.org/10.1016/j.lithos.2020.105374

Bachmann, R., Glodny, J., Oncken, O., Seifert, W., 2009. Abandonment of the South Penninic–Austroalpine palaeosubduction zone, Central Alps, and shift from subduction erosion to accretion: constraints from Rb/Sr geochronology. Journal of the Geological Society 166, 217–231. https://doi.org/10.1144/0016-76492008-024

Balestro, G., Festa, A., Borghi, A., Castelli, D., Gattiglio, M., Tartarotti, P., 2018. Role of Late Jurassic intra-oceanic structural inheritance in the Alpine tectonic evolution of the Monviso meta-ophiolite Complex (Western Alps). Geol. Mag. 155, 233–249. https://doi.org/10.1017/S0016756817000553

Balestro, G., Festa, A., Dilek, Y., 2019. Structural architecture of the Western Alpine Ophiolites, and the Jurassic seafloor spreading tectonics of the Alpine Tethys. Journal of the Geological Society 176, 913–930. https://doi.org/10.1144/jgs2018-099

Ballèvre, M., Merle, O., 1993. The Combin Fault : compressional reactivation of a Late Cretaceous-Early Tertiary detachment fault in the Western Alps. Schweizerische Mineralogische Und Petrographische Mitteilungen 73, 205–227. https://doi.org/10.5169/SEALS-55570

Ballèvre, M, Lagabrielle, Y, 1994. Garnet in blueschist-facies marbles from the Queyras unit (Western Alps): its occurrence and its significance. Schweizerische Mineralogische Und Petrographische Mitteilungen 74, 203–212.

Ballèvre, M., Kienast, J.-R., Vuichard, J.-P., 1986. La “nappe de la Dent-Blanche” (Alpes occidentales) : deux unités austroalpines indépendantes. Eclogae Geologicae Helvetiae 79, 57–74. https://doi.org/10.5169/SEALS-165826

Ballèvre, M., Lagabrielle, Y., Merle, O., 1990. Tertiary ductile normal faulting as a consequence of lithospheric stacking in the western Alps. Mémoires de la Société géologique de France 156, 227–236.

Barféty, J.-C., Polino, R, Mercier, D, 2006. Notice explicative de la feuille Névache-Bardonecchia-Modane à 1/50000 (799) - Orléans : BRGM.

Bearth, P, 1959. Uber Eklogite, Glaukophanschiefer und metamorphe Pillowlaven. Schweizerische Mineralogische Und Petrographische Mitteilungen 39, 267–286.

Bearth, P, 1962. Versuch einer Gliederung alpinmetamorpher Serien der Westalpen. Schweizerische Mineralogische Und Petrographische Mitteilungen 42, 127–137.

Bearth, P, 1967. Die Ophiolite der Zone von Zermatt – Saas Fee. Beitr. Geol.Karte Schweiz 132.

Bebout, G.E., Agard, P., Kobayashi, K., Moriguti, T., Nakamura, E., 2013. Devolatilization history and trace element mobility in deeply subducted sedimentary rocks: Evidence from Western Alps HP/UHP suites. Chemical Geology 342, 1–20. https://doi.org/10.1016/j.chemgeo.2013.01.009

Behr, W.M., Becker, T.W., 2018. Sediment control on subduction plate speeds. Earth and Planetary Science Letters 502, 166–173. https://doi.org/10.1016/j.epsl.2018.08.057

Behr, W.M., Bürgmann, R., 2021. What’s down there? The structures, materials and environment of deep-seated slow slip and tremor. Phil. Trans. R. Soc. A. 379, 20200218. https://doi.org/10.1098/rsta.2020.0218

Behr, W.M., Kotowski, A.J., Ashley, K.T., 2018. Dehydration-induced rheological heterogeneity and the deep tremor source in warm subduction zones. Geology 46, 475–478. https://doi.org/10.1130/G40105.1

Bellahsen, N., Mouthereau, F., Boutoux, A., Bellanger, M., Lacombe, O., Jolivet, L., Rolland, Y., 2014. Collision kinematics in the western external Alps: Kinematics of the Alpine collision. Tectonics 33, 1055–1088. https://doi.org/10.1002/2013TC003453

Berger, A., Bousquet, R., 2008. Subduction-related metamorphism in the Alps: review of isotopic ages based on petrology and their geodynamic consequences. Geological Society, London, Special Publications 298, 117–144. https://doi.org/10.1144/SP298.7

Beyssac, O., Goffé, B., Chopin, C., Rouzaud, J.N., 2002. Raman spectra of carbonaceous material in metasediments: a new geothermometer. Journal of Metamorphic Geology 20, 859–871. https://doi.org/10.1046/j.1525-1314.2002.00408.x

Beyssac, O., Goffé, B., Petitet, J.-P., Froigneux, E., Moreau, M., Rouzaud, J.-N., 2003. On the characterization of disordered and heterogeneous carbonaceous materials by Raman spectroscopy. Spectrochimica Acta Part A: Molecular and Biomolecular Spectroscopy 59, 2267–2276. https://doi.org/10.1016/S1386-1425(03)00070-2

Bocchio, R., Benciolini, L., Martin, S., Tartarotti, P., 2000. Geochemistry of eclogitised Fe-Ti-gabbros from various lithological settings (Aosta Valley ophiolites, Italian western Alps). Protolith composition and eclogitic paragenesis. Periodico di Mineralogia 69, 217–237.

Bocquet, J, 1974. Etudes minéralogiques et pétrologiques sur les métamorphismes d'âge alpin dans les alpes françaises. PhD thesis Université de Grenoble.

Bodinier, J.-L., Menzies, M.A., Thirlwall, M.F., 1991. Continental to Oceanic Mantle Transition--REE and Sr-Nd Isotopic Geochemistry of the Lanzo Lherzolite Massif. Journal of Petrology Special_Volume, 191–210. https://doi.org/10.1093/petrology/Special_Volume.2.191

Bonnet, G., Agard, P., Angiboust, S., Monié, P., Jentzer, M., Omrani, J., Whitechurch, H., Fournier, M., 2018. Tectonic slicing and mixing processes along the subduction interface: The Sistan example (Eastern Iran). Lithos 310–311, 269–287. https://doi.org/10.1016/j.lithos.2018.04.016

Bonnet, G, Chopin, C, Locatelli, M, Kylander-Clark, A. R. C., Hacker, B. R., submitted. Protracted subduction of the European hyperextended margin exposed in the Dora-Maira massif (W. Alps).

Bourbon, M, Caron, J.M., Lemoine, M, Tricart, P, 1979. Stratigraphie des schistes lustrés piémontais dans les Alpes cottiennes (Alpes occidentales franco-italiennes): nouvelle interprétation et conséquences géodynamiques. Bulletin de la Societe Geologique de France 180–2182.

Bousquet, R., 2008. Metamorphic heterogeneities within a single HP unit: Overprint effect or metamorphic mix? Lithos 103, 46–69. https://doi.org/10.1016/j.lithos.2007.09.010

Bousquet, R., Oberhansli, R., Goffe, B., Jolivet, L., Vidal, O., 1998. High-pressure-low-temperature metamorphism and deformation in the Bundnerschiefer of the Engadine window: implications for the regional evolution of the eastern Central Alps. J Metamorph Geol 16, 657–674. https://doi.org/10.1111/j.1525-1314.1998.00161.x

Bousquet, R., Goffé, B., Vidal, O., Oberhänsli, R., Patriat, M., 2002. The tectono-metamorphic history of the Valaisan domain from the Western to the Central Alps: New constraints on the evolution of the Alps. Geological Society of America Bulletin 114, 207–225. https://doi.org/10.1130/0016-7606(2002)114<0207:TTMHOT>2.0.CO;2

Bousquet, R., Oberhänsli, R., Goffé, B., Wiederkehr, M., Koller, F., Schmid, S.M., Schuster, R., Engi, M., Berger, A., Martinotti, G., 2008. Metamorphism of metasediments at the scale of an orogen: a key to the Tertiary geodynamic evolution of the Alps. Geological Society, London, Special Publications 298, 393–411. https://doi.org/10.1144/SP298.18

Bowtell, S.A., Cliff, R.A., Barnicoat, A.C., 1994. Sm-Nd isotopic evidence on the age of eclogitization in the Zermatt-Saas ophiolite. J Metamorph Geol 12, 187–196. https://doi.org/10.1111/j.1525-1314.1994.tb00013.x

Broadwell, K.S., Locatelli, M., Verlaguet, A., Agard, P., Caddick, M.J., 2019. Transient and periodic brittle deformation of eclogites during intermediate-depth subduction. Earth and Planetary Science Letters 521, 91–102. https://doi.org/10.1016/j.epsl.2019.06.008

Bucher, K., Grapes, R., 2009. The Eclogite-facies Allalin Gabbro of the Zermatt-Saas Ophiolite, Western Alps: a Record of Subduction Zone Hydration. Journal of Petrology 50, 1405–1442. https://doi.org/10.1093/petrology/egp035

Bucher, S., Schmid, S.M., Bousquet, R., Fugenschuh, B., 2003. Late-stage deformation in a collisional orogen (Western Alps): nappe refolding, back-thrusting or normal faulting? Terra Nova 15, 109–117. https://doi.org/10.1046/j.1365-3121.2003.00470.x

Bucher, K., Fazis, Y, De Capitani, C, Grapes, R, 2005. Blueschists, eclogites, and decompression assemblages of the Zermatt-Saas ophiolite: High-pressure metamorphism of subducted Tethys lithosphere. American Mineralogist 90, 821–835. https://doi.org/10.2138/am.2005.1718

Busigny, V., Cartigny, P., Philippot, P., 2011. Nitrogen isotopes in ophiolitic metagabbros: A re-evaluation of modern nitrogen fluxes in subduction zones and implication for the early Earth atmosphere. Geochimica et Cosmochimica Acta 75, 7502–7521. https://doi.org/10.1016/j.gca.2011.09.049

Busigny, V., Chen, J., Philippot, P., Borensztajn, S., Moynier, F., 2018. Insight into hydrothermal and subduction processes from copper and nitrogen isotopes in oceanic metagabbros. Earth and Planetary Science Letters 498, 54–64. https://doi.org/10.1016/j.epsl.2018.06.030

Caby, R., 1996. Low-angel extrusion of high-pressure rocks and the balance between outward and inward displacements of Middle Penninic units in the western Alps. Eclogae Geologicae Helvetiae 89/1, 229–267. https://doi.org/10.5169/SEALS-167901

Caby, R, Kienast, J. R., Saliot, P, 1976. Modèle d'évolution structurale des Alpes occidentales. Colloque International CNRS, Ecologie et Géologie de l'Himalaya 85–92.

Caby, R., Kienast, J.-R., Saliot, P., 1978. Structure, métamorphisme et modèle d'évolution tectonique des Alpes occidentales. Revue de géographie physique et de géologie dynamique Paris, 20, 307–322.

Cadoppi, P, Castelletto, M, Sacchi, R, Baggio, P, Carraro, F, Giraud, V, 2002. Note illustrative della carta geologica d'Italia alla scala 1:50000: foglio 154 Susa. ISPRA, Servizio Geologico d'Italia.

Caron, J.-M., 1974. Rapports entre diverses" generations" de lawsonite et les deformations dans les Schistes lustres des Alpes cottiennes septentrionales (France et Italie). Bulletin de la Société Géologique de France 7, 256–263.

Caron, J.M., 1977. Lithostratigraphie et tectonique des Schistes Lustrés dans les Alpes Cottiennes septentrionales et en Corse orientale. PhD thesis, université de Strasbourg.

Chopin, C, 1978. Les paragenèses réduites ou oxydées de concentrations manganésifères des «schistes lustrés» de Haute-Maurienne (Alpes françaises). Bulletin de Minéralogie 101, 514–531.

Chopin, C, 1979. De la Vanoise au massif du Grand Paradis, Une approche pétrographique et radiochronologique de la signification géodynamique du métamorphisme de haute pression. PhD thesis Université Pierre et Marie Curie, Paris 6.

Chopin, C., 1984. Coesite and pure pyrope in high-grade blueschists of the Western Alps: a first record and some consequences. Contr. Mineral. and Petrol. 86, 107–118. https://doi.org/10.1007/BF00381838

Chopin, C, Maluski, H, 1980. 40Ar-39Ar dating of high pressure metamorphic micas from the Gran Paradiso area (Western Alps): Evidence against the blocking temperature concept. Contributions to Mineralogy and Petrology 74, 109–122.

Compagnoni, R., Rolfo, F., 2003. UHPM units in the Western Alps, in: Papp, G., Weiszburg, T.G., Carswell, D.A., Compagnoni, R., Rolfo, F. (Eds.), Ultrahigh Pressure Metamorphism. Mineralogical Society of Great Britain and Ireland, Budapest, pp. 13–49. https://doi.org/10.1180/EMU-notes.5.2

Connolly, J. A. D., 1990. Multivariable phase diagrams: an algorithm based on generalized thermodynamics. American Journal of Science 290, 666–718.

Connolly, J.A.D., 2005. Computation of phase equilibria by linear programming: A tool for geodynamic modeling and its application to subduction zone decarbonation. Earth and Planetary Science Letters 236, 524–541. https://doi.org/10.1016/j.epsl.2005.04.033

Connolly, J.A.D., 2009. The geodynamic equation of state: What and how. Geochem. Geophys. Geosyst. 10, n/a-n/a. https://doi.org/10.1029/2009GC002540

Corno, A., Mosca, P., Borghi, A., Gatteggio, M., 2019. Lithostratigraphy and petrography of the Monte Banchetta-Punta Rognosa oceanic succession (Troncea and Chisonetto Valleys, Western Alps). Ofioliti 44. https://doi.org/10.4454/ofioliti.v44i2.526

Corno, A., Groppo, C., Mosca, P., Borghi, A., Gattiglio, M., 2021. Eclogitic metamorphism in the Alpine far-west: petrological constraints on the Banchetta-Rognosa tectonic unit (Val Troncea, Western Alps). Swiss J Geosci 114, 16. https://doi.org/10.1186/s00015-021-00393-7

Cubas, N, Agard, P, Tissandier, R, submitted. Predicting earthquake ruptures from topography.

Dal Piaz, G.V., 1974a. Le métamorphisme de haute pression et basse température dans l'évolution structurale du bassin ophiolitique alpino-apenninique. 1ère partie : Considérations paléogéographiques. Bolletino della Societa Geologica Italiana 93, 437–467.

Dal Piaz, G.V., 1974b. Le métamorphisme de haute pression et basse température dans l'évolution structurale du bassin ophiolitique alpino-apenninique. Schweizerische Mineralogische Und Petrographische Mitteilungen 54, 399–424.

Dal Piaz, G.V., Cortiana, G, Del Moro, A, Martin, S, Pennachioni, G, Tartarotti, P, 2001. Tertiary age and paleostructural inferences of the eclogitic imprint in the Austroalpine outliers and Zermatt-Saas ophiolite, western Alps. International Journal of Earth Sciences (Geol Rundsch) 90, 668–684.

Dal Piaz, G.V., Gianotti, F, Monopoli, B, Pennachioni, G, Tartarotti, P, Schiavo, A, 2010. Note illustrative della carta geologica d'Italia alla scala 1:50000: foglio 091 Chatillon. ISPRA, Servizio Geologico d'Italia.

de Meyer, C.M.C., Baumgartner, L.P., Beard, B.L., Johnson, C.M., 2014. Rb–Sr ages from phengite inclusions in garnets from high pressure rocks of the Swiss Western Alps. Earth and Planetary Science Letters 395, 205–216. https://doi.org/10.1016/j.epsl.2014.03.050

De Togni, M., Gattiglio, M., Ghignone, S., Festa, A., 2021. Pre-Alpine Tectono-Stratigraphic Reconstruction of the Jurassic Tethys in the High-Pressure Internal Piedmont Zone (Stura di Viù Valley, Western Alps). Minerals 11, 361. https://doi.org/10.3390/min11040361

De Wever, P., Caby, R., 1981. Datation de la base des schistes lustrés postophiolitiques par des radiolaires (Oxfordien-Kimmeridgien moyen) dans les Alpes Cottiennes (Saint Véran, France). Comptes Rendus de l'Académie des Sciences de Paris 292, 467–472.

De Wever, P., Baumgartner, P.O., Polino, R., 1987a. Précision sur les datations de la base des Schistes Lustrés postophiolitiques dans les Alpes cottiennes. Comptes Rendus de l'Académie des Sciences de Paris 305, 487–491.

De Wever, P., Danelian, T., Durand-Delga, M., Cordey, M., Kito, N., 1987b. Datations des radiolarites post-ophiolitiques de Corse alpine à l'aide des Radiolaires. Comptes Rendus de l'Académie des Sciences de Paris 305, 893–900.

Debelmas, J, Caby, R, Desmons, J, 1991. Notice explicative de la feuille Sainte-Foy-Tarentaise à 1/50000 (728) - Orléans : BRGM.

Debret, B., Nicollet, C., Andreani, M., Schwartz, S., Godard, M., 2013. Three steps of serpentinization in an eclogitized oceanic serpentinization front (Lanzo Massif - Western Alps). Journal of Metamorphic Geology 31, 165–186. https://doi.org/10.1111/jmg.12008

Decandia, F.A., Elter, P, 1969. Riflessioni sul problema delle ofioliti nell'Appennino settentrionale (Nota preliminare). Atti Societa Toscana delle Science Naturali : memorie Serie A, 76, 1–9.

Decandia, F.A., Elter, P, 1972. La" zona" ofiolitifera del Bracco nel settore compreso fra Levanto e la Val Gravena (Apennino ligure). Bolletino della Societa Geologica Italiana 11, 37–64.

Decrausaz, T., Müntener, O., Manzotti, P., Lafay, R., Spandler, C., 2021. Fossil oceanic core complexes in the Alps. New field, geochemical and isotopic constraints from the Tethyan Aiguilles Rouges Ophiolite (Val d'Hérens, Western Alps, Switzerland). Swiss J Geosci 114, 3. https://doi.org/10.1186/s00015-020-00380-4

Delaloye, M., Desmons, J., 1976. K-Ar Radiometric Age Determinations of White Micas from the Piemont Zone, French-Italian Western Alps. Contributions to Mineralogy and Petrology 57, 297–303. https://doi.org/10.1007/BF03542939

Deville, E, 1986. La klippe de la Pointe du Grand Vallon (Vanoise-Alpes occidentales) : un lambeau de métasédiments à foraminifères du Maastrichtien supérieur couronnant les nappes de « schistes lustrés ». Comptes rendus de l'Académie des sciences. Série 2, Mécanique, Physique, Chimie, Sciences de l'univers, Sciences de la Terre 303, 1221–1226.

Deville, E, 1987. Etude géologique en Vanoise orientale (Alpes occidentales, Savoie). De la naissance à la structuration d'un secteur de la paléo-marge européenne et de l'océan téthysien : aspects stratigraphiques, pétrographiques et tectoniques. PhD thesis Université de Savoie.

Deville, E., Fudral, S., Lagabrielle, Y., Marthaler, M., Sartori, M., 1992. From oceanic closure to continental collision: A synthesis of the" Schistes lustrés" metamorphic complex of the Western Alps. Geological Society of America Bulletin 104, 127–139.

Dragovic, B., Angiboust, S., Tappa, M.J., 2020. Petrochronological close-up on the thermal structure of a paleo-subduction zone (W. Alps). Earth and Planetary Science Letters 547, 116446. https://doi.org/10.1016/j.epsl.2020.116446

Droop, G.T.R., Lombardo, B, Pognante, U, 1990. Formation and distribution of eclogite facies rocks in the Alps. In: Carswell, D.A. (Ed.), Eclogite Facies Rocks: Glasgow. Blackie, United Kingdom, 225–259.

Duchène, S., Blichert-Toft, J., Luais, B., Télouk, P., Lardeaux, J.-M., Albarède, F., 1997. The Lu–Hf dating of garnets and the ages of the Alpine high-pressure metamorphism. Nature 387, 586–589. https://doi.org/10.1038/42446

Duesterhoeft, E., Quinteros, J., Oberhänsli, R., Bousquet, R., de Capitani, C., 2014. Relative impact of mantle densification and eclogitization of slabs on subduction dynamics: A numerical thermodynamic/thermokinematic investigation of metamorphic density evolution. Tectonophysics 637, 20–29. https://doi.org/10.1016/j.tecto.2014.09.009

Dumitru, T.A., Wakabayashi, J., Wright, J.E., Wooden, J.L., 2010. Early Cretaceous transition from nonaccretionary behavior to strongly accretionary behavior within the Franciscan subduction complex: ACCRETION IN THE FRANCISCAN COMPLEX. Tectonics 29. https://doi.org/10.1029/2009TC002542

Dumont, T, Lemoine, M, Tricart, P, 1984. Pérennité de la sédimentation pélagique du Jurassique supérieur jusque dans le crétacé supérieur au-dessus de la croûte océanique téthysienne ligure : la série supra-ophiolitique du lac des Cordes (zone piémontaise des Alpes occidentales au SE de Briançon). Comptes rendus de l'Académie des sciences. Série 2, Mécanique, Physique, Chimie, Sciences de l'univers, Sciences de la Terre 7, 921–933.

Ellero, A., Loprieno, A., 2018. Nappe stack of Piemonte–Ligurian units south of A osta V alley: New evidence from Urtier Valley (Western Alps). Geological Journal 53, 1665–1684. https://doi.org/10.1002/gj.2984

Elter, G, 1971. Schistes lustrés et ophiolites de la zone piémontaise entre Orco et Doire Baltée (Alpes Graies). Hypothèses sur l'origine des ophiolites. Géologie Alpine 47, 147–169.

Tobin, H., Hirose, T., Ikari, M., Kanagawa, K., Kimura, G., Kinoshita, M., Kitajima, H., Saffer, D., Yamaguchi, A., Eguchi, N., Maeda, L., Toczko, S., 2019. Expedition 358 Preliminary Report: NanTroSEIZE Plate Boundary Deep Riser 4: Nankai Seismogenic/Slow Slip Megathrust, International Ocean Discovery Program Preliminary Report. International Ocean Discovery Program. https://doi.org/10.14379/iodp.pr.358.2019

Frezzotti, M.L., Selverstone, J., Sharp, Z.D., Compagnoni, R., 2011. Carbonate dissolution during subduction revealed by diamond-bearing rocks from the Alps. Nature Geosci 4, 703–706. https://doi.org/10.1038/ngeo1246

Fudral, S., 1996. Etude géologique de la suture tethysienne dans les Alpes franco-italiennes Nord-Occidentales de la Doire Ripaire (Italie) à la région de Bourg Saint-Maurice. PhD thesis Université de Savoie.

Fudral, S., Deville, E., Marthaler, M., 1987. Distinction de trois ensembles d'unités dans les «Schistes lustrés» compris entre la Vanoise et le Val de Suse (Alpes franco-italiennes septentrionales): aspects lithostratigraphiques, paléogéographiques et géodynamiques. Comptes rendus de l'Académie des sciences. Série 2, Mécanique, Physique, Chimie, Sciences de l'univers, Sciences de la Terre, 305, 467–472.

Gabalda, S., Beyssac, O., Jolivet, L., Agard, P., Chopin, C., 2009. Thermal structure of a fossil subduction wedge in the Western Alps. Terra Nova 21, 28–34. https://doi.org/10.1111/j.1365-3121.2008.00849.x

Garber, J.M., Smye, A.J., Feineman, M.D., Kylander-Clark, A.R.C., Matthews, S., 2020a. Decoupling of zircon U–Pb and trace-element systematics driven by U diffusion in eclogite-facies zircon (Monviso meta-ophiolite, W. Alps). Contrib Mineral Petrol 175, 55. https://doi.org/10.1007/s00410-020-01692-2

Garber, J.M., Rioux, M., Kylander-Clark, A.R.C., Hacker, B.R., Vervoort, J.D., Searle, M.P., 2020b. Petrochronology of Wadi Tayin Metamorphic Sole Metasediment, With Implications for the Thermal and Tectonic Evolution of the Samail Ophiolite (Oman/UAE). Tectonics 39. https://doi.org/10.1029/2020TC006135

Ghignone, S., Borghi, A., Balestro, G., Castelli, D., Gattiglio, M., Groppo, C., 2021a. HP tectono-metamorphic evolution of the Internal Piedmont Zone in Susa Valley (Western Alps): New petrologic insight from garnet+chloritoid-bearing micaschists and Fe–Ti metagabbro. Journal of Metamorphic Geology 39, 391-416.

Ghignone, S., Sudo, M., Balestro, G., Borghi, A., Gattiglio, M., Ferrero, S., van Schijndel, V., 2021b. Timing of exhumation of meta-ophiolite units in the Western Alps: New tectonic implications from 40Ar/39Ar white mica ages from Piedmont Zone (Susa Valley). Lithos 404–405, 106443. https://doi.org/10.1016/j.lithos.2021.106443

Goffé, B., Chopin, C., 1986. High-pressure metamorphism in the Western Alps : zoneography of metapelites, chronology and consequences. Schweizerische Mineralogische Und Petrographische Mitteilungen 66, 41–52. https://doi.org/10.5169/SEALS-50880

Goffé, B., Bousquet, R., 1997. Ferrocarpholite, chloritoid and lawsonite in metapelites of the Versoyen and Petit St Bernard units (Valais zone, Western Alps). Schweizerische Mineralogische und Petrographische Mitteilunge 77, 137–147.

Goffé, B., Schwartz, S., Lardeaux, J.-M., Bousquet, R., 2004. Explanatory notes of the map: metamorphic structure of the Alps Western and Ligurian Alps. MITT.ÖSTERR.MINER.GES. 125–144.

Gouzu, C., Itaya, T., Hyodo, H., Matsuda, T., 2006. Excess 40Ar-free phengite in ultrahigh-pressure metamorphic rocks from the Lago di Cignana area, Western Alps. Lithos 92, 418–430. https://doi.org/10.1016/j.lithos.2006.03.056

Gouzu, C., Yagi, K., Thanh, N.X., Itaya, T., Compagnoni, R., 2016. White mica K–Ar geochronology of HP–UHP units in the Lago di Cignana area, western Alps, Italy: Tectonic implications for exhumation. Lithos 248–251, 109–118. https://doi.org/10.1016/j.lithos.2016.01.015

Groppo, C., Castelli, D., 2010. Prograde P–T Evolution of a Lawsonite Eclogite from the Monviso Meta-ophiolite (Western Alps): Dehydration and Redox Reactions during Subduction of Oceanic FeTi-oxide Gabbro. Journal of Petrology 51, 2489–2514. https://doi.org/10.1093/petrology/egq065

Groppo, C., Beltrando, M., Compagnoni, R., 2009. The P-T path of the ultra-high pressure Lago Di Cignana and adjoining high-pressure meta-ophiolitic units: insights into the evolution of the subducting Tethyan slab. Journal of Metamorphic Geology 27, 207–231. https://doi.org/10.1111/j.1525-1314.2009.00814.

Guillot, S., Hattori, K., Agard, P., Schwartz, S., Vidal, O., 2009. Exhumation Processes in Oceanic and Continental Subduction Contexts: A Review, in: Lallemand, S., Funiciello, F. (Eds.), Subduction Zone Geodynamics, Frontiers in Earth Sciences. Springer Berlin Heidelberg, Berlin, Heidelberg, pp. 175–205. https://doi.org/10.1007/978-3-540-87974-9_10

Guillot, S., Schwartz, S., Reynard, B., Agard, P., Prigent, C., 2015. Tectonic significance of serpentinites. Tectonophysics 646, 1–19. https://doi.org/10.1016/j.tecto.2015.01.020

Hacker, B.R., Peacock, S.M., Abers, G.A., Holloway, S.D., 2003. Subduction factory 2. Are intermediate-depth earthquakes in subducting slabs linked to metamorphic dehydration reactions?: SUBDUCTION ZONE EARTHQUAKES AND DEHYDRATION. J. Geophys. Res. 108. https://doi.org/10.1029/2001JB001129

Handy, M.R., 2010. Reconciling plate-tectonic reconstructions of Alpine Tethys with the geological–geophysical record of spreading and subduction in the Alps 38.

Henry, C., Burkhard, M., Goffé, B., 1996. Evolution of synmetamorphic veins and their wallrocks through a Western Alps transect: no evidence for large-scale fluid flow. Stable isotope, major- and trace-element systematics. Chemical Geology 127, 81–109. https://doi.org/10.1016/0009-2541(95)00106-9

Hertgen, S., Yamato, P., Morales, L.F.G., Angiboust, S., 2017. Evidence for brittle deformation events at eclogite-facies P-T conditions (example of the Mt. Emilius klippe, Western Alps). Tectonophysics 706–707, 1–13. https://doi.org/10.1016/j.tecto.2017.03.028

Herviou, C., Verlaguet, A., Agard, P., Locatelli, M., Raimbourg, H., Lefeuvre, B., Dubacq, B., 2021. Along-dip variations of subduction fluids: The 30–80 km depth traverse of the Schistes Lustrés complex (Queyras-Monviso, W. Alps). Lithos 394–395, 106168. https://doi.org/10.1016/j.lithos.2021.106168

Holland, T.J.B., Powell, R., 1998. An internally consistent thermodynamic data set for phases of petrological interest: AN INTERNALLY CONSISTENT THERMODYNAMIC DATA SET. Journal of Metamorphic Geology 16, 309–343. https://doi.org/10.1111/j.1525-1314.1998.00140.x

Holland, T., Baker, J., Powell, R., 1998. Mixing properties and activity-composition relationships of chlorites in the system MgO-FeO-Al2O3-SiO2-H2O. ejm 10, 395–406. https://doi.org/10.1127/ejm/10/3/0395

Ikari, M.J., Kopf, A.J., Hüpers, A., Vogt, C., 2018. Lithologic control of frictional strength variations in subduction zone sediment inputs. Geosphere 14, 604–625. https://doi.org/10.1130/GES01546.1

Incel, S., Hilairet, N., Labrousse, L., John, T., Deldicque, D., Ferrand, T., Wang, Y., Renner, J., Morales, L., Schubnel, A., 2017. Laboratory earthquakes triggered during eclogitization of lawsonite-bearing blueschist. Earth and Planetary Science Letters 459, 320–331. https://doi.org/10.1016/j.epsl.2016.11.047

Jolivet, L., Goffé, B., Monié, P., Truffert-Luxey, C., Patriat, M., Bonneau, M., 1996. Miocene detachment in Crete and exhumation P-T-t paths of high-pressure metamorphic rocks. Tectonics 15, 1129–1153. https://doi.org/10.1029/96TC01417

Jolivet, L., Faccenna, C., Goffé, B., Mattei, M., Rossetti, F., Brunet, C., Storti, F., Funiciello, R., Cadet, J.P., d'Agostino, N., Parra, T., 1998. Midcrustal shear zones in postorogenic extension: Example from the northern Tyrrhenian Sea. J. Geophys. Res. 103, 12123–12160. https://doi.org/10.1029/97JB03616

Kameda, J., Inoue, S., Tanikawa, W., Yamaguchi, A., Hamada, Y., Hashimoto, Y., Kimura, G., 2017. Alteration and dehydration of subducting oceanic crust within subduction zones: implications for décollement step-down and plate-boundary seismogenesis. Earth Planets Space 69, 52. https://doi.org/10.1186/s40623-017-0635-1

Karig, D.E., Sharman, G.F., 1975. Subduction and Accretion in Trenches. Geol Soc America Bull 86, 377–389. https://doi.org/10.1130/0016-7606(1975)86<377:SAAIT>2.0.CO;2

Kerswell, B.C., Kohn, M.J., Gerya, T.V., 2021. Backarc Lithospheric Thickness and Serpentine Stability Control Slab-Mantle Coupling Depths in Subduction Zones. Geochem Geophys Geosyst 22. https://doi.org/10.1029/2020GC009304

Kienast, J. R., 1973. Sur l'existence de deux séries différentes au sein de l'ensemble schistes lustrés-ophiolites du val d'Aoste ; quelques arguments fondés sur l'étude des roches métamorphiques. Comptes Rendus de l'Académie des Sciences de Paris 276, 2621–2624.

Kimura, G., Ludden, J., 1995. Peeling oceanic crust in subduction zones. Geol 23, 217–220. https://doi.org/10.1130/0091-7613(1995)023<0217:POCISZ>2.3.CO;2

Kimura, G., Maruyama, S., Isozaki, Y., Terabayashi, M., 1996. Well-preserved underplating structure of the jadeitized Franciscan complex, Pacheco Pass, California. Geol 24, 75. https://doi.org/10.1130/0091-7613(1996)024<0075:WPUSOT>2.3.CO;2

Kimura, G., Kitamura, Y., Hashimoto, Y., Yamaguchi, A., Shibata, T., Ujiie, K., Okamoto, S., 2007. Transition of accretionary wedge structures around the up-dip limit of the seismogenic subduction zone. Earth and Planetary Science Letters 255, 471–484. https://doi.org/10.1016/j.epsl.2007.01.005

Kita, S., Okada, T., Nakajima, J., Matsuzawa, T., Hasegawa, A., 2006. Existence of a seismic belt in the upper plane of the double seismic zone extending in the along-arc direction at depths of 70–100 km beneath NE Japan. Geophys. Res. Lett. 33, L24310. https://doi.org/10.1029/2006GL028239

Kunz, P., 1988. Ophiolites penniques et sédiments associés dans la région d'Arolla (val d'Hérens, Valais, Suisse). Eclogae Geologicae Helvetiae 81, 115–124. https://doi.org/10.5169/SEALS-166172

Lagabrielle, Y., 1987. Les ophiolites : Marqueurs de l'histoire tectonique des domaines océaniques. PhD thesis Brest.

Lagabrielle, Y, Polino, R, 1988. Un schéma structural du domaine des Schistes lustrés ophiolitifères au nord-ouest du massif du Mont Viso (Alpes Sud-Occidentales) et ses implications. Comptes rendus de l'Académie des sciences. Série 2, Mécanique, Physique, Chimie, Sciences de l'univers, Sciences de la Terre, 306, 921–928.

Lagabrielle, Y., Cannat, M., 1990. Alpine Jurassic ophiolites resemble the modern central Atlantic basement. Geology 18, 319–322.

Lagabrielle, Y., Fudral, S., Kienast, J.-R., 1990. La couverture océanique des ultrabasites de Lanzo (Alpes occidentales) : arguments lithostratigraphiques et pétrologiques. Geodinamica Acta 4, 43–55. https://doi.org/10.1080/09853111.1990.11105199

Lagabrielle, Y., Vitale Brovarone, A., Ildefonse, B., 2015. Fossil oceanic core complexes recognized in the blueschist metaophiolites of Western Alps and Corsica. Earth-Science Reviews 141, 1–26. https://doi.org/10.1016/j.earscirev.2014.11.004

Lahfid, A., Beyssac, O., Deville, E., Negro, F., Chopin, C., Goffé, B., 2010. Evolution of the Raman spectrum of carbonaceous material in low-grade metasediments of the Glarus Alps (Switzerland): RSCM in low-grade metasediments. Terra Nova 22, 354–360. https://doi.org/10.1111/j.1365-3121.2010.00956.x

Lanari, P, 2012. Micro-cartographie P-T-ε dans les roches métamorphiques. Applications aux Alpes et à l'Himalaya. PhD thesis, Université de Grenoble.

Lapen, T.J., Johnson, C.M., Baumgartner, L.P., Mahlen, N.J., Beard, B.L., Amato, J.M., 2003. Burial rates during prograde metamorphism of an ultra-high-pressure terrane: an example from Lago di Cignana, western Alps, Italy. Earth and Planetary Science Letters 215, 57–72. https://doi.org/10.1016/S0012-821X(03)00455-2

Lay, T., Kanamori, H., Ammon, C.J., Koper, K.D., Hutko, A.R., Ye, L., Yue, H., Rushing, T.M., 2012. Depth-varying rupture properties of subduction zone megathrust faults: MEGATHRUST RUPTURE DOMAINS. J. Geophys. Res. 117, n/a-n/a. https://doi.org/10.1029/2011JB009133

Le Pichon, X., Bergerat, F., Roulet, M., 1988. Plate kinematics and tectonics leading to the Alpine belt formation: a new analysis. Geological Society of America Special Issue 218, 111–131.

Lefeuvre, B., Agard, P., Verlaguet, A., Dubacq, B., Plunder, A., 2020. Massive formation of lawsonite in subducted sediments from the Schistes Lustrés (W. Alps): Implications for mass transfer and decarbonation in cold subduction zones. Lithos 370–371, 105629. https://doi.org/10.1016/j.lithos.2020.105629

Lemoine, M, 1959. Remarques a propos de quelques faits et hypotheses concernant l'age des Schistes lustres piemontais dans les Alpes cottiennes et brianconnaises. Bulletin de la Société Géologique de France 7, 90–92.

Lemoine, M, 1971. Données nouvelles sur la série du Gondran près Briançon (Alpes Cottiennes). Réflexions sur les problèmes stratigraphique et paléographique de la zone piémontaise. Géologie Alpine 47, 181–201.

Lemoine, M., 2003. Schistes lustrés from Corsica to Hungary : back to the original sediments and tentative dating of partly azoic metasediments. Bulletin de la Société Géologique de France 174, 197–209. https://doi.org/10.2113/174.3.197

Lemoine, M., Tricart, P., 1986. Les Schistes lustrés piémontais des Alpes Occidentales : approche stratigraphique, structurales et sédimentologique. Eclogae Geologicae Helvetiae 79, 271–294. https://doi.org/10.5169/SEALS-165835

Lemoine, M, Steen, D.M., Vuagnat, M, 1970. Sur le problème stratigraphique des ophiolites piémontaises et des roches sédimentaires associées: observations dans le massif de Chabrière en Haute-Ubaye (Basses-Alpes, France). Compte rendu des séances de la Société de physique et d'histoire naturelle de Genève 5, 44–59.

Lemoine, M., Marthaler, M., Caron, M., Sartori, M., Amaudric du Chaffaut, S., 1984. Découverte de foraminifères planctoniques du Crétacé supérieur dans les schistes lustrés du Queyras (Alpes occidentales). Conséquences paléogéographiques et tectoniques. Comptes-rendus des séances de l'Académie des sciences. Série 2, Mécanique-physique, chimie, sciences de l'univers, sciences de la terre 299, 727–732.

Lemoine, M., Bas, T., Arnaud-Vanneau, A., Arnaud, H., Dumont, T., Gidon, M., Bourbon, M., de Graciansky, P.-C., Rudkiewicz, J.-L., Megard-Galli, J., Tricart, P., 1986. The continental margin of the Mesozoic Tethys in the Western Alps. Marine and Petroleum Geology 3, 179-199.

Liewig, N, 1981. Les phengites : marqueurs géométriques, chimiques et isotopiques de l'histoire des roches métamorphiques : application aux schistes lustres des Alpes cottiennes. PhD thesis, université de Strasbourg.

Locatelli, M., Verlaguet, A., Agard, P., Federico, L., Angiboust, S., 2018. Intermediate-depth brecciation along the subduction plate interface (Monviso eclogite, W. Alps). Lithos 320–321, 378–402. https://doi.org/10.1016/j.lithos.2018.09.028

Locatelli, M., Federico, L., Agard, P., Verlaguet, A., 2019a. Geology of the southern Monviso metaophiolite complex (W-Alps, Italy). Journal of Maps 15, 283–297. https://doi.org/10.1080/17445647.2019.1592030

Locatelli, M., Verlaguet, A., Agard, P., Pettke, T., Federico, L., 2019b. Fluid Pulses During Stepwise Brecciation at Intermediate Subduction Depths (Monviso Eclogites, W. Alps): First Internally Then Externally Sourced. Geochem. Geophys. Geosyst. 20, 5285–5318. https://doi.org/10.1029/2019GC008549

Lombardo, B., Nervo, R., Compagnoni, R., Messiga, B., Kienast, J. R., Mevel, C., Fiora, L., Piccardo, G. B., Lanza, R., 1978. Osservazioni preliminari sulle ofioliti metamorfiche del Monviso (Alpi Occidentali). Rendiconti Della Soc. Ital. Mineral. E Petrol. 34, 235–305.

Malusà, M.G., Polino, R., Zattin, M., Bigazzi, G., Martin, S., Piana, F., 2005. Miocene to Present differential exhumation in the Western Alps: Insights from fission track thermochronology: EXHUMATION IN THE WESTERN ALPS. Tectonics 24, n/a-n/a. https://doi.org/10.1029/2004TC001782

Manatschal, G., Sauter, D., Karpoff, A.M., Masini, E., Mohn, G., Lagabrielle, Y., 2011. The Chenaillet Ophiolite in the French/Italian Alps: An ancient analogue for an Oceanic Core Complex? Lithos 124, 169–184. https://doi.org/10.1016/j.lithos.2010.10.017

Manzotti, P., Ballèvre, M., Pitra, P., Schiavi, F., 2021. Missing lawsonite and aragonite found: P–T and fluid composition in meta-marls from the Combin Zone (Western Alps). Contrib Mineral Petrol 176, 60. https://doi.org/10.1007/s00410-021-01818-0

Marthaler, M., 1984. Géologie des unités penniques entre le val d'Anniviers et le val de Tourtemagne (Valais, Suisse). Eclogae Geologicae Helvetiae 77, 395–448. https://doi.org/10.5169/SEALS-165516

Marthaler, M., Stampfli, G.M., 1989. Les Schistes lustrés à ophiolites de la nappe du Tsaté : un ancien prisme d'accrétion de la marge active apulienne? Schweizerische Mineralogische und Petrographische Mitteilunge 69, 211–216. https://doi.org/10.5169/SEALS-52789

Martin, S., Rebay, G., Kienast, J.-R., Mével, C., 2008. AN ECLOGITISED OCEANIC PALAEO-HYDROTHERMAL FIELD FROM THE ST. MARCEL VALLEY (ITALIAN WESTERN ALPS) 33, 16.

Massonne, H.J., 1992. Thermochemical determination of water activities relevant to eclogitic rocks. In: Water-Rock Interaction (eds Kharaka, Y. K., and Maest, A.S.). Balkema, Rotterdam 1523–1526.

Massonne, H.J., 1995. Experimental and petrogenetic study of UHPM. In: Coleman, R.G. and Wang, X., Eds., 1995.Ultrahigh pressure metamorphism. Cambridge University Press, Cambridge 33–95.

Massonne, H.-J., Schreyer, W., 1987. Phengite geobarometry based on the limiting assemblage with K-feldspar, phlogopite, and quartz. Contr. Mineral. and Petrol. 96, 212–224. https://doi.org/10.1007/BF00375235

Massonne, H.J., Schreyer, W, 1989. Stability field of the high-pressure assemblage, talc+ phengite and two new phengite barometers. European Journal of Mineralogy 1, 391–410.

Menant, A., Angiboust, S., Gerya, T., 2019. Stress-driven fluid flow controls long-term megathrust strength and deep accretionary dynamics. Sci Rep 9, 9714. https://doi.org/10.1038/s41598-019-46191-y

Menant, A., Angiboust, S., Gerya, T., Lacassin, R., Simoes, M., Grandin, R., 2020. Transient stripping of subducting slabs controls periodic forearc uplift. Nat Commun 11, 1823. https://doi.org/10.1038/s41467-020-15580-7

Michard, A., Goffé, B., Chopin, C., Henry, C., 1996. Did the Western Alps develop through an Oman-type stage? The geotectonic setting of high-pressure metamorphism in two contrasting Tethyan transects. Eclogae Geologicae Helvetiae 89, 43–80.

Michard, A., Avigad, D., Goffé, B., Chopin, C., 2004. The high-pressure metamorphic front of the south Western Alps (Ubaye-Maira transect, France, Italy). Schweizerische Mineralogische Und Petrographische Mitteilungen 84, 215–235.

Monié, P., Agard, P., 2009. Coeval blueschist exhumation along thousands of kilometers: Implications for subduction channel processes. Geochem. Geophys. Geosyst. 10, n/a-n/a. https://doi.org/10.1029/2009GC002428

Moore, J.C., 1975. Selective subduction. Geol 3, 530. https://doi.org/10.1130/0091-7613(1975)3<530:SS>2.0.CO;2

Müntener, O., Piccardo, G.B., Polino, R., Zanetti, A., 2005. REVISITING THE LANZO PERIDOTITE (NW-ITALY): 'ASTHENOSPHERIZATION' OF ANCIENT MANTLE LITHOSPHERE. Ofioliti 30, 111–124.

Negro, F., Bousquet, R., Vils, F., Pellet, C.-M., Hänggi-Schaub, J., 2013. Thermal structure and metamorphic evolution of the Piemont-Ligurian metasediments in the northern Western Alps. Swiss J Geosci 106, 63–78. https://doi.org/10.1007/s00015-013-0119-7

Okazaki, K., Hirth, G., 2016. Dehydration of lawsonite could directly trigger earthquakes in subducting oceanic crust. Nature 530, 81–84. https://doi.org/10.1038/nature16501

Paulatto, M., Laigle, M., Galve, A., Charvis, P., Sapin, M., Bayrakci, G., Evain, M., Kopp, H., 2017. Dehydration of subducting slow-spread oceanic lithosphere in the Lesser Antilles. Nat Commun 8, 15980. https://doi.org/10.1038/ncomms15980

Peacock, S.M., 1993. The importance of blueschist → eclogite dehydration reactions in subducting oceanic crust. Geological Society of America Bulletin 105, 684–694. https://doi.org/10.1130/0016-7606(1993)105<0684:TIOBED>2.3.CO;2

Pelletier, L., Müntener, O., 2006. High-pressure metamorphism of the Lanzo peridotite and its oceanic cover, and some consequences for the Sesia–Lanzo zone (northwestern Italian Alps). Lithos 90, 111–130. https://doi.org/10.1016/j.lithos.2006.01.006

Pennacchioni, G., Scambelluri, M., Bestmann, M., Notini, L., Nimis, P., Plümper, O., Faccenda, M., Nestola, F., 2020. Record of intermediate-depth subduction seismicity in a dry slab from an exhumed ophiolite. Earth and Planetary Science Letters 548, 116490. https://doi.org/10.1016/j.epsl.2020.116490

Philippot, P., 1990. Opposite vergence of Nappes and crustal extension in the French-Italian western Alps. Tectonics 9, 1143–1164. https://doi.org/10.1029/TC009i005p01143

Piccardo, G.B., Zanetti, A., Müntener, O., 2007. Melt/peridotite interaction in the Southern Lanzo peridotite: Field, textural and geochemical evidence. Lithos 94, 181–209. https://doi.org/10.1016/j.lithos.2006.07.002

Platt, J.P., 1986. Dynamics of orogenic wedges and the uplift of high-pressure metamorphic rocks. Geol Soc America Bull 97, 1037–1053. https://doi.org/10.1130/0016-7606(1986)97<1037:DOOWAT>2.0.CO;2

Platt, J.P., 1988. The mechanics of frontal imbrication: a first-order analysis. Geol Rundsch 77, 577–589. https://doi.org/10.1007/BF01832399

Platt, J.P., Xia, H., Schmidt, W.L., 2018. Rheology and stress in subduction zones around the aseismic/seismic transition. Prog Earth Planet Sci 5, 24. https://doi.org/10.1186/s40645-018-0183-8

Plunder, A., Agard, P., Dubacq, B., Chopin, C., Bellanger, M., 2012. How continuous and precise is the record of P-T paths? Insights from combined thermobarometry and thermodynamic modelling into subduction dynamics (Schistes Lustrés, W. Alps): TOWARDS Continuous P-T PATHS? Journal of Metamorphic Geology 30, 323–346. https://doi.org/10.1111/j.1525-1314.2011.00969.x

Plunder, A., Agard, P., Chopin, C., Pourteau, A., Okay, A.I., 2015. Accretion, underplating and exhumation along a subduction interface: From subduction initiation to continental subduction (Tavşanlı zone, W. Turkey). Lithos 226, 233–254. https://doi.org/10.1016/j.lithos.2015.01.007

Pognante, U, 1980. Preliminary data on the Piemonte ophiolite nappe in the lower Val Susa – Val Chisone area, Italian western Alps. Ofioliti 2, 221–240.

Pognante, U, 1984. Eclogitic versus blueschist metamorphism in the internal Western Alps along the Susa valley traverse. Sciences Géologiques, bulletins et mémoires 37, 29–36.

Pognante, U., 1985. Coronitic reactions and ductile shear zones in eclogitised ophiolite metagabbro, Western Alps, North Italy. Chemical Geology 50, 99–109. https://doi.org/10.1016/0009-2541(85)90114-7

Pognante, U., 1991. Petrological constraints on the eclogite- and blueschistfacies metamorphism and P-T-t paths in the Western Alps. J Metamorph Geol 9, 5–17. https://doi.org/10.1111/j.1525-1314.1991.tb00501.x

Polino, R, Lemoine, M, 1984. Détritisme mixte d'origine continentale et océanique dans les sédiments jurassico-crétacés supra-ophiolitiques de la Téthys ligure: la série du Lago Nero (Alpes Occidentales franco-italiennes). Comptes rendus de l'Académie des sciences. Série 2, Mécanique, Physique, Chimie, Sciences de l'univers, Sciences de la Terre 298, 359–364.

Polino, R, Dela Pierre, F, Borghi, A, Carraro, F, Fioraso, G, Giardino, M, 2002. Note illustrative della carta geologica d'Italia alla scala 1:50000: foglio 132-152-153 Bardonecchia. ISPRA, Servizio Geologico d'Italia.

Polino, R, Malusà, M.G., Martin, S, Carraro, F, Gianotti, F, Bonetto, F, 2015. Note illustrative della carta geologica d'Italia alla scala 1:50000: foglio 090 Aosta. ISPRA, Servizio Geologico d'Italia.

Rebay, G., Zanoni, D., Langone, A., Luoni, P., Tiepolo, M., Spalla, M.I., 2018. Dating of ultramafic rocks from the Western Alps ophiolites discloses Late Cretaceous subduction ages in the Zermatt-Saas Zone. Geol. Mag. 155, 298–315. https://doi.org/10.1017/S0016756817000334

Reddy, S.M., Wheeler, J., Butler, R.W.H., Cliff, R.A., Freeman, S., Inger, S., Pickles, C., Kelley, S.P., 2003. Kinematic reworking and exhumation within the convergent Alpine Orogen. Tectonophysics 365, 77–102. https://doi.org/10.1016/S0040-1951(03)00017-9

Reinecke, T., 1991. Very-high-pressure metamorphism and uplift of coesite-bearing metasediments from the Zermatt-Saas zone, Western Alps. ejm 3, 7–18. https://doi.org/10.1127/ejm/3/1/0007

Reinecke, T., 1998. Prograde high- to ultrahigh-pressure metamorphism and exhumation of oceanic sediments at Lago di Cignana, Zermatt-Saas Zone, western Alps. Lithos 42, 147–189. https://doi.org/10.1016/S0024-4937(97)00041-8

Reynard, B., Ballèvre, M., 1988. Coexisting amphiboles in an eclogite from the Western Alps: new constraints on the miscibility gap between sodic and calcic amphiboles. Journal of Metamorphic Geology 6, 333-350.

Robert, D, 1979. Contribution à l'étude géologique de la haute vallée de l'Arc-Région de Bonneval-Savoie. PhD thesis Université de Paris 6.

Rolland, Y., Lardeaux, J.-M., Guillot, S., Nicollet, C., 2000. Extension syn-convergence, poinçonnement vertical et unités métamorphiques contrastées en bordure ouest du Grand Paradis (Alpes Franco-Italiennes). Geodinamica Acta 13, 133–148. https://doi.org/10.1080/09853111.2000.11105369

Rubatto, D., Hermann, J, 2001. Exhumation as fast as subduction? Geology 29, 3–6.

Rubatto, D., Hermann, J., 2003. Zircon formation during fluid circulation in eclogites (Monviso, Western Alps): implications for Zr and Hf budget in subduction zones. Geochimica et Cosmochimica Acta 67, 2173–2187.

Rubatto, D., Angiboust, S., 2015. Oxygen isotope record of oceanic and high-pressure metasomatism: a P–T–time–fluid path for the Monviso eclogites (Italy). Contrib Mineral Petrol 170, 44. https://doi.org/10.1007/s00410-015-1198-4

Rubatto, D., Gebauer, D., Fanning, M., 1998. Jurassic formation and Eocene subduction of the Zermatt-Saas-Fee ophiolites: implications for the geodynamic evolution of the Central and Western Alps. Contributions to Mineralogy and Petrology 132, 269–287. https://doi.org/10.1007/s004100050421

Ruff, L., Kanamori, H., 1980. Seismicity and the subduction process. Physics of the Earth and Planetary Interiors 23, 240–252. https://doi.org/10.1016/0031-9201(80)90117-X

Ruh, J.B., Le Pourhiet, L., Agard, Ph., Burov, E., Gerya, T., 2015. Tectonic slicing of subducting oceanic crust along plate interfaces: Numerical modeling. Geochem. Geophys. Geosyst. 16, 3505–3531. https://doi.org/10.1002/2015GC005998

Rüpke, L., 2004. Serpentine and the subduction zone water cycle. Earth and Planetary Science Letters 223, 17–34. https://doi.org/10.1016/j.epsl.2004.04.018

Saffer, D.M., Tobin, H.J., 2011. Hydrogeology and Mechanics of Subduction Zone Forearcs: Fluid Flow and Pore Pressure. Annu. Rev. Earth Planet. Sci. 39, 157–186. https://doi.org/10.1146/annurev-earth-040610-133408

Saliot, Pierre, 1978. Le métamorphisme dans les Alpes françaises. PhD thesis Université Paris-Sud.

Saliot, P., Velde, B., 1982. Phengite compositions and post-nappe high-pressure metamorphism in the pennine zone of the French Alps. Earth and Planetary Science Letters 57, 133–138. https://doi.org/10.1016/0012-821X(82)90179-0

Sartori, M., 1987. Structure de la zone du Combin entre les Diablons et Zermatt (Valais). Eclogae Geologicae Helvetiae 80, 789–814. https://doi.org/10.5169/SEALS-166026

Scambelluri, M., Pennacchioni, G., Gilio, M., Bestmann, M., Plümper, O., Nestola, F., 2017. Fossil intermediate-depth earthquakes in subducting slabs linked to differential stress release. Nature Geoscience 10, 960–966. https://doi.org/10.1038/s41561-017-0010-7

Schmid, S.M., Pfiffner, O.A., Froitzheim, N., Schönborn, G., Kissling, E., 1996. Geophysical-geological transect and tectonic evolution of the Swiss-Italian Alps. Tectonics 15, 1036–1064. https://doi.org/10.1029/96TC00433

Schmid, S.M., Kissling, E., Diehl, T., van Hinsbergen, D.J.J., Molli, G., 2017. Ivrea mantle wedge, arc of the Western Alps, and kinematic evolution of the Alps–Apennines orogenic system. Swiss J Geosci 110, 581–612. https://doi.org/10.1007/s00015-016-0237-0

Scholl, D.W., von Huene, R., Vallier, T.L., Howell, D.G., 1980. Sedimentary masses and concepts about tectonic processes at underthrust ocean margins. Geology 8, 564–568. https://doi.org/10.1130/0091-7613(1980)8<564:SMACAT>2.0.CO;2

Schwartz, Stéphane, 2000. La zone Piémontaise des Alpes occidentales : un paléo-complexe de subduction. Arguments métamorphiques, géochronologiques et structuraux. PhD thesis, Université Claude Bernard-Lyon I.

Schwartz, S., Lardeaux, J.-M., Guillot, S., Tricart, P., 2000a. Diversité du métamorphisme éclogitique dans le massif ophiolitique du Monviso (Alpes occidentales, Italie). Geodinamica Acta 13, 169–188. https://doi.org/10.1080/09853111.2000.11105371

Schwartz, S., Lardeaux, J.-M., Tricart, P., 2000b. La zone d'Acceglio (Alpes cottiennes) :un nouvel exemple de croûte continentale éclogitisée dans les Alpes occidentales. Comptes Rendus de l'Académie des Sciences - Series IIA - Earth and Planetary Science 330, 859–866. https://doi.org/10.1016/S1251-8050(00)00218-4

Schwartz, S., Lardeaux, J.M., Tricart, P., Guillot, S., Labrin, E., 2007. Diachronous exhumation of HP-LT metamorphic rocks from south-western Alps: evidence from fission-track analysis. Terra Nova 19, 133–140. https://doi.org/10.1111/j.1365-3121.2006.00728.x

Schwartz, S., Guillot, S., Reynard, B., Lafay, R., Debret, B., Nicollet, C., Lanari, P., Auzende, A.L., 2013. Pressure–temperature estimates of the lizardite/antigorite transition in high pressure serpentinites. Lithos 178, 197–210. https://doi.org/10.1016/j.lithos.2012.11.023

Schwartz, S., Gautheron, C., Ketcham, R.A., Brunet, F., Corre, M., Agranier, A., Pinna-Jamme, R., Haurine, F., Monvoin, G., Riel, N., 2020. Unraveling the exhumation history of high-pressure ophiolites using magnetite (U-Th-Sm)/He thermochronometry. Earth and Planetary Science Letters 543, 116359. https://doi.org/10.1016/j.epsl.2020.116359

Selverstone, J., Sharp, Z.D., 2013. Chlorine isotope constraints on fluid-rock interactions during subduction and exhumation of the Zermatt-Saas ophiolite: CHLORINE ISOTOPES IN SUBDUCTED OPHIOLITE. Geochem. Geophys. Geosyst. 14, 4370–4391. https://doi.org/10.1002/ggge.20269

Simon-Labric, T., Rolland, Y., Dumont, T., Heymes, T., Authemayou, C., Corsini, M., Fornari, M., 2009. 40 Ar/ 39 Ar dating of Penninic Front tectonic displacement (W Alps) during the Lower Oligocene (31-34 Ma). Terra Nova 21, 127–136. https://doi.org/10.1111/j.1365-3121.2009.00865.x

Skora, S., Mahlen, N.J., Johnson, C.M., Baumgartner, L.P., Lapen, T.J., Beard, B.L., Szilvagyi, E.T., 2015. Evidence for protracted prograde metamorphism followed by rapid exhumation of the Zermatt-Saas Fee ophiolite. J. Metamorph. Geol. 33, 711–734. https://doi.org/10.1111/jmg.12148

Soret, M., Larson, K.P., Cottle, J., Ali, A., 2021. How Himalayan collision stems from subduction. Geology 49, 894–898. https://doi.org/10.1130/G48803.1

Stampfli, G.M., Marthaler, M., 1990. Divergent and convergent margins in the North-Western alps confrontation to actualistic models. Geodinamica Acta 4, 159–184. https://doi.org/10.1080/09853111.1990.11105208

Stampfli, G.M., Mosar, J., Marquer, D., Marchant, R., Baudin, T., Borel, G., 1998. Subduction and obduction processes in the Swiss Alps. Tectonophysics 296, 159–204. https://doi.org/10.1016/S0040-1951(98)00142-5

Stern, R.J., 2002. SUBDUCTION ZONES. Rev. Geophys. 40, 3-1-3–38. https://doi.org/10.1029/2001RG000108

Syracuse, E.M., van Keken, P.E., Abers, G.A., 2010. The global range of subduction zone thermal models. Physics of the Earth and Planetary Interiors 183, 73–90. https://doi.org/10.1016/j.pepi.2010.02.004

Tartarotti, P., Martin, S., Festa, A., Balestro, G., 2021. Metasediments Covering Ophiolites in the HP Internal Belt of the Western Alps: Review of Tectono-Stratigraphic Successions and Constraints for the Alpine Evolution. Minerals 11, 411. https://doi.org/10.3390/min11040411

Tatsumi, Y., 1986. Formation of the volcanic front in subduction zones. Geophys. Res. Lett. 13, 717–720. https://doi.org/10.1029/GL013i008p00717

Tewksbury-Christle, C.M., Behr, W.M., Helper, M.A., 2021. Tracking Deep Sediment Underplating in a Fossil Subduction Margin: Implications for Interface Rheology and Mass and Volatile Recycling. Geochem Geophys Geosyst 22. https://doi.org/10.1029/2020GC009463

Tricart, P, 1974. Les Schistes lustrés du Haut-Cristillan (Alpes cottiennes, France) : litostratigraphie, architecture et tectogenèse. Géologie Alpine 50, 131–152.

Tricart, P., Schwartz, S., 2006. A north-south section across the Queyras Schistes lustrés (Piedmont zone, Western Alps): Syn-collision refolding of a subduction wedge. Eclogae geol. Helv. 99, 429–442. https://doi.org/10.1007/s00015-006-1197-6

van Keken, P.E., Hacker, B.R., Syracuse, E.M., Abers, G.A., 2011. Subduction factory: 4. Depth-dependent flux of H 2 O from subducting slabs worldwide. J. Geophys. Res. 116, B01401. https://doi.org/10.1029/2010JB007922

Vannucchi, P., Spagnuolo, E., Aretusini, S., Di Toro, G., Ujiie, K., Tsutsumi, A., Nielsen, S., 2017. Past seismic slip-to-the-trench recorded in Central America megathrust. Nature Geosci 10, 935–940. https://doi.org/10.1038/s41561-017-0013-4

Velde, B, 1967. Si+ 4 content of natural phengites. Contributions to Mineralogy and Petrology 14, 250–258.

Villa, I.M., Bucher, S., Bousquet, R., Kleinhanns, I.C., Schmid, S.M., 2014. Dating Polygenetic Metamorphic Assemblages along a Transect across the Western Alps. Journal of Petrology 55, 803–830. https://doi.org/10.1093/petrology/egu007

Vitale Brovarone, A., Picatto, M., Beyssac, O., Lagabrielle, Y., Castelli, D., 2014. The blueschist–eclogite transition in the Alpine chain: P–T paths and the role of slow-spreading extensional structures in the evolution of HP–LT mountain belts. Tectonophysics 615–616, 96–121. https://doi.org/10.1016/j.tecto.2014.01.001

von Huene, R., Scholl, D.W., 1991. Observations at convergent margins concerning sediment subduction, subduction erosion, and the growth of continental crust. Rev. Geophys. 29, 279–316. https://doi.org/10.1029/91RG00969

Wada, I., Wang, K., 2009. Common depth of slab-mantle decoupling: Reconciling diversity and uniformity of subduction zones. Geochem. Geophys. Geosyst. 10, n/a-n/a. https://doi.org/10.1029/2009GC002570

Wassmann, S., Stöckhert, B., 2013. Rheology of the plate interface — Dissolution precipitation creep in high pressure metamorphic rocks. Tectonophysics 608, 1–29. https://doi.org/10.1016/j.tecto.2013.09.030

Weber, S., Sandmann, S., Miladinova, I., Fonseca, R.O.C., Froitzheim, N., Münker, C., Bucher, K., 2015. Dating the initiation of Piemonte-Liguria Ocean subduction: Lu–Hf garnet chronometry of eclogites from the Theodul Glacier Unit (Zermatt-Saas zone, Switzerland). Swiss J Geosci 108, 183–199. https://doi.org/10.1007/s00015-015-0180-5

Willner, A.P., 2005. Pressure–Temperature Evolution of a Late Palaeozoic Paired Metamorphic Belt in North–Central Chile (34°–35°30′S). Journal of Petrology 46, 1805–1833. https://doi.org/10.1093/petrology/egi035

Zanoni, D., Rebay, G., Spalla, M.I., 2016. Ocean floor and subduction record in the Zermatt-Saas rodingites, Valtournanche, Western Alps. J. Metamorph. Geol. 34, 941–961. https://doi.org/10.1111/jmg.12215

Table captions

Table 1: Lithological ratio (sediment versus mafic-ultramafic) and aerial exposure of the Liguro-Piemont slices. See text (§4.2) for details in the methodology.

Table 2: RSCM temperatures of the Liguro-Piemont slices. All the compiled RSCM temperatures (from this study and literature) are presented in Sup. Mat 1.

Table 3: Maximum Si a.p.f.u. values of phengite ($Si^{max}Ph$) and estimated peak pressure for Liguro-Piemont slices. Peak pressures were estimated by crossing RSCM temperatures (see Table 1; Fig. 4a-c, 5a-e) with the calculated isopleths of Si a.p.f.u. in phengite for a representative rock composition (Fig. 9a). Selected $Si^{max}Ph$, RSCM temperature for the same samples and all estimated pressure values are presented in Sup. mat. 3.

Figure captions

Figure 1: Maps of the Western Alps focused on the Liguro-Piemont (L-P) domain. A) Distribution of sediments and mafic-ultramafic rocks across the L-P domain and location of the stratigraphic columns presented in figure 3b and the tectonic contacts separating L-P slices. B) Zoneography of index metamorphic minerals of L-P metasediments, both from field observations (this study) and compiled from literature (Bocquet, 1974; Agard et al., 2001a; Goffé et al., 2004; Bousquet et al., 2008; Manzotti et al., 2021). C) Distribution of blueschist- and eclogite-facies metamorphism across the L-P domain and location of the L-P tectonic slices described in literature. References for the different slices are in the text (see §3). Che: Chenaillet. Abbreviations for the tectonic slices: AG: Aigle; ALB: Albergian; ATF: Avise-Tsaboc-Feluma; AV: Avic; BY: By unit; CC: Cerogne-Ciantiplagna; CH: Chardonnet klippe; CO: Cornet; CS: Calcschist unit; GU: Grivola-Urtier; GS: Grande-Sassière klippe; GV: Grand Vallon klippe; JO: Jovet klippe; LA: Lamet klippe; LN: Lago Nero; LS: Lago Superiore; MB: Mirabouc-Bouchet; MV: Monviso unit; OR: Orsiera-Rocciavrè; PT: Pelvas-Taillante; PY: Puys; SLU: Savoy Lower Unit; SMU: Savoy Middle Unit; SN-L: Lower Sana klippe; SN-U: Upper Sana klippe; VN: Venaus; VV: Vin Vert; W-SS: West-Sesia unit; ZS: Zermatt-Saas.

Figure 2: Panoramic pictures of the Liguro-Piemont domain exposing the present slice-stacking. A) Savoy-Susa transect from Rocciamelone summit. B) Cottian Alps transect. C) Queyras-Monviso transect from Bric-Froid summit. B) and C) are modified after Agard (2021).

Figure 3: Stratigraphy and paleogeography of the Liguro-Piemont rocks. A) Schematic cross-section of the European margin and Liguro-Piemont ocean before subduction with emphasis on the paleogeograhic unknowns. Grey sticks with question marks correspond to potential locations for the stratigraphic columns of figure 3b. B) Compilation of stratigraphic columns of the L-P domain. Description, references of the different stratigraphic columns, stratigraphic formations and events are in the text (§4.1). Location of the stratigraphic columns across the L-P complex are in figure 1a. Stratigraphic column 1 (Chabrière-series) corresponds to the reference complete succession of L-P deposits ranging from Middle-Upper Jurassic to Upper Cretaceous deposits. Most of the blueschist-facies slices have an almost similar stratigraphic succession with only few formations missing. Few blueschist-facies slices (column 3, 8, 10, 11, 13) (almost) only have Upper Cretaceous sediments. All stratigraphic colums from eclogite-facies slices are devoid of Upper Cretaceous. Abbreviations for the tectonic slices: AV: Avic; AG: Aigle; CS: Calcschist unit; CO: Cornet; GV: Grand Vallon klippe; LA: Lamet klippe; LN: Lago Nero; MB: Mirabouc-Bouchet; MV: Monviso unit; PT: Pelvas-Taillante; SLU: Savoy Lower Unit; SMU: Savoy Middle Unit; VV: Vin Vert; ZS: Zermatt-Saas.

Figure 4: Distribution and interpolation of RSCM temperatures across the Liguro-Piemont domain. A) RSCM temperatures and L-P tectonic contacts across the domain notably highlighting the eastward metamorphic gradient. B) Interpolation of RSCM temperatures across the L-P domain with 25°C intervals. C) Smoothed interpolation of RSCM temperatures across the domain and tectonic contacts of the L-P slices. This map as C) highlights the burial temperature recorded by rocks across the whole L-P domain and the specific temperature range of each tectonic slice. Some slices have blue color corresponding to 300-400°C while other have green-to yellow colors highlighting ~400-500°C T_{max}. Finally, easternmost slices (eclogite-facies) have orange-to red colors corresponding to T_{max} above 500°C. Most of the slices expose an internal eastward increase in T_{max}. For the three maps, square symbols correspond to our samples (108 samples) while round symbols correspond to RSCM temperatures compiled from literature (289 samples; Beyssac et al., 2002; Gabalda

et al., 2009; Angiboust et al., 2009; 2012b, 2014; Angiboust and Agard, 2010; Plunder et al., 2012; Negro et al., 2013; Schwartz et al., 2013; Decrausaz et al., 2021; Manzotti et al., 2021). Samples description, temperature and mineral assemblages as well as compiled RSCM temperatures from literature are presented in Sup. mat. 1.

Figure 5: Statistical distribution of RSCM temperatures in Liguro-Piemont domain**.** A) Bar chart of all RSCM temperatures showing a trimodal distribution with peaks at 370-380°C, 460-470°C and ~540°C. B) to E) Cumulative bar charts of RSCM temperatures along Valais-Aosta, Savoy-Susa, Cottian Alps and Queyras-Monviso transects, all showing the same three temperature clusters of A). Slices were color-coded according to their specific temperature ranges (Table 1). Fo all charts, RSCM temperatures are both from this study and compiled from literature (see Fig. 4 caption)

Figure 6: Microphotographs highlighting the successive deformation structures observed in our representative metasedimentary samples. A) to B) S1 and S2 foliation are marked by phengite (Ph) and chlorite crystals. D3 deformation corresponds to small shear bands cross-cutting S1 and S2. Index minerals, such as chloritoid (Cld), lawsonite, Fe-Mg carpholite or garnet often show textural equilibrium with S1 phengite.

Figure 7: Phengite composition. A) Ternary diagram of point electron microprobe analyses of phengite. B) Maximum Si values of phengite ($Si^{max}Ph$; peak pressure indicator) versus RSCM temperatures of the same samples or samples from the same locality. Most samples plot on a linear trend, highlighting the increase of $Si^{max}Ph$ with temperature and the efficiency of Si value use as peak pressure indicator. Square/round symbols correspond to our samples/literature $Si^{max}Ph$ (Bocquet, 1974; Liewig, 1981; Agard et al., 2001a; Bonnet et al., submitted). Light-blue symbols with dotted contours correspond to samples in which phengite with peak burial Si values was not preserved or not found. Representative compositions of analyzed phengite are presented in Sup. mat. 2 and selected $Si^{max}Ph$ values are presented in Sup. mat. 3.

Figure 8: Distribution of maximum Si values of phengite ($Si^{max}Ph$) across the L-P domain, in Cottian Alps and Queyras-Monviso region. $Si^{max}Ph$ values progressively increase toward east, showing an eastward pressure gradient as highlighted for temperature in figure 4a-c. Square symbols correspond to our samples while round symbols correspond to literature data (see Fig. 7 caption). Symbols with dotted contours correspond to samples where peak burial Si values were not preserved or foundd. Selected $Si^{max}Ph$ values are presented in Sup. mat. 3.

Figure 9: Thermodynamic modelling for a representative composition of Liguro-Piemont metasediments. A) Pseudosection (system NaCaKFMASH, with all assemblages containing quartz, phengite and H_2O) calculated using Perple_X software (Connolly, 1990, 2005, 2009) for the bulk composition of CBas912m sample of Henry et al. (1996) considered as representative of most Liguro-Piemont calcschists. Calculated isopleths of Si a.p.f.u. in phengite are represented. The red line corresponds to a 8°C/km gradient. Calculated B) evolution of mineral modes and C) H_2O content and major dehydration reactions, along a 8°C/km gradient (from 300°C-1.25 GPa to 600°C-2.5GPa) for the pseudosection presented in A). Mineral abbreviations: Car: carpholite; Chl: Chlorite; Cld: chloritoid; Gln: glauchophane; Grt: grenat; Jd: jadeite; Ky: kyanite; Lws: lawsonite; Pg: paragonite; Ph: phengite; Qz: quartz; Zo: zoisite. Reaction abbreviations: Car-: carpholite-out; Chl-: chlorite-out; Cld+: chloritoid-in; Cld- chloritoid-out; Lws-: lawsonite-out. Mineral assemblages in A) 1: Car Jd Lws Stp; 2: Car Chl Jd Lws Stp; 3: Car Jd Lws Pg Stp; 4: Car Chl Jd Lws Pg; 5: Chl Cld Lws Pg Zo; 6: Car Gln Jd Lws; 7: Car Chl Gln Jd Lws; 8: Car Gln Grt Jd Lws; 9: Car Cld Gln Jd Lws; 10: Car Grt

Jd Lws; 11: Cld Car Gln Lws Pg; 12: Cld Gln Lws Pg; 13: Car Chl Cld Jd Lws; 14: Car Grt Jd Lws Pg; 15: Car Gln Grt Lws Pg; 16: Gln Grt Ky Lws Pg; 17: Car Cld Grt Lws Jd; 18: Cld Gln Jd Lws Pg; 19: Gln Grt Jd Ky; 20: Cld Gln Grt Ky Pg; 21: Cld Gln Grt Pg; 22: Chl Cld Grt Pg.

Figure 10: A) Mean peak P-T conditions (circles) for the Liguro-Piemont slices. Slices were plotted in this P-T grid using their mean RSCM temperature and mean pressure retrieved from $Si^{max}Ph$ and the pseudosection (Fig. 9), or estimated in literature (§3). Increasing thickness of symbol contours represents increasing sediment/mafic-ultramafic ratio (table 1) in the slices: Sed.+: ≥ 90% of sediments; Maf.Umaf.+: ~60% of sediments. Maf.Umaf.++: ~40% of sediments (MUM units of Agard, 2021). The three major clusters of peak P-T conditions correspond to groups of slices with distinct sediment/mafic-ultramafic ratios. The major dehydration reactions of figure 9c are also reported. B) Subuction ages of Liguro-Piemont slices. Symbols correspond to the peak burial of the slices while dotted arrows depict their paths. This figure highlights the successive slicing of LPU, LPM, sediment-rich LPL and mafic-ultramafic-rich LPL from the downgoing slab and their stacking at ~36-35 Ma. Slices only composed by Upper Cretaceous deposits may be the last units sliced as highlighted by the peak burial age of CS. References for ages are in the text (§3; 7.2, 7.3). LPU: Liguro-piemont Upper units; LPM: Liguro-Piemont Middle units; LPL: Liguro-Piemont Lower units. Slice abbreviations: ALB: Albergian; ATF: Avise-Tsaboc-Feluma; AV: Avic; BY: By unit; CO: Cornet; CS: Calcschist unit; GU: Grivola-Urtier; LN: Lago Nero; LS: Lago Superiore; MB: Mirabouc-Bouchet; SLU: Savoy Lower Unit; SMU: Savoy Middle Unit; ZS: Zermatt-Saas. Abbreviations for continental units: DM: Dora-Maira; GP: Gran Paradiso; MR: Monte Rosa. Modified after Agard (2021).

Figure 11: Simplified map showing the distribution of the three Liguro-Piemont units across the Western Alps. Location of cross-sections shown in figure 12 is indicated (A-A'; B-B'; C-C'; D-D'). LPU: Liguro-Piemont Upper units; LPM: Liguro-Piemont Middle units; LPL: Liguro-Piemont Lower units.

Figure 12: Cross-sections of the four major Liguro-Piemont transects described in this study exposing the actual stacking of the different slices and units. Cross-section locations are indicated in figure 11. A) to D) were repectively modified after Negro et al. (2013); Plunder et al. (2012); Agard (2021); Lagabrielle (1987). LPU: Liguro-Piemont Upper units; LPM: Liguro-Piemont Middle units; LPL: Liguro-Piemont Lower units. Slice abbreviations: BY: By unit; CC: Cerogne-Ciantiplagna; CO: Cornet; CS: Calcschist unit; GV: Grand Vallon klippe; LA: Lamet klippe; LN: Lago Nero; LS: Lago Superiore; MB: Mirabouc-Bouchet; MV: Monviso; OR: Orsiera-Rocciavrè; PT: Pelvas-Taillante; SLU: Savoy Lower Unit; SMU: Savoy Middle Unit; ZS: Zermatt-Saas.

Figure 13: Statistical distribution of RSCM temperatures in the Liguro-Piemont units. A) Boxplots of RSCM temperature for the three Liguro-Piemont units, both from this study and compiled from literature (see Fig. 4 caption). B) Boxplots of $Si^{max}Ph$ for the three Liguro-Piemont units, both from this study and compiled from literature (see Fig. 7 caption). inside boxes, lines and crossed circles correspond to median and mean values of each boxplot, given in the text (§7.1). LPU: Liguro-Piemont Upper units; LPM: Liguro-Piemont Middle units; LPL: Liguro-Piemont Lower units.

Figure 14: Sketch of the slicing and stacking of Liguro-Piemont slices. A) Idealized view of the Alpine subduction zone at ~50-45 Ma, showing the relative location of the slices (for the four transects) discuted in the text. At this time, Chabrière-type LPU and LPM are already offscraped from the slab and are exhuming, as for the sedimentary-dominated LPL. Mafic-Ultramafic LPL, initially close to the continental margin are being sliced. Upper Cretaceous LPU and LPM will be the last to offscraped from the downgoing slab. Two different transects

defined by Agard (2021) are represented (sectors A and B). Modified after Agard (2021). B) to E) RSCM temperature versus longitude for the four transects detailed in the text (see also Fig. 11, 12). These graphs show the increase of peak temperature from W to E and the current stacking of the L-P units, with LPU structurally at the top of LPM and LPL. Square/round symbols correspond to our samples/literature data respectively (see Fig. 4 caption). Abbreviations: LPU: Liguro-Piemont Upper units; LPM: Liguro-Piemont Middle units; LPL: Liguro-Piemont Lower units. AG: Aigle; ALB: Albergian; ATF: Avise-Tsaboc-Feluma; AV: Avic; BY: By unit; CC: Cerogne-Ciantiplagna; CO: Cornet; CS: Calcschist unit; GU: Grivola-Urtier; LN: Lago Nero; LS: Lago Superiore; MB: Mirabouc-Bouchet; MV: Monviso; OR: Orsiera-Rocciavrè; PT: Pelvas-Taillante; PY: Puys; SLU: Savoy Lower Unit; SMU: Savoy Middle Unit; SUU: Savoy Upper Unit; VV: Vin Vert; W-SS: West-Sesia unit; ZS: Zermatt-Saas. U.K. slices: slices mostly made by Upper Cretaceous sediments such as the Savoy Upper Unit at Grand Vallon or Lamet klippe.

Figure 15: A) Potential paleogeographic position of Liguro-Piemont units before subduction. B) Suggested slicing and stacking sequence of Liguro-Piemont units. C) Stratigraphic columns with recovered portion of the different Liguro-Piemont units and suggested decollement layers and offscraping mechanisms. For the Upper-Cretaceous LPU and LPM, the initial basement may either have been made of continental or oceanic rocks. We suggest that strain localization leading to LPU and LPM units' slicing mostly occurred due to major lithological contrasts in the pile, such as levels of pelagic sediments or serpentinized mantle acting as rheological weaknesses, possibly under high fluid pressure conditions. On the other side, LPL units slicing at eclogite facies conditions may be linked to major dehydration reactions (as lawsonite breakdown in sediments), under high fluid pressure conditions, responsible for rocks embrittlement. LPU: Liguro-Piemont Upper units; LPM: Liguro-Piemont Middle units; LPL: Liguro-Piemont Lower units.

Figure 16: Depth clusters and mechanisms of slicing in the Liguro-Piemont subduction zone. A) Bar chart of underplating depth (distributed deformation along the plate interface) along the Chilean margin (after Cubas et al., submitted). Mean peak burial depths estimated in this study for the Liguro-Piemont units LPU an LPM are in good agreement with the underplating depth clusters observed along the Chilean margin. The peak burial depth of the eclogite-facies LPL units is similar tot the estimated peak burial depth for most of worldwide recovered eclogites (after Agard et al., 2018). B) Schematic peak P-T depth conditions for the Liguro-Piemont units, and suggested major slicing mechanisms, i.e. major litholical heterogeneities for LPU and LPM and fluid release combined with lithological heterogeneities for LPL. C) Schematic view of a subducting slab with discontinuous oceanic crust, subjected to three main depths of slicing at ~35-45 km, 55-65 km and 70-80 km. The heterogeneously distributed deformation leads to slicing of the slab, underplating and topographic build-up responsible for the nucleation of earthquakes propagating across the B and C domains. Modified after Cubas et al. (submitted). Abbreviations: LPU: Liguro-Piemont Upper units; LPM: Liguro-Piemont Middle units; LPL: Liguro-Piemont Lower units.

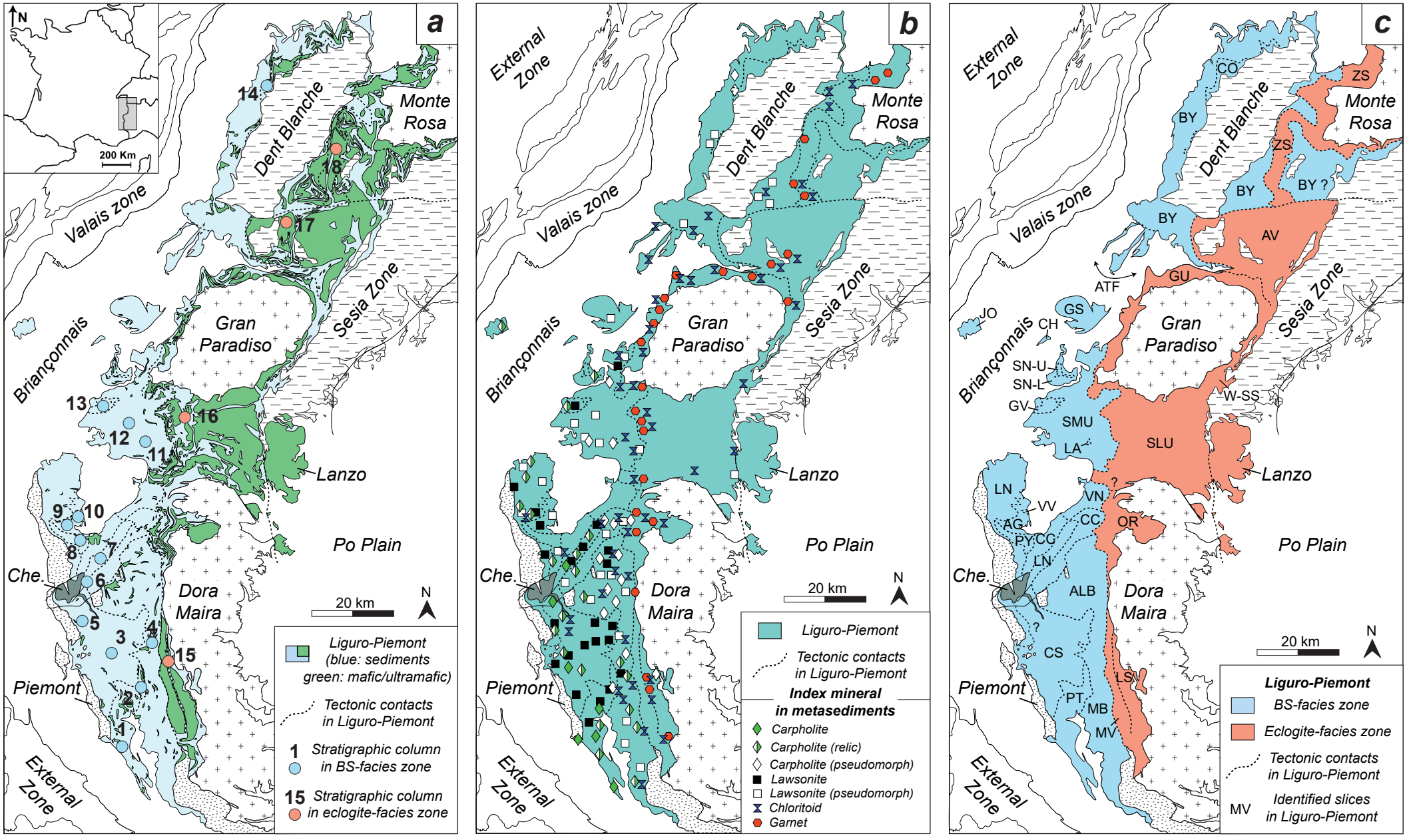
a
b
c
N
200 Km
Valais zone
External Zone
Briançonnais
Dent Blanche
Monte Rosa
Gran Paradiso
Sesia Zone
Lanzo
Po Plain
Dora Maira
Che.
Piemont
20 km
Liguro-Piemont (blue: sediments green: mafic/ultramafic)
Tectonic contacts in Liguro-Piemont
1 Stratigraphic column in BS-facies zone
15 Stratigraphic column in eclogite-facies zone
Liguro-Piemont
Tectonic contacts in Liguro-Piemont
Index mineral in metasediments
Carpholite
Carpholite (relic)
Carpholite (pseudomorph)
Lawsonite
Lawsonite (pseudomorph)
Chloritoid
Garnet
CO
ZS
BY
BY ?
AV
ATF
GU
JO
GS
CH
SN-U
SN-L
GV
W-SS
SMU
SLU
LA
LN
VV
VN
AG
CC
OR
PY
CG
ALB
CS
LS
PT
MB
MV
Liguro-Piemont
BS-facies zone
Eclogite-facies zone
Tectonic contacts in Liguro-Piemont
Identified slices in Liguro-Piemont

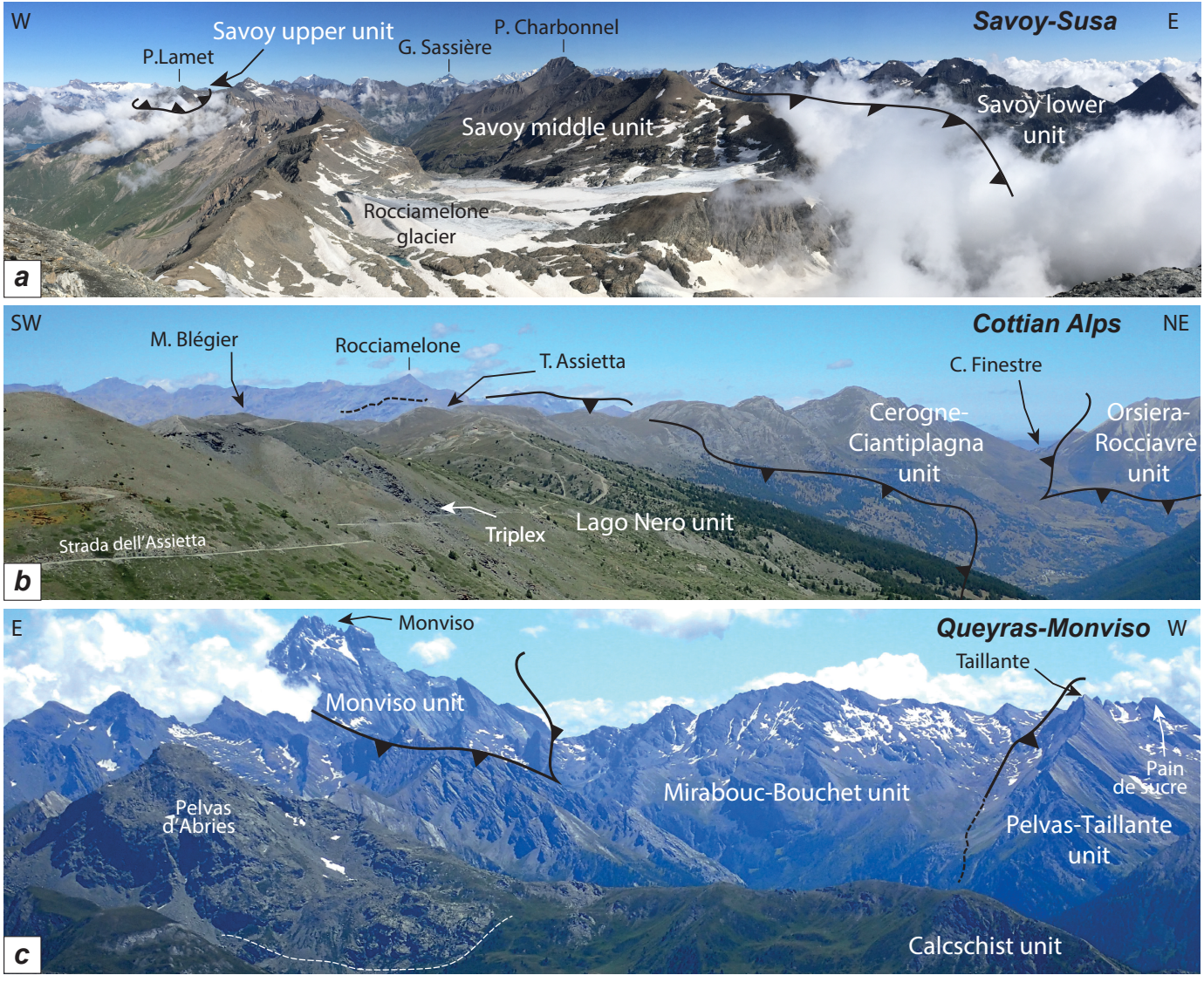
W
Savoy upper unit
P.Lamet
G. Sassière
P. Charbonnel
Savoy-Susa
E
Savoy middle unit
Savoy lower unit
Rocciamelone glacier
a
SW
M. Blégier
Rocciamelone
T. Assietta
Cottian Alps
NE
C. Finestre
Cerogne-Ciantiplagna unit
Orsiera-Rocciavrè unit
Triplex
Lago Nero unit
Strada dell'Assietta
b
E
Monviso
Queyras-Monviso
W
Taillante
Monviso unit
Pain de sucre
Mirabouc-Bouchet unit
Pelvas d'Abries
Pelvas-Taillante unit
Calcschist unit
c

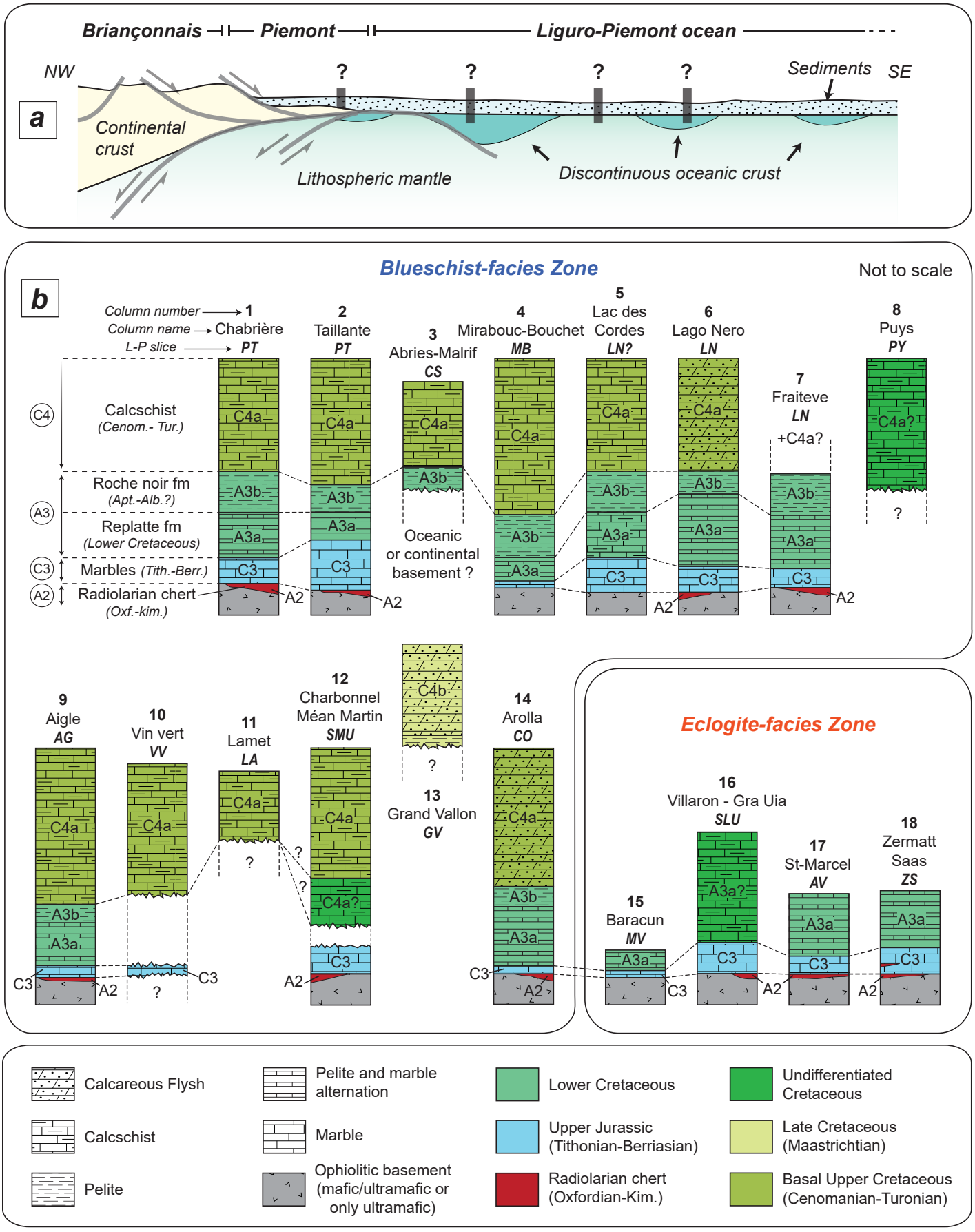
Briançonnais
Piemont
Liguro-Piemont ocean
a
NW
SE
Sediments
Continental crust
Lithospheric mantle
Discontinuous oceanic crust
Blueschist-facies Zone
Not to scale
b
Column number
Column name
L-P slice
1 Chabrière PT
2 Taillante PT
3 Abries-Malrif CS
4 Mirabouc-Bouchet MB
5 Lac des Cordes LN?
6 Lago Nero LN
7 Fraiteve LN +C4a?
8 Puys PY
C4 Calcschist (Cenom.- Tur.)
A3 Roche noir fm (Apt.-Alb.?)
Replatte fm (Lower Cretaceous)
C3 Marbles (Tith.-Berr.)
A2 Radiolarian chert (Oxf.-kim.)
Oceanic or continental basement ?
9 Aigle AG
10 Vin vert VV
11 Lamet LA
12 Charbonnel Méan Martin SMU
13 Grand Vallon GV
14 Arolla CO
Eclogite-facies Zone
15 Baracun MV
16 Villaron - Gra Uia SLU
17 St-Marcel AV
18 Zermatt Saas ZS
Calcareous Flysh
Calcschist
Pelite
Pelite and marble alternation
Marble
Ophiolitic basement (mafic/ultramafic or only ultramafic)
Lower Cretaceous
Upper Jurassic (Tithonian-Berriasian)
Radiolarian chert (Oxfordian-Kim.)
Undifferentiated Cretaceous
Late Cretaceous (Maastrichtian)
Basal Upper Cretaceous (Cenomanian-Turonian)

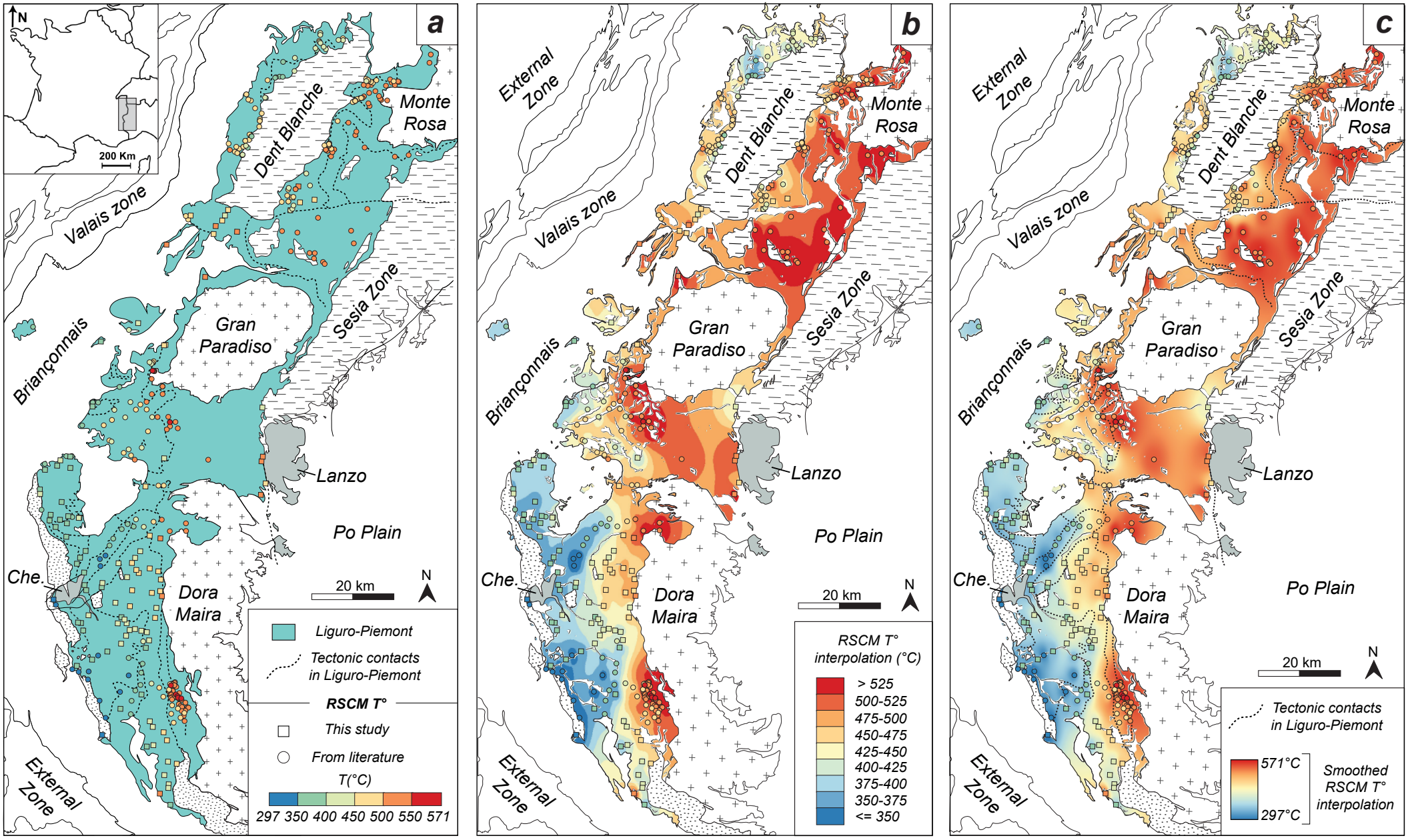
a
b
c
N
200 Km
Valais zone
External Zone
Briançonnais
Dent Blanche
Monte Rosa
Gran Paradiso
Sesia Zone
Lanzo
Po Plain
Che.
Dora Maira
20 km
Liguro-Piemont
Tectonic contacts in Liguro-Piemont
RSCM T°
This study
From literature
T(°C)
297 350 400 450 500 550 571
RSCM T° interpolation (°C)
> 525
500-525
475-500
450-475
425-450
400-425
375-400
350-375
<= 350
571°C
297°C
Smoothed RSCM T° interpolation

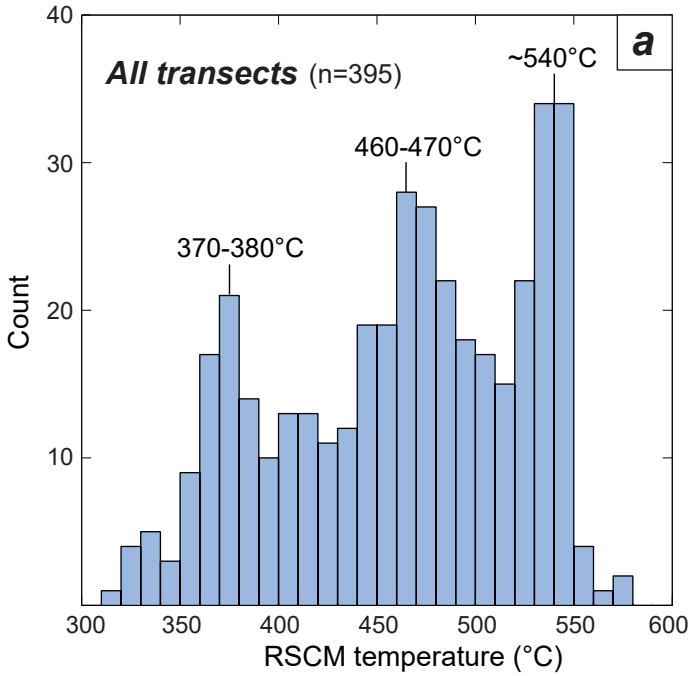
a
All transects (n=395)
~540°C
460-470°C
370-380°C
Count
RSCM temperature (°C)

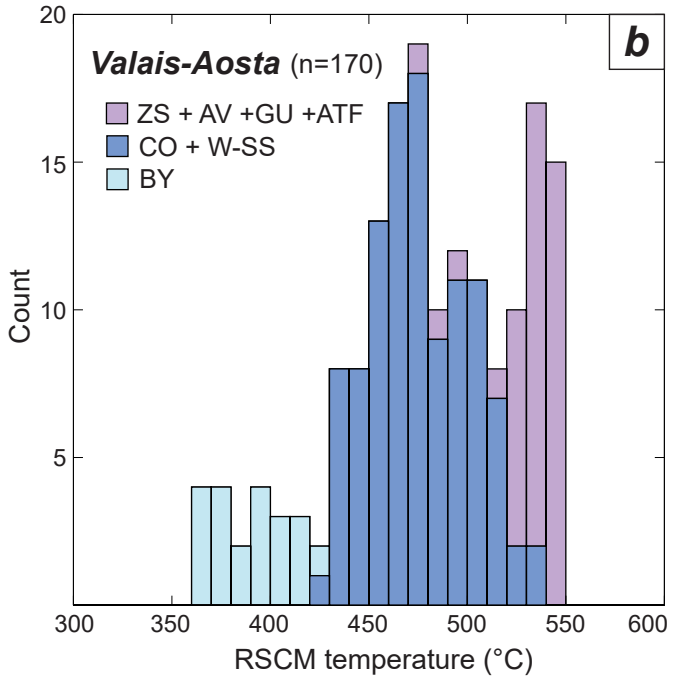
b
Valais-Aosta (n=170)
ZS + AV +GU +ATF
CO + W-SS
BY
Count
RSCM temperature (°C)

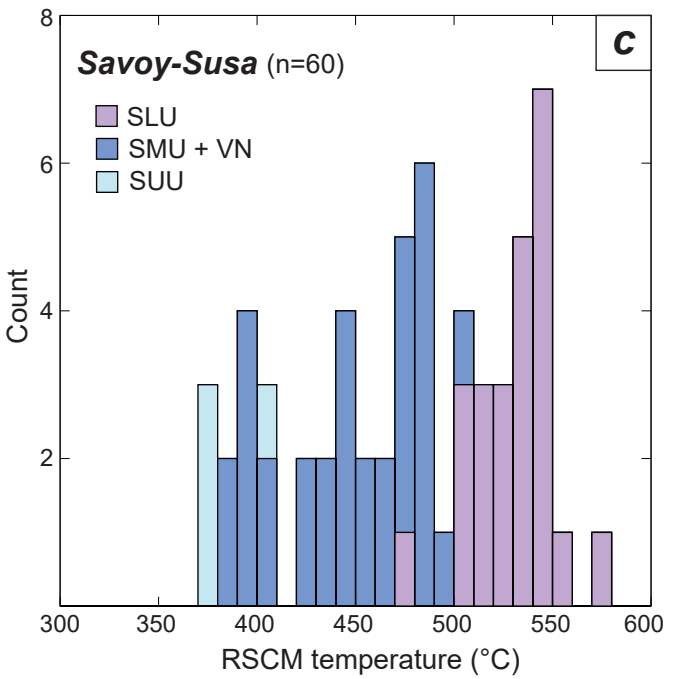
c
Savoy-Susa (n=60)
SLU
SMU + VN
SUU
Count
RSCM temperature (°C)

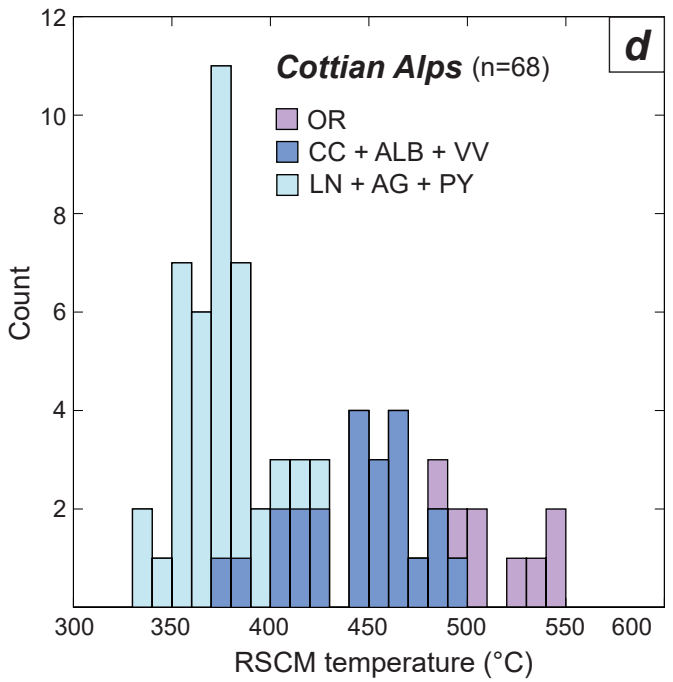
d
Cottian Alps (n=68)
OR
CC + ALB + VV
LN + AG + PY
Count
RSCM temperature (°C)

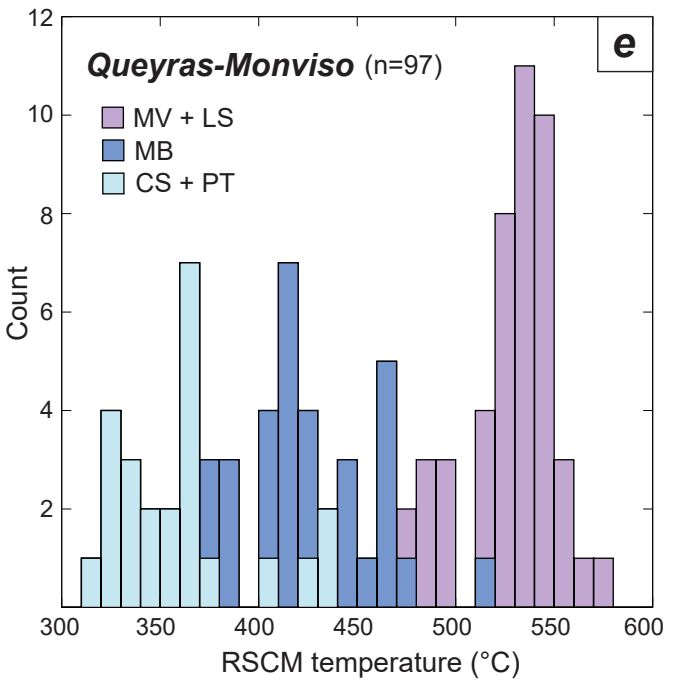
e
Queyras-Monviso (n=97)
MV + LS
MB
CS + PT
Count
RSCM temperature (°C)

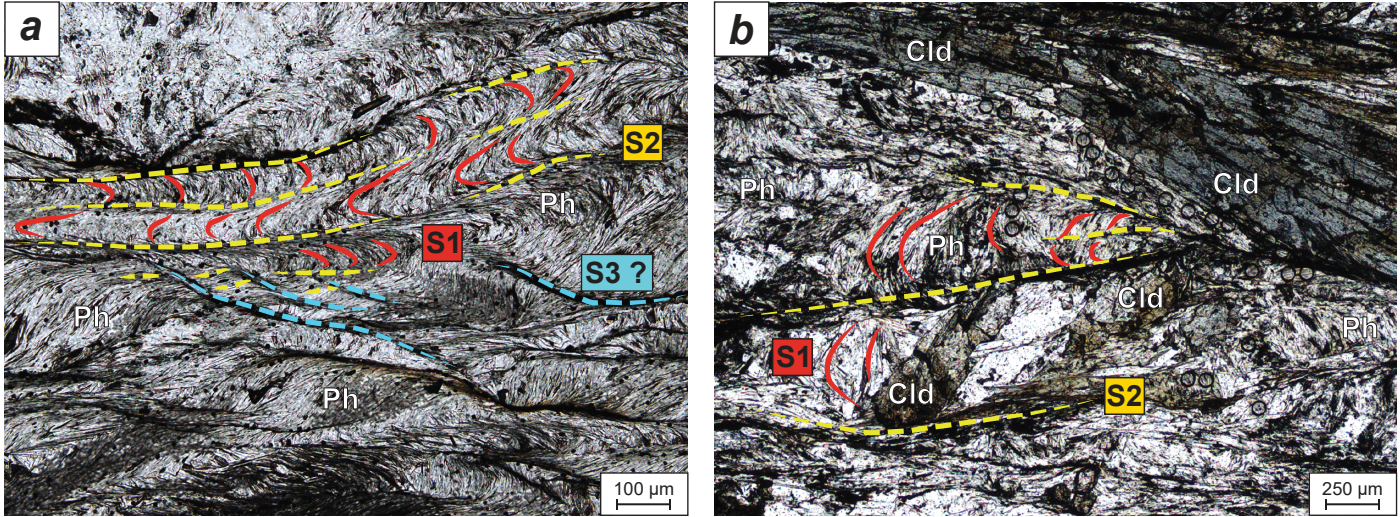
a
S2
Ph
S1
S3 ?
Ph
Ph
100 µm
b
Cld
Ph
Cld
Ph
Cld
Ph
S1
Cld
S2
250 µm

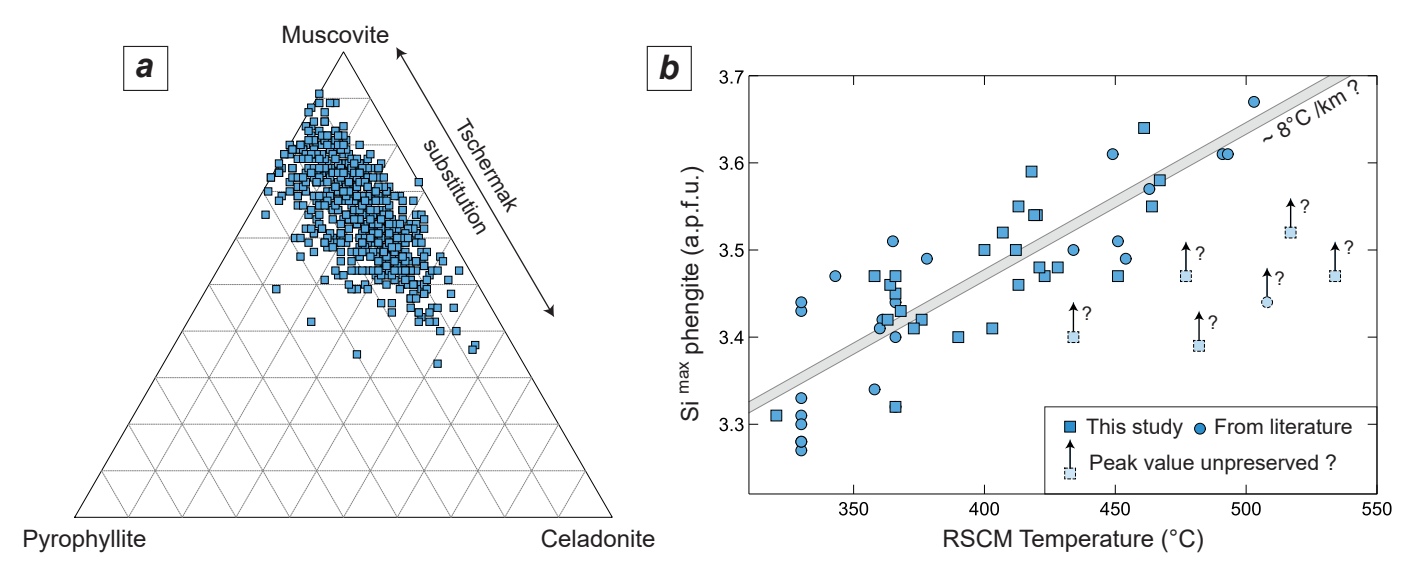
a
Muscovite
Tschermak
substitution
Pyrophyllite
Celadonite
b
Si max phengite (a.p.f.u.)
3.7
3.6
3.5
3.4
3.3
~ 8°C /km ?
This study
From literature
Peak value unpreserved ?
350
400
450
500
550
RSCM Temperature (°C)

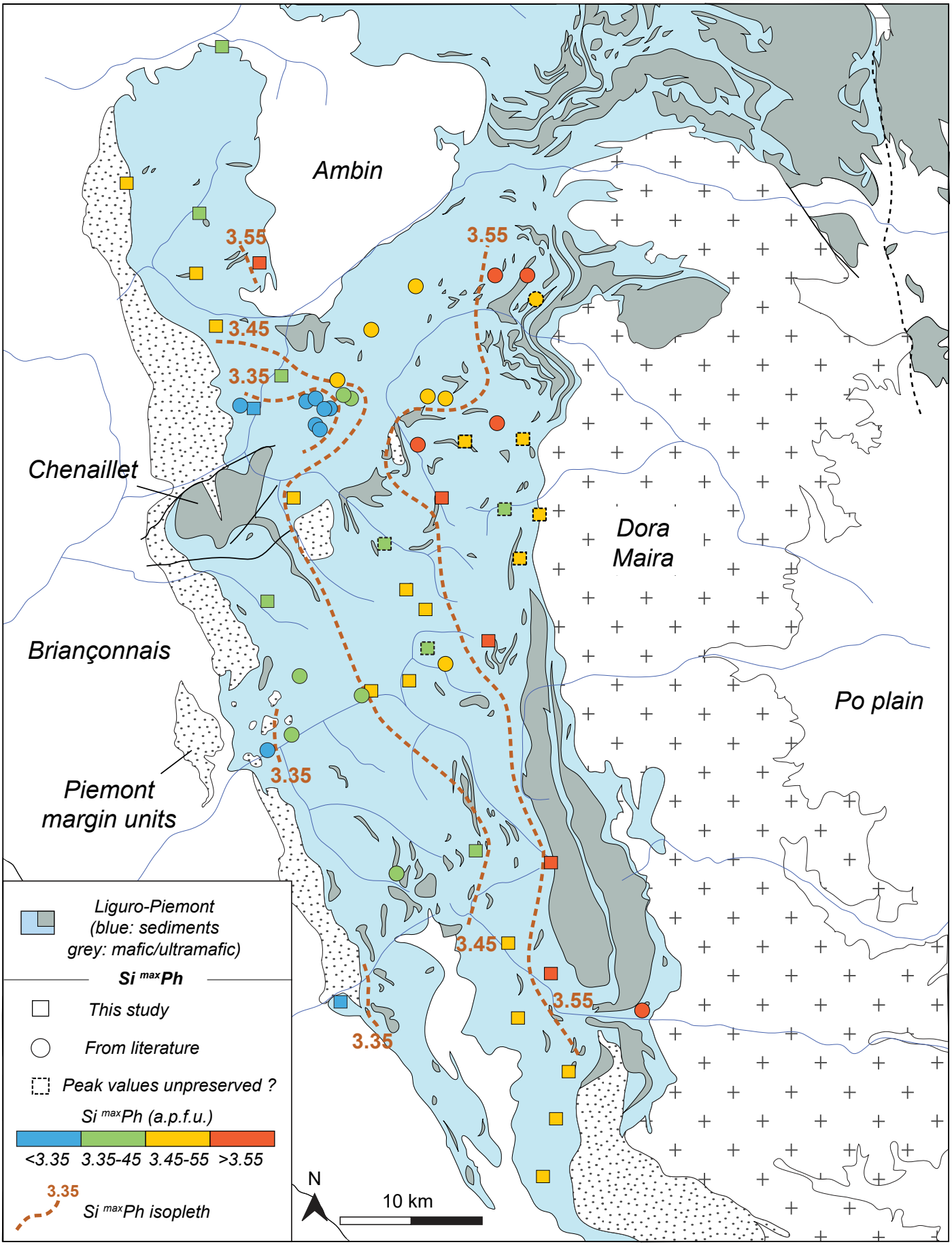
Ambin
Chenaillet
Briançonnais
Piemont
margin units
Dora
Maira
Po plain
3.55
3.45
3.35
3.35
3.55
3.45
3.55
3.35
Liguro-Piemont
(blue: sediments
grey: mafic/ultramafic)
Si max Ph
This study
From literature
Peak values unpreserved ?
Si max Ph (a.p.f.u.)
<3.35 3.35-45 3.45-55 >3.55
3.35
Si max Ph isopleth
N
10 km

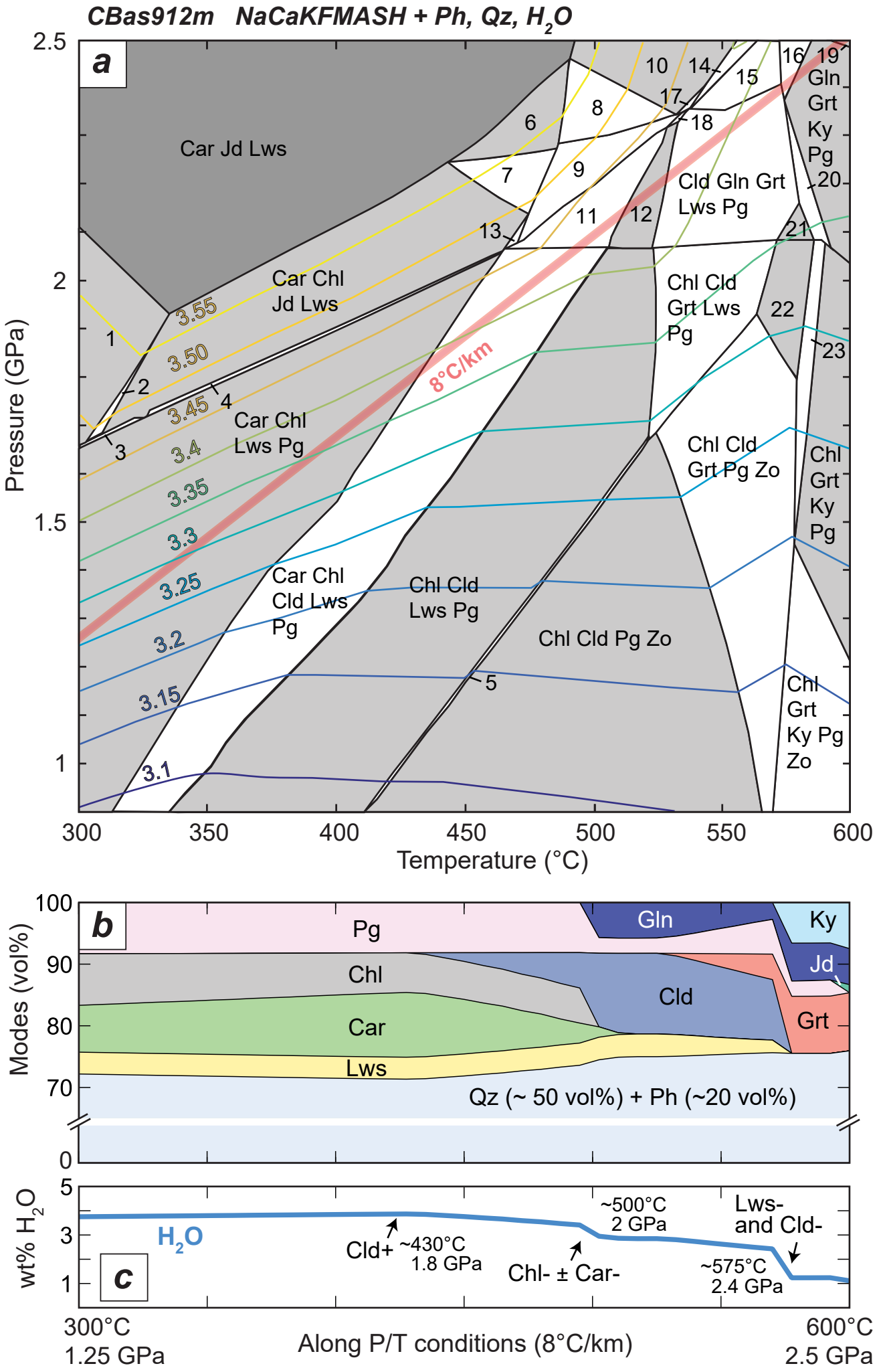
CBas912m NaCaKFMASH + Ph, Qz, H2O
a
Car Jd Lws
Car Chl Jd Lws
Car Chl Lws Pg
Car Chl Cld Lws Pg
Chl Cld Lws Pg
Chl Cld Pg Zo
Cld Gln Grt Lws Pg
Chl Cld Grt Lws Pg
Chl Cld Grt Pg Zo
Gln Grt Ky Pg
Chl Grt Ky Pg
Chl Grt Ky Pg Zo
3.55
3.50
3.45
3.4
3.35
3.3
3.25
3.2
3.15
3.1
8°C/km
Pressure (GPa)
Temperature (°C)
b
Pg
Chl
Car
Lws
Gln
Ky
Jd
Cld
Grt
Qz (~ 50 vol%) + Ph (~20 vol%)
Modes (vol%)
c
H2O
wt% H2O
Cld+ ~430°C 1.8 GPa
Chl- ± Car-
~500°C 2 GPa
Lws- and Cld-
~575°C 2.4 GPa
300°C 1.25 GPa
Along P/T conditions (8°C/km)
600°C 2.5 GPa

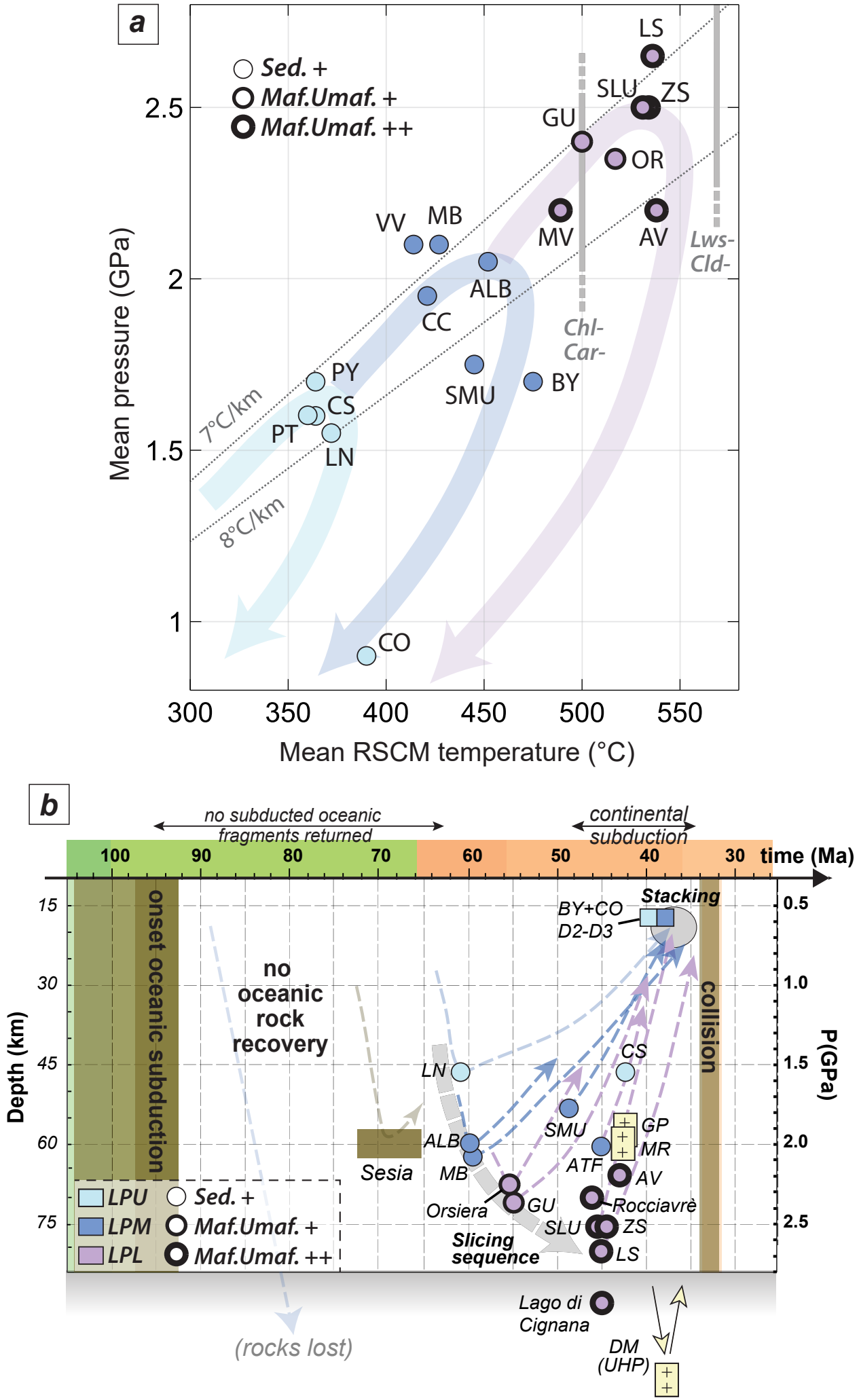
a
Sed. +
Maf.Umaf. +
Maf.Umaf. ++
LS
SLU
ZS
GU
OR
VV
MB
MV
AV
Lws-
Cld-
ALB
CC
Chl-
Car-
PY
SMU
BY
CS
PT
LN
7°C/km
8°C/km
CO
Mean pressure (GPa)
Mean RSCM temperature (°C)
b
no subducted oceanic fragments returned
continental subduction
time (Ma)
onset oceanic subduction
no oceanic rock recovery
Stacking
BY+CO D2-D3
collision
Depth (km)
P(GPa)
LN
CS
SMU
GP
MR
ATF
AV
ALB
MB
Sesia
Orsiera
GU
Rocciavrè
SLU
ZS
LS
Slicing sequence
LPU
LPM
LPL
Sed. +
Maf.Umaf. +
Maf.Umaf. ++
(rocks lost)
Lago di Cignana
DM (UHP)

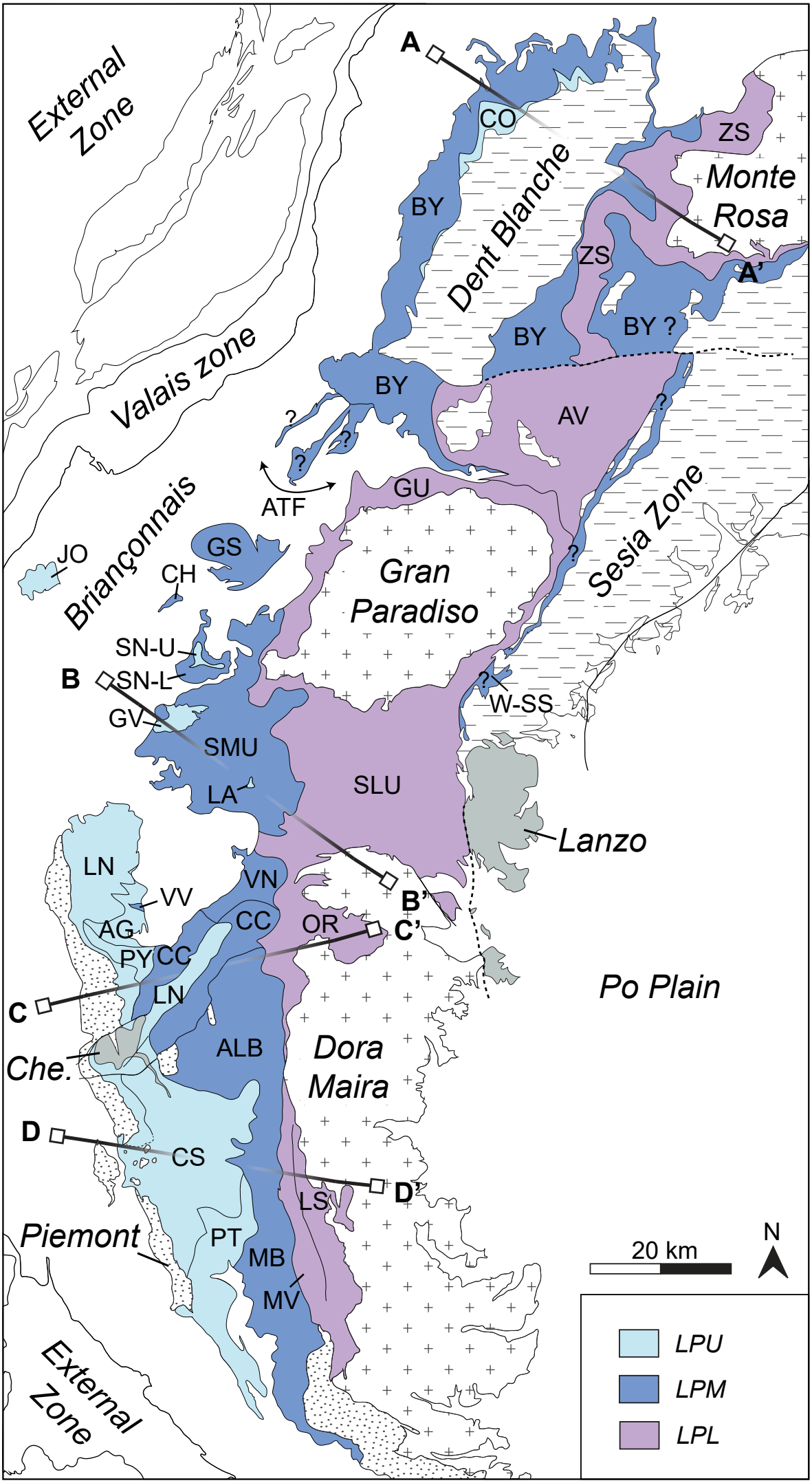
External Zone
Valais zone
Briançonnais
Dent Blanche
Monte Rosa
Gran Paradiso
Sesia Zone
Lanzo
Po Plain
Dora Maira
Che.
Piemont
External Zone
A
A'
B
B'
C
C'
D
D'
CO
ZS
BY
BY ?
AV
GU
ATF
JO
CH
GS
SN-U
SN-L
GV
SMU
LA
SLU
W-SS
LN
VV
VN
AG
CC
OR
PY
ALB
CS
LS
PT
MB
MV
20 km
N
LPU
LPM
LPL

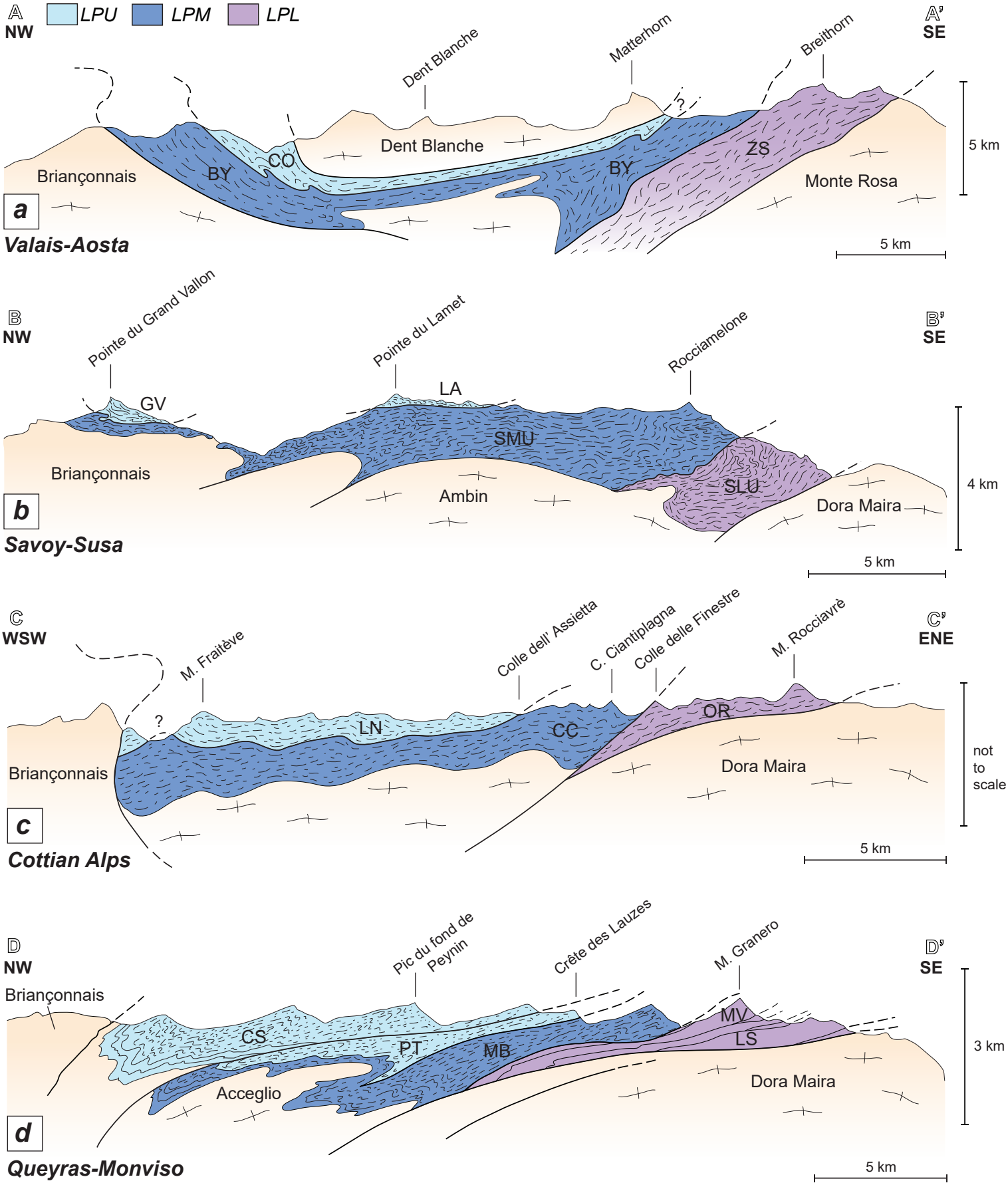
A
NW
LPU
LPM
LPL
A'
SE
Dent Blanche
Matterhorn
Breithorn
Dent Blanche
Briançonnais
BY
CO
BY
ZS
Monte Rosa
5 km
a
Valais-Aosta
5 km
B
NW
Pointe du Grand Vallon
Pointe du Lamet
Rocciamelone
B'
SE
GV
LA
SMU
Briançonnais
Ambin
SLU
Dora Maira
4 km
b
Savoy-Susa
5 km
C
WSW
M. Fraitève
Colle dell' Assietta
C. Ciantiplagna
Colle delle Finestre
M. Rocciavrè
C'
ENE
LN
CC
OR
Briançonnais
Dora Maira
not to scale
c
Cottian Alps
5 km
D
NW
Pic du fond de Peynin
Crête des Lauzes
M. Granero
D'
SE
Briançonnais
CS
PT
MB
MV
LS
Acceglio
Dora Maira
3 km
d
Queyras-Monviso
5 km

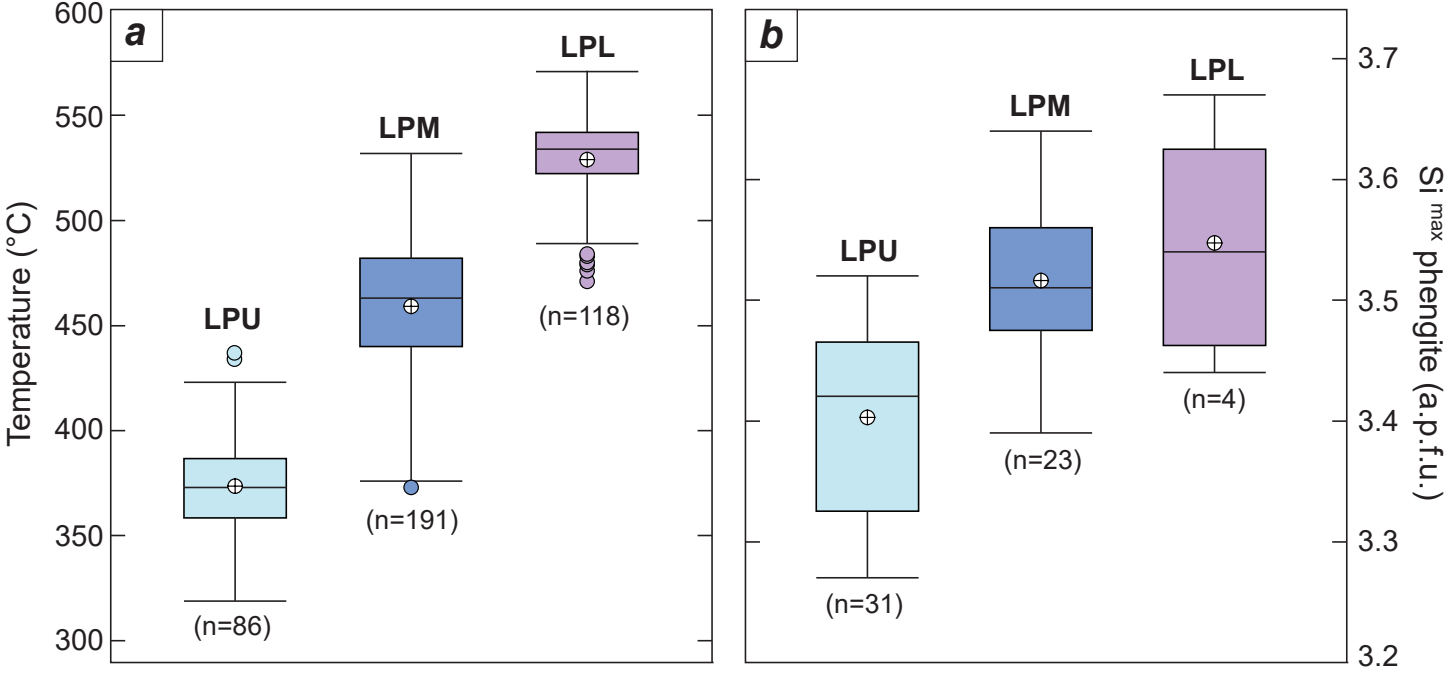
a
b
LPU
LPM
LPL
(n=86)
(n=191)
(n=118)
(n=31)
(n=23)
(n=4)
Temperature (°C)
Si max phengite (a.p.f.u.)
600
550
500
450
400
350
300
3.7
3.6
3.5
3.4
3.3
3.2

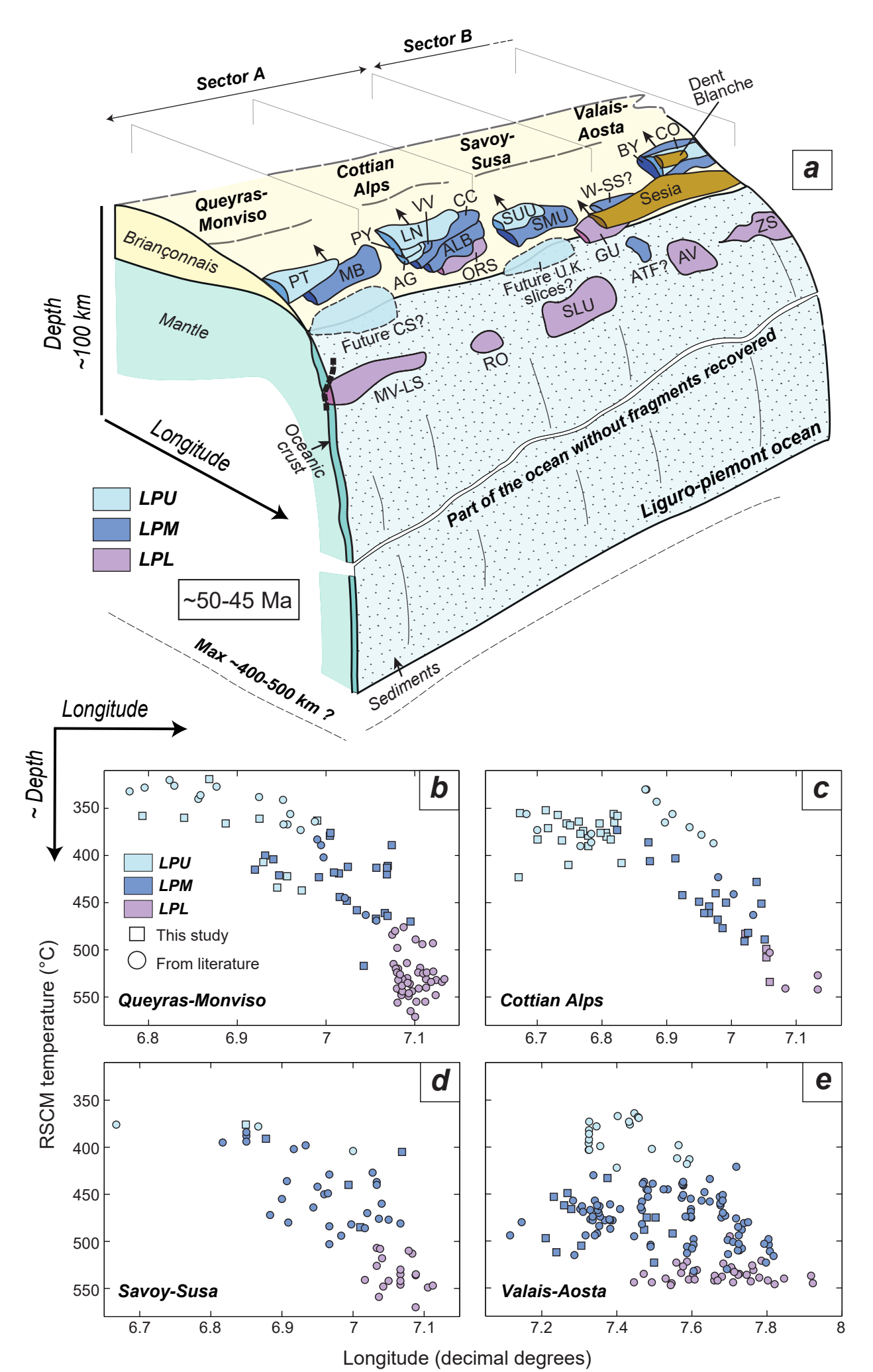
Sector A
Sector B
Dent Blanche
Valais-Aosta
Savoy-Susa
Cottian Alps
Queyras-Monviso
Briançonnais
Mantle
Depth ~100 km
Longitude
Oceanic crust
Sediments
Max ~400-500 km ?
Part of the ocean without fragments recovered
Ligure-piemont ocean
Future CS?
Future U.K. slices?
Future U.K. slices
MV-LS
RO
SLU
SUU
SMU
W-SS?
Sesia
ZS
GU
ATF?
AV
BY
CO
VV
CC
LN
PY
ALB
AG
ORS
PT
MB
LPU
LPM
LPL
~50-45 Ma
a
~ Depth
Longitude
b
c
d
e
This study
From literature
Queyras-Monviso
Cottian Alps
Savoy-Susa
Valais-Aosta
RSCM temperature (°C)
Longitude (decimal degrees)

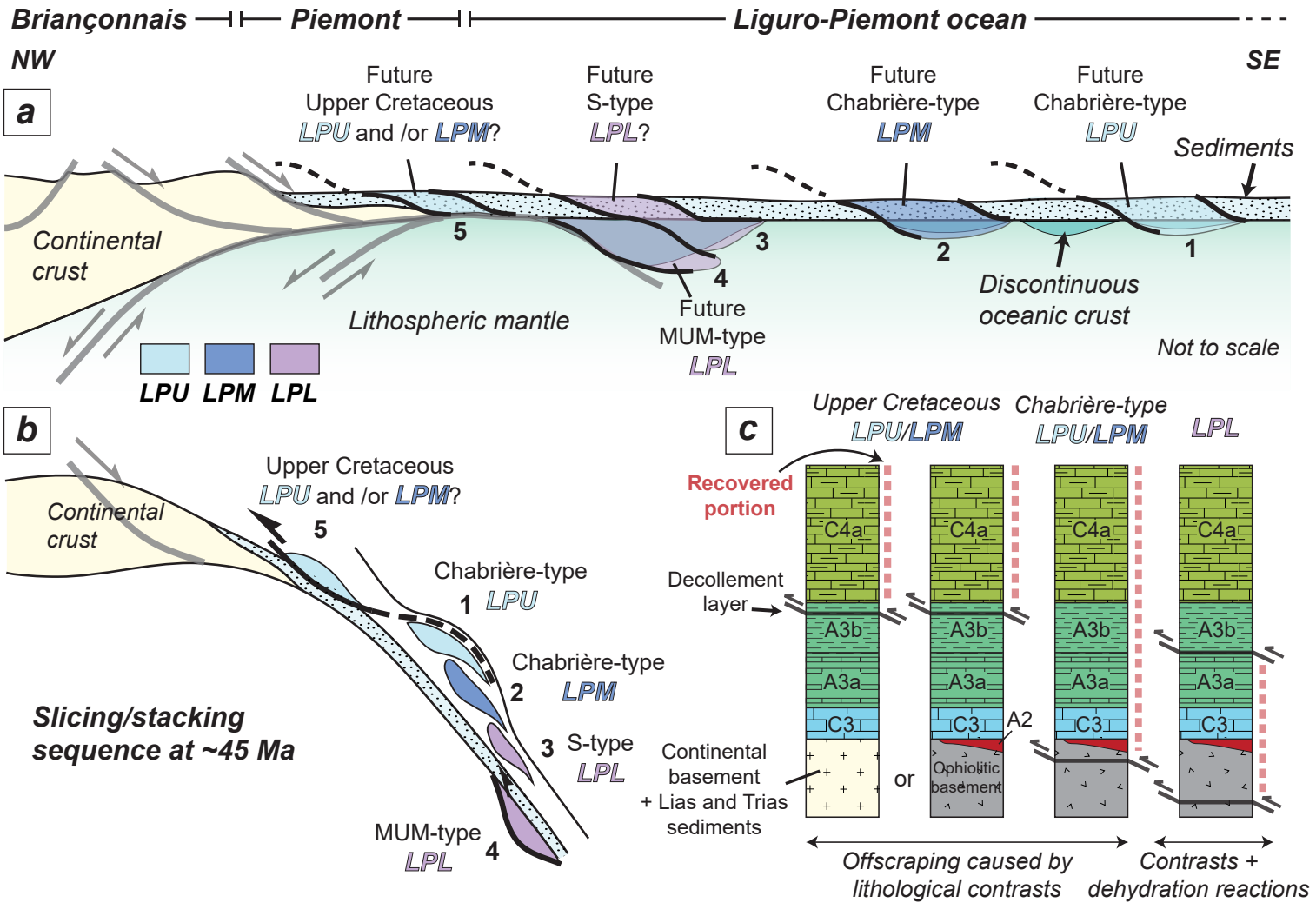
Briançonnais
Piemont
Liguro-Piemont ocean
NW
SE
a
Future
Upper Cretaceous
LPU and /or LPM?
Future
S-type
LPL?
Future
Chabrière-type
LPM
Future
Chabrière-type
LPU
Sediments
Continental
crust
Lithospheric mantle
Future
MUM-type
LPL
Discontinuous
oceanic crust
Not to scale
LPU LPM LPL
b
Continental
crust
Upper Cretaceous
LPU and /or LPM?
Chabrière-type
LPU
Chabrière-type
LPM
S-type
LPL
MUM-type
LPL
Slicing/stacking
sequence at ~45 Ma
c
Upper Cretaceous
LPU/LPM
Chabrière-type
LPU/LPM
LPL
Recovered
portion
Decollement
layer
C4a
A3b
A3a
C3
A2
Continental
basement
+ Lias and Trias
sediments
or
Ophiolitic
basement
Offscraping caused by
lithological contrasts
Contrasts +
dehydration reactions

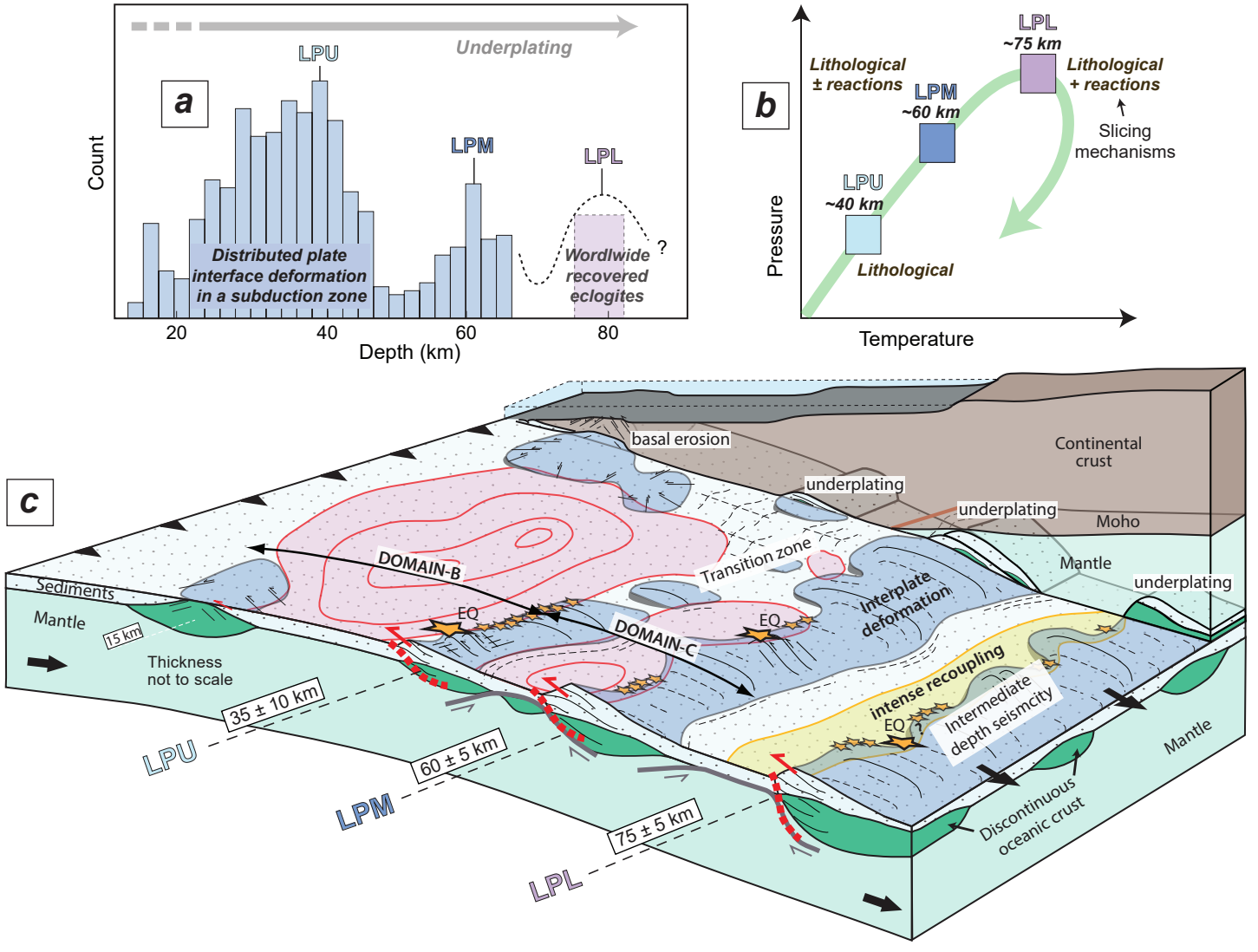
a
Underplating
LPU
LPM
LPL
Count
Distributed plate interface deformation in a subduction zone
Wordlwide recovered eclogites
?
20
40
60
80
Depth (km)
b
LPL
~75 km
Lithological ± reactions
LPM
~60 km
Lithological + reactions
Slicing mechanisms
LPU
~40 km
Lithological
Pressure
Temperature
c
basal erosion
Continental crust
underplating
underplating
Moho
Mantle
underplating
Transition zone
DOMAIN-B
DOMAIN-C
EQ
EQ
Interplate deformation
Sediments
Mantle
15 km
Thickness not to scale
35 ± 10 km
LPU
60 ± 5 km
LPM
75 ± 5 km
LPL
intense recoupling
EQ ?
Intermediate depth seismcity
Mantle
Discontinuous oceanic crust

Slice	*Metamorphic zone*	*Sediments %*	*Mafic-ultramafic %*	*~ outcroping surface (km^2)*
All Liguro-Piemont domain	Blueschist and eclogite facies zones	71	29	2477
All Blueschist-facies slices	Blueschist-facies zone	91	9	1516
All Eclogite-facies slices	Eclogite-facies zone	38	62	961
Aigle + Vin vert	Blueschist-facies zone	98	2	20
Albergian + Mirabouc-Bouchet	"	96	4	258
Cerogne-Ciantiplagna	"	95	5	78
Chardonnet klippe (Savoy Middle Unit)	"	100	0	2
Combin (By + Cornet)	"	76	24	433
Calcschist unit	"	99	1	161
Grande-Sassière klippe (Savoy Middle Unit)	"	99	1	38
Grand Vallon klippe (Savoy Upper Unit)	"	100	0	9
Jovet klippe (Savoy Upper Unit)	"	100	0	9
Lamet klippe (Savoy Upper Unit)	"	100	0	<1
Lago Nero	"	99	1	134
Pelvas-Taillante	"	90	10	70
Puys	"	99	1	14
Savoy Middle Unit	"	98	2	181
Lower Sana klippe (Savoy Middle Unit)	"	96	4	14
Upper Sana klippe (Savoy Upper Unit)	"	91	9	3
Venaus	"	99	1	28
Avise-Tsaboc-Feluma	?	99	1	28
West-Sesia	?	93	7	34
Avic unit	Eclogite-facies zone	28	72	211
Grivola-Urtier	"	61	39	113
Monviso unit + Lago Superiore	"	40	60	101
Orsiera-Rocciavrè	"	59	41	70
Savoy Lower Unit	"	36	64	314
Zermatt-Saas	"	35	65	152

Table 1: Lithological ratio (sediment versus mafic-ultramafic) and aerial exposure of the Liguro-Piemont slices. See text (§4.2) for details in the methodology.

Transect	Slice	Mean T (°C)	Med. T (°C)	sd	n samples	T range (°C)	References
Valais-Aosta	Cornet (Combin)	390	392	18	21	364-422	Negro et al. (2013); Angiboust et al. (2014); Decrausaz et al. (2021); Manzotti et al. (2021)
"	By (Combin)	476	474	25	106	421-532	This study; Angiboust et Agard (2010); Negro et al. (2013); Angiboust et al. (2014); Decrausaz et al. (2021); Manzotti et al. (2021)
"	Zermatt-Saas	533	536	12	26	495-546	Angiboust et al. (2009); Angiboust et Agard (2010); Negro et al. (2013)
"	Avic	538	538	7	12	523-547	Angiboust et al. (2009); Angiboust et Agard (2010)
"	Grivola-Urtier	499	483	31	3	479-534	This study
"	Avise-Tsaboc-Feluma	/	/	/	1	522	This study
"	West-Sesia	/	/	/	1	433	This study
Savoy-Susa	Savoy Upper Unit	384	377	14	4	376-404	This study; Gabalda et al. (2009); Plunder et al. (2012)
"	Savoy Middle Unit	445	449	36	31	384-503	This study; Gabalda et al. (2009); Plunder et al. (2012)
"	Venaus	/	/	/	1	484	This study
"	Savoy Lower Unit	530	533	21	24	471-580	This study; Gabalda et al. (2009); Plunder et al. (2012)
Cottian Alps	Lago Nero	372	373	20	33	330-423	This study; Beyssac et al. (2002); Gabalda et al. (2009)
"	Puys	/	/	/	1	364	This study
"	Aigle	373	377	15	3	357-386	This study; Gabalda et al. (2009)
"	Vin Vert	414	414	3	2	413-416	This study
"	Cerogne-Ciantiplagna	421	423	34	5	373-463	This study; Beyssac et al. (2002)
"	Albergian	452	453	29	16	386-491	This study
"	Orsiera-Rocciavrè	517	517	22	8	483-542	This study; Beyssac et al. (2002); Gabalda et al. (2009)
Queyras-Monviso	Calcschist unit	364	349	43	14	320-437	This study; Schwartz et al. (2013)
"	Pelvas-Taillante	355	362	17	10	319-363	This study; Schwartz et al. (2013)
"	Mirabouc-Bouchet	427	419	34	29	376-517	This study; Schwartz et al. (2013)
"	Monviso unit	488	489	8	7	476-498	Angiboust et al. (2011); Schwartz et al. (2013)
"	Lago Superiore	536	534	14	37	514-571	Angiboust et al. (2011); Schwartz et al. (2013)

Table 2: RSCM temperatures of the Liguro-Piemont slices. All the compiled RSCM temperatures (from this study and literature) are presented in Sup. Mat 1.

Slice	$Si^{max}Ph$	Mean $Si^{max}Ph$	Med. $Si^{max}Ph$	sd	n samples	Relative pressure (GPa)	References for $Si^{max}Ph$
Lago Nero	3.27-3.5	3.39	3.42	0.082	19	~1.3 - ~1.9	This study; Agard et al. (2001); Liewig (1981)
Puys	3.46	/	/	/	1	1.7-1.8	This study
Vin Vert	3.55	/	/	/	1	2.1	This study
Cerogne-Ciantiplagna	3.4-3.57	3.49	3.49	0.113	2	1.7- ~2.2	This study; Agard et al. (2001)
Albergian	3.39-3.64	3.5	3.48	0.082	11	1.8- ~2.3	This study; Agard et al. (2001)
Orsiera-Rocciavrè	3.47-3.67	3.53	3.47	0.125	3	2.2- ~2.5	This study; Agard et al. (2001)
Calcschist unit	3.34-3.5	3.43	3.42	0.059	8	1.4-2	This study; Liewig (1981)
Pelvas-Taillante	3.31-3.42	3.37	3.37	0.077	2	1.4-1.7	This study; Bocquet (1974)
Mirirabouc-Bouchet	3.48-3.59	3.53	3.54	0.037	9	1.9- ~2.4	This study
Lago Superiore	3.61	/	/	/	1	> 2.4	Bonnet et al. (submitted)

Table 3: Maximum Si a.p.f.u. values of phengite ($Si^{max}Ph$) and estimated peak pressure for Liguro-Piemont slices. Peak pressures were estimated by crossing RSCM temperatures (see Table 1; Fig. 4a-c, 5a-e) with the calculated isopleths of Si a.p.f.u. in phengite for a representative rock composition (Fig. 9a). Selected $Si^{max}Ph$, RSCM temperature for the same samples and all estimated pressure values are presented in Sup. mat. 3.